NEARSHORE WAVE PREDICTION MODELING FOR THE SOUTHERN-WEST COASTS OF THE BLACK SEA AND COMPARISON WITH THE WAVE MEASUREMENT DATA

A Thesis Submitted to
the Graduate School of Engineering and Sciences of
İzmir Institute of Technology
in Partial Fulfillment of the Requirements for the Degree of

MASTER OF SCIENCE

in Civil Engineering

by
Muzaffer GÜLER

December 2019
İZMİR

We approve the thesis of **Muzaffer GÜLER**

Examining Committee Members:

Assist. Prof. Bergüzar ÖZBAHÇECİ
Department of the Civil Engineering, İzmir Institute of Technology

Prof. Şebnem ELÇİ
Department of the Civil Engineering, İzmir Institute of Technology

Assoc. Prof. Mustafa DOĞAN
Department of the Civil Engineering, Dokuz Eylül University

19 December 2019

Assist. Prof. Bergüzar ÖZBAHÇECİ
Supervisor, Department of the Civil Engineering
İzmir Institute of Technology

Prof. Gökmen TAYFUR
Head of the Department of the
Civil Engineering

Prof. Mehtap EANES
Dean of the Graduate School of
Engineering and Sciences

ACKNOWLEDGMENTS

I would like to thank my dear advisor Assist. Prof. Bergüzar Özbahçeci who guided and supported me with her valuable knowledge and experiences during my thesis. I could not have studied with a better advisor.

My thanks also go to the European Centre for Medium-Range Weather Forecasts (ECMWF) for providing ERA-5 wave data.

Last but not least, I would like to thank my family: my parents Ayşegül Güler, Hamdi Güler, my lovely sister Saadet Güler and my aunt Mine Kongül for supporting me throughout my life.

ABSTRACT

NEARSHORE WAVE PREDICTION MODELING FOR THE SOUTHERN-WEST COASTS OF THE BLACK SEA AND COMPARISON WITH THE WAVE MEASUREMENT DATA

While waves propagate towards shallow areas where most of the coastal structures are constructed, their properties like wave height and direction may change. The change in the wave properties in shallow areas called wave transformation may happen due to a decrease in water depth, sea bottom configurations or some obstacles like islands. Therefore, it should be calculated to find the wave properties used in coastal engineering projects. In this study, the main purpose is to model the waves in the near-shore region of the Filyos coast in Zonguldak province of Turkey by a 3rd generation nearshore wave model, SWAN (Simulating Waves Nearshore). The newest re-analysis data, ERA5, of The European Centre for Medium-Range Weather Forecasts (ECMWF) are used as SWAN model input in deep water. The data are calibrated with satellite radar altimeter data before using the model input data. One of the targets of the study is to verify the developed model using data of an in-situ measurement campaign organized by the Turkish Ministry of Transport. A verification study is performed using not only all data but also using the storm data with higher waves. For the selected storms, statistical and spectral analyses of the raw data are also performed. Results of the verification study show that wave predictions obtained from the developed nearshore wave model using SWAN fit to in-situ measurements well. Results are also compared with the previous studies and it is concluded that error results are much better for the wave period.

ÖZET

GÜNEYBATI KARADENİZ İÇİN YAKIN KIYI DALGA TAHMİN MODELİ GELİŞTİRİLMESİ VE ÖLÇÜMLERLE KARŞILAŞTIRILMASI

Dalgalar, kıyı yapılarının çoğunun inşa edildiği sığ alanlara doğru ilerlerken, yüksekliği ve yönü gibi özellikleri değişebilir. Dalga dönüşümü olarak adlandırılan sığ alanlardaki dalga özelliklerinde oluşan bu değişim, su derinliği, deniz tabanı konfigurasyonları veya adalar gibi bazı etkenler nedeniyle meydana gelebilir. Bu nedenle, kıyı mühendisliği projelerinde gerekli dalga parametrelerinin bulunmasında dikkate alınmalıdır. Bu çalışmada temel amaç, güneybatı Karadeniz kesimindeki Zonguldak ilinin Filyos ilçesi kıyıları için 3. nesil yakın kıyı dalga modeli olan SWAN (Simulating Waves Nearshore) ile dalga modellemesi yapmaktır. Avrupa Orta Aralıklı Hava Tahminleri Merkezi'nin (ECMWF) en güncel yeniden analiz veri seti olan ERA5, derin suda SWAN modeli girdisi olarak kullanılmıştır. Model girdisi olarak kullanılmadan önce veriler uydu radar altimetre verisi ile kalibre edilmiştir. Çalışmanın hedeflerinden biri, ölçümleri Ulaştırma Bakanlığı tarafından gerçekleştirilen dalga verilerini kullanarak geliştirilen modeli doğrulamaktır. Doğrulama çalışması sadece tüm veriler kullanılarak değil, aynı zamanda daha yüksek dalgalara sahip fırtına verileri kullanılarak da gerçekleştirilmiştir. Seçilen fırtınalar için ham verilerin istatistiksel ve spektral analizleri de yapılmıştır. Doğrulama çalışmasının sonuçları, SWAN kullanılarak geliştirilen yakın kıyı dalga modelinden elde edilen dalga tahminlerinin yerinde ölçümlerle uyumlu olduğunu göstermektedir. Sonuçlar önceki çalışmalarla da karşılaştırılmış ve hata sonuçlarının dalga periyodu için daha iyi olduğu sonucuna varılmıştır.

TABLE OF CONTENTS

LIST OF FIGURES

Figure **Page**

Figure **Page**

Figure **Page**

Figure **Page**

Figure **Page**

LIST OF TABLES

CHAPTER 1

INTRODUCTION

1.1. Motivation

Existing waters on the earth, ocean-sea-lake, have a great impact on shipping, transportation, fishing, recreation, and construction. The movements of these water bodies, called waves have been examined frequently in order to use in almost all coastal and marine activities. The fact that some waves may result in a catastrophe has led to the need to get to know the atmosphere, the air, and the sea better.

Second World War has been accepted as the born of modern coastal engineering. Since then various wind-wave prediction methods have been derived. SMB (Sverdrup-Munk-Bretschneider) was the first nomogram method to estimate the wave height and period using wind speed, duration, and distance of water area that wind is blowing to generate waves called as fetch. Then through the JONSWAP (Joint North Sea Wave Project), Hasselman et al. (1973) derived a parametric method to estimate wave properties. Then numerical models have been developed as computer technology develops. All of the methods can predict the waves in deep water. However, while waves propagate towards shallow areas where most of the coastal structures are constructed due to economic reasons, their properties like wave height and direction may change. The change in the wave properties in shallow areas also called wave transformation may happen due to a decrease in water depth, sea bottom configurations or some obstacles like islands. Wave shoaling, refraction, breaking and diffraction are the components of the wave transformation. Therefore, those components should be calculated to use in coastal engineering activities.

Wave transformation can be calculated using analytical methods derived from linear wave theory under the assumption that bottom contours are parallel to the coastline. Goda (2010) calculated wave transformation considering wave randomness. However, his formulas and user-friendly charts are correct for the same assumption of parallel bottom contours. To calculate the changes in the wave properties for irregular bottom configurations as in nature, numerical models have been developed. SWAN

developed by the Technical University of Delft is one of the commonly used numerical models to calculate the wave properties in the near-shore. In-situ measurements are generally used to verify the numerical models.

In-situ measurements produce one of the most reliable sources of wave data. However, due to the practical problems associated with the measurements and financial problems, measurement data can be usually obtained for a short term and they are used for the calibration and verification purposes (Ozbahceci 2019). One of them was organized within the framework of the NATO TU-WAVES project (Ozhan and Abdalla 1999). Five directional wave buoys were deployed at Alanya, Dalaman, Bozcaada, Sinop, and Hopa along the Turkish coasts. Due to several problems like loss and damages, wave buoys are not in use for the time being. Measurement details can be found in Ozhan and Abdalla (1999). State Meteorological Organization in Turkey started to permanent wave measurements in İstanbul, Çanakkale, Antalya, and Mersin in 2015. Buoy deployment depths are more than 50 m in both of the measurement campaigns. It is a deep water condition for the seas along the Turkish coasts. Using in-situ measurement data in deep water, it is possible to verify the numerical models in deep water conditions. Akpınar et al. (2014) used in-situ data of NATO TU-WAVES to verify their SWAN model in deep water. However, for most of the coastal activities, near-shore wave information is necessary. Thus, numerical models to predict the waves in the near-shore should be verified with the measurements conducted in the near-shore. There are only two measurement campaigns in near-shore of the Turkish coasts. One of them is in Filyos and conducted by the Turkish Ministry of Transport, General Directorate of Infrastructure, Research Department in the years of 1994 and 1996. Wave height, period and direction were measured by pressure type wave gauge in 12.5m water depth. Therefore, this data can be a good source to verify the near-shore wave prediction model.

1.2. Purpose and Scope of the Study

In this study, the main purpose is to model the waves in the near-shore region by a 3rd generation nearshore wave model, SWAN (Simulating Waves Nearshore). SWAN is chosen for the numerical model since it has many advantages like modeling in stationary and non-stationary modes, including triad and quadruplet non-linear wave

interactions and it is user –friendly and widely used in all around the world. Filyos coast of Zonguldak province of Turkey in the southwestern part of the Black Sea was chosen as the study area. There is a new port project of the Turkish government in Filyos. Therefore in-situ wave measurement campaign was organized in 1994. The newest re-analysis data, ERA5, of The European Centre for Medium-Range Weather Forecasts (ECMWF) are used as SWAN model input in deep water. The data is calibrated with satellite radar altimeter data before using it as model input data. One of the targets of the study is to verify the developed model using in-situ measurements. A verification study is performed using not only all data but also using the storm data with higher waves. For the selected storms, statistical and spectral analyses of the row data are also performed.

1.3. The Structure of the Thesis

The structure of this thesis is as follows. A review of the literature survey is provided in Chapter 2. Data-used and calibration studies are elaborated in Chapter 3, this is followed by numerical modeling (SWAN) described in Chapter 4. Verification study is provided in Chapter 5 and this thesis concludes with a discussion of the presented study in Chapter 6.

CHAPTER 2

LITERATURE REVIEW

2.1. Wave Properties

Waves are created by energy passing through water, causing it to move in a circular motion. The surface water never travels, but the waves transmit energy across if not obstructed by any obstacles. Waves can be classified according to generating force and period. Classification of waves in accordance with the phenomena, generating force and period is given in Table 1.

Table 1. Waves, their causes and periods (Source: Ergin 2009)

Phenomenon	Generating Force (Cause)	Period
Short Period Waves • Wind Waves	Wind Shear	Up to 15 sec
• Swell	Wind Wave	Up to 30 sec
Long Period Waves • Tsunami	At the sea bed: Earthquake, landslide, volcanic eruption, meteor impact.	5 to 60 min
• Tidal wave	Gravitational action of the moon and the sun	About 12-24 h
• Storm Surge	Wind stress and atmospheric pressure reduction	1 to 30 days
• Harbor Resonance	Tsunami, surf beat	2 to 40 min
• Seiche	Wind Variation	2 to 40 min
• Surf Beat	Wave Group	1 to 5 min

The terms that describe waves that are propagating at a constant rate and not changing significantly over time are presented in Figure 1.

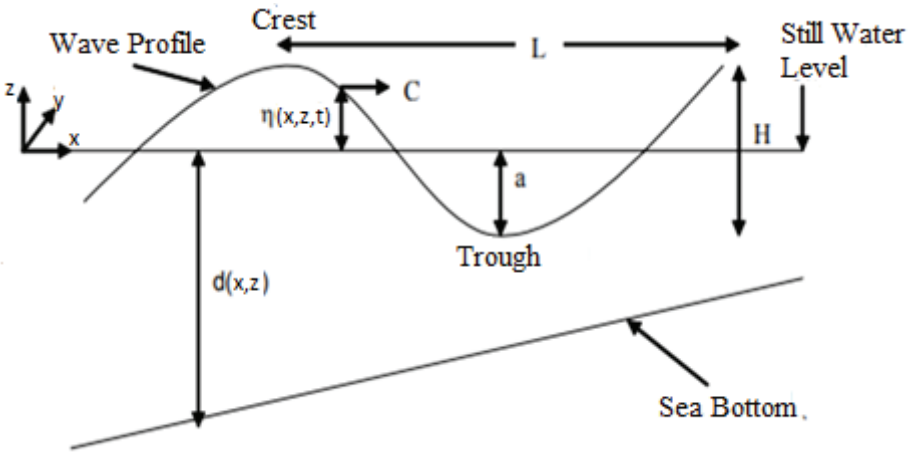

Figure 1. Definition sketch for sinusoidal wave (Source: Lecture notes, Coastal Hydraulics (CE479))

- Wave Profile(h)= Vertical displacement of the sea surface from the still water level (SWL) as a function of time and space.
- Wave Crest = The highest point of the wave profile.
- Wave Trough = The lowest point of the wave profile.
- WaveLength (L)= The horizontal distance between two successive crests or troughs(m).
- Wave Height(H) = The vertical distance from wave trough to the wave crest. It is equal to twice the wave amplitude(m).
- Wave Steepness(H/L) = The ratio of wave height to wavelength.
- Wave Amplitude(a) = The vertical distance from the still water level to wave crest.
- Wave Period(T) = Time for one full wavelength to pass a given point (s).
- Wave frequency(f) = The number of waves to pass a given point per unit time (f = 1/T)
- Wavenumber (k)= 2p times the number of waves per unit horizontal distance. ($k = \frac{2\pi}{L}$)
- Angular wave frequency(s)= It is equal to the wave frequency times 2s($\sigma = \frac{2\pi}{T}$)
- Water depth(d)= Distance from SWL to bottom.
- Wave celerity(C)= The speed at which a waveform moves. ($C = L/T$)

Basic parameters of a wave are wave height, wave period and wavelength.

2.2. Classification after Height, Length and Depth

Waves may be classified with respect to the assumptions employed in their mathematical development. For wind waves occurring in nature the wave steepness *H/L* is usually at most 0.02 to 0.05 and due to this small value could believe that the linearization by neglecting H^2/L^2 in comparison with terms, H/L represents a good approximation for all practical purposes (Ergin 2009). The resulting waves are called Linear waves and small amplitude wave theory is applicable for linear waves.

If the wave height is finite height, the effect of higher-order terms is taken into account and the resulting waves are called nonlinear waves. Finite amplitude wave theory is applicable for nonlinear waves.

Classification of small amplitude waves and finite-amplitude waves with respect to relative depth is shown in Figure 2.

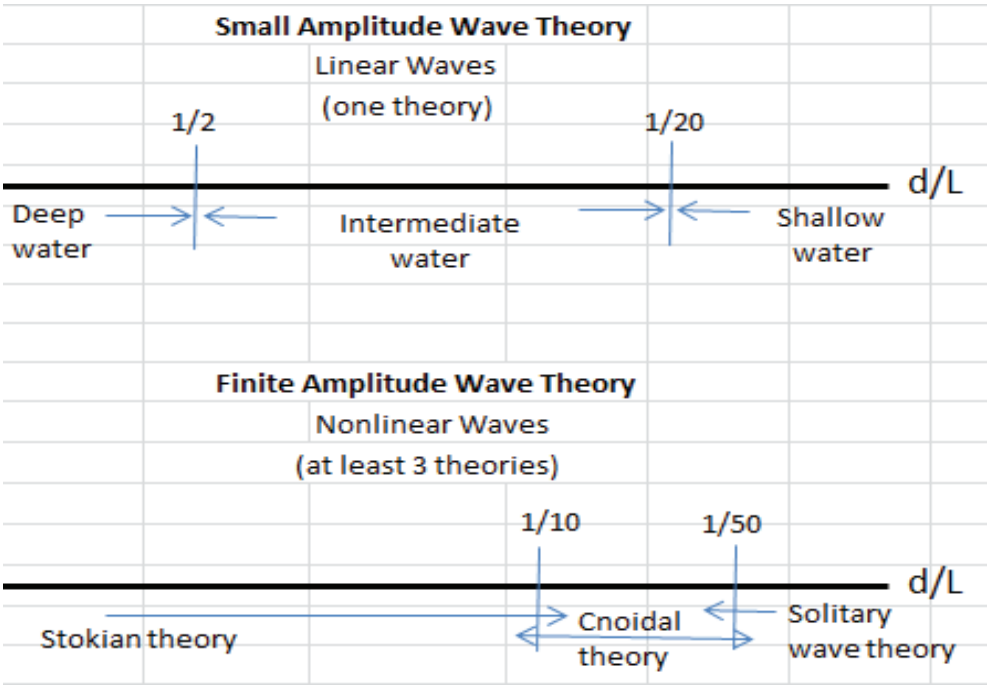

Figure 2. Classification of waves with respect to relative depth (Source: IPPEN 1996)

2.3. Wave Transformation

Wave Transformation refers to changes in wave characteristics during propagation, generally propagating from deep through shallow water. Waves are continuously subjected to transformations due to their interaction with the sea bottom, the shoreline, and forms that are encountered while propagating. The primary processes affecting wave transformations are refraction, diffraction, shoaling, dissipation (breaking), and nonlinear effects. Wave transformation is concerned with the changes in H, L, C and α, the wave angle with the bottom contours; wave period T remains constant throughout the process.

2.3.1. Wave Shoaling

While waves are propagating from deep water towards the shore, the bottom friction effect starts when the water depth becomes less than about half the wavelength. As waves slow-down in shallow water, wave-length reduces and wave height increases. The increase in wave height is referred to as wave shoaling. It is calculated as given in Equation10.

$$\frac{H}{H_0} = K_S = \left[tanh\left(\frac{2\pi d}{L}\right)\right]^{-0.5}\left[1 + \frac{4\pi d/L}{sinh(4\pi d/L)}\right]^{-0.5} \quad (1)$$

K_s: Shoaling coefficient, $Ks=\sqrt{\frac{n_0}{n}\frac{C_0}{C}}$ (2)

2.3.2. Wave Refraction

Wave refraction is a process affecting the distribution of wave energy and power. It occurs from a change in local wave propagation speed due primarily to local depth changes and can end up with convergence or divergence of the wave energy-producing changes in wave height as well as wave direction in the nearshore. When the energy flux is conserved between the wave rays, then;

Energy flux= EC_g ; C_g=Cn (3)

$$ECnb = constant \quad (4)$$

$$\frac{H}{H0} = \sqrt{\frac{n_0}{n}\frac{C_0}{C}}\sqrt{\frac{b_0}{b}} = KsKr \quad (5)$$

Kr: Coefficient of refraction, Kr=$\sqrt{\frac{b_0}{b}}$ (6)

Another way to calculate Kr using the wave direction of propagation by Snell's Law. It is shown in Figure 3.

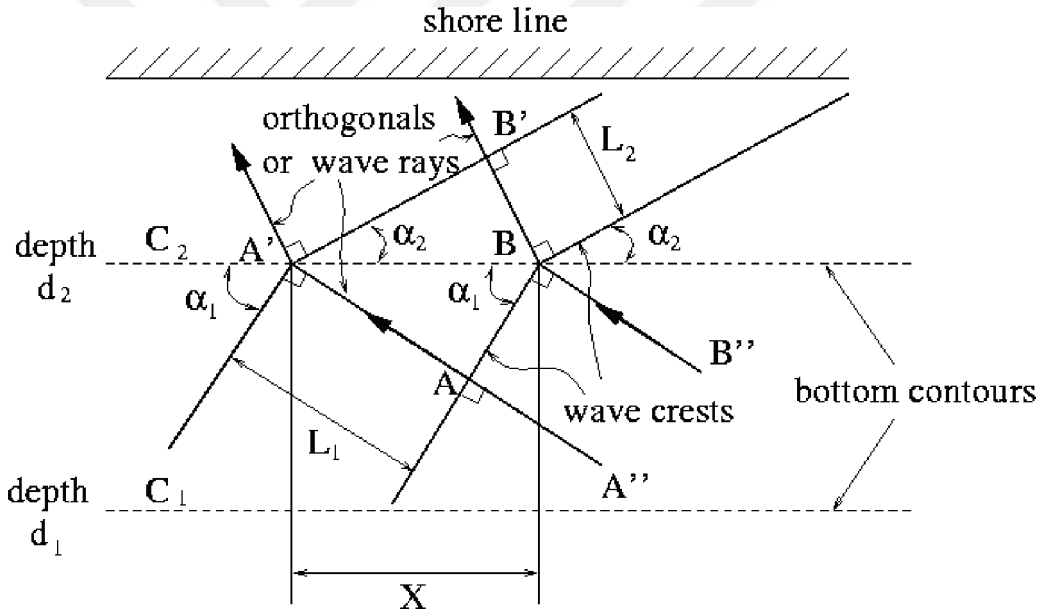

Figure 3. Snell's law (Source: http://cavity.caee.utexas.edu/kinnas/wow /public _html / waveroom/linapp/node3.html)

$$xsin\propto_1 = L_1\,, xsin\propto_2 = L_2 \quad (7)$$

$$\frac{sin\propto_1}{sin\propto_2} = \frac{C_1}{C_2} = \frac{L_1}{L_2} = \tanh kd \quad (8)$$

$$b_0 = x\cos\propto_0\,, b = x\cos\propto \quad (9)$$

$$Kr = \sqrt{\frac{b_0}{b}} = \sqrt{\frac{cos\propto_0}{cos\propto}} \quad (10)$$

2.3.3. Wave Diffraction

The diffraction of waves is a phenomenon in which energy is transferred laterally along the wave crest because of any obstacles. The diffraction of waves is described in Figure 4. In this figure, it is seen that incident waves cannot move directly into the shadow region. However, the wave motion is transmitted into the shadow region by means of lateral energy transfer and so that it causes a change in wave height and wave direction.

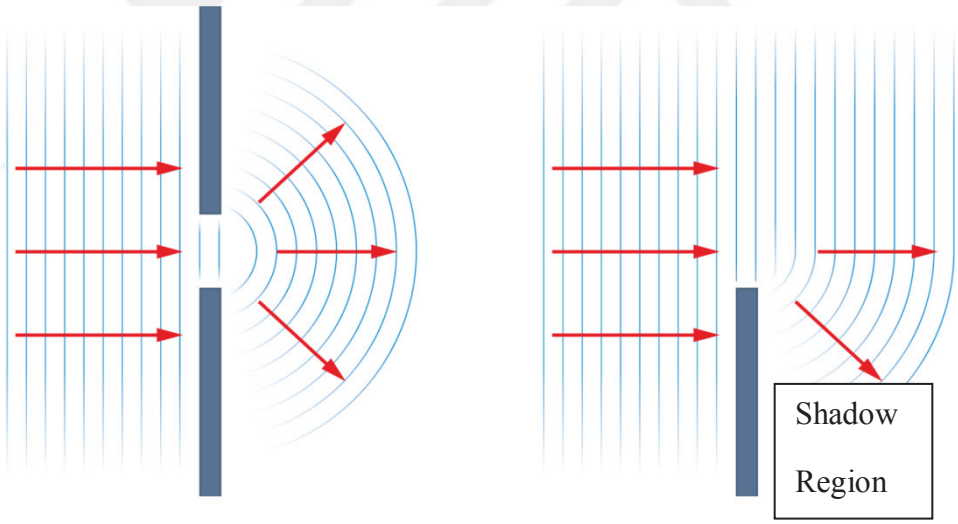

Figure 4. Wave diffraction (Source: https://roguephysicist.com/wave_behaviour.htm)

Waves in the shadow region are called as the diffracted waves. The ratio between the diffracted (H_d) and incident wave heights (H_i) is given by diffraction coefficient (K_d);

$$K_d = \frac{H_d}{Hi} \quad (11)$$

Wave diffraction calculations are carried out usually to determine wave height within the structure sites or near structure sites located on the shores of bays sheltered by the natural coastline configuration. The calculation of wave diffraction is quite complicated. For preliminary calculations, however, it is often sufficient to use diffraction diagrams. One such diagram is presented in Figure 5.

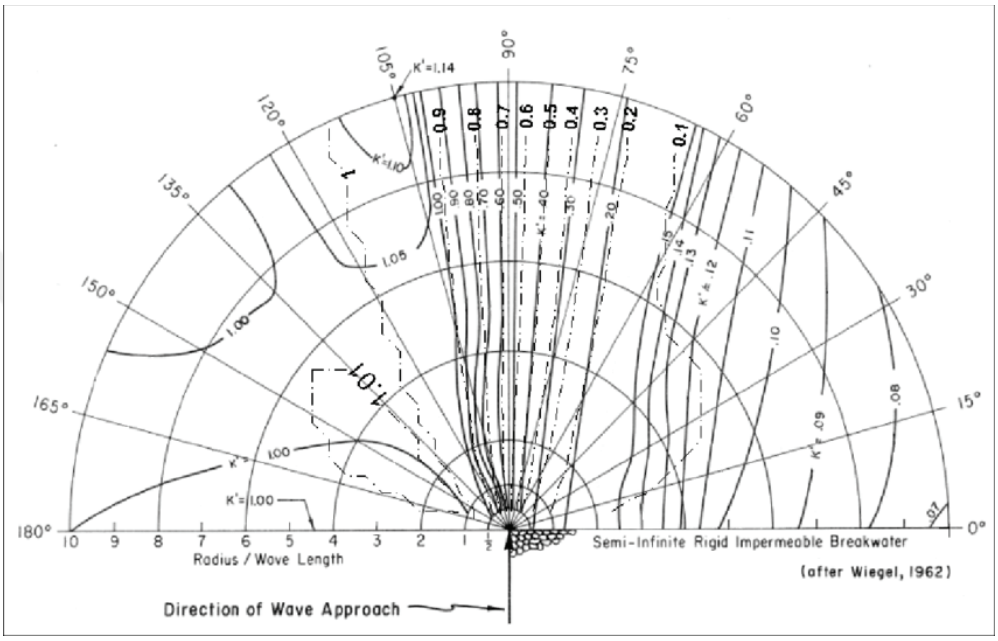

Figure 5. Wave diffraction diagram for the approach angle between a wave orthogonal and the breakwater alignment (β_{app}=90˚) (Source: https://www.researchgate.net/figure /Wave-diffraction-diagram-and-calculated-normalized-diffraction-wave-height-K-dash-dot_fig5_235103047)

2.3.4. Wave Breaking

As waves move into shoaling water, they eventually become unstable and break. Breaker index that is the ratio between breaking depth db and breaking height Hb is given in Eq. 18.

$$\frac{Hb}{db} = f(m, \frac{H_0}{L_0},) \tag{12}$$

m: Beach slope

β: deep-water approach angle

Definition sketch for breaking wave height and depth is shown in Figure 6.

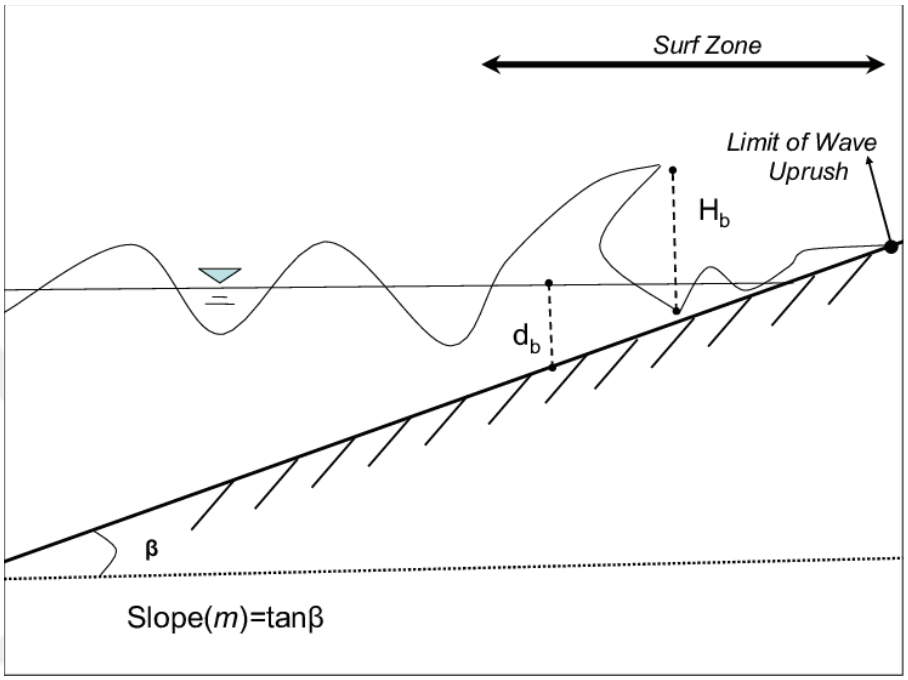

Figure 6. Definition sketch for breaking wave height and depth (Source: https: // www. researchgate.net/figure/Definition-sketch-for-breaking-wave-height-and-depth_fig7_322150522)

The maximum height of the wave is limited by a certain limitation while a wave will move in shallow water. This limitation is considered to be the wave orthogonality value.

Critical Wave Steepness:

$$\left(\frac{H}{L}\right)_{max} = \frac{1}{7} tanh\left(\frac{2\pi d}{L}\right) \quad (13)$$

In the deepwater:

$$\left(\frac{H_0}{L_0}\right)_{max} = \frac{1}{7} \cong 0.142 \tag{14}$$

Breaking waves are generally divided into four main types, depending on the steepness of the waves and the slope of the shoreface: spilling, plunging, surging and collapsing. A non-dimensional number, Irribaren number, is used to determine the wave breaking type. It is defined as:

$$\boldsymbol{\xi}_0 = \frac{m}{\sqrt{H_0/L_0}} = \frac{\tan\propto}{\sqrt{H_0/L_0}} \tag{15}$$

Table 2 shows types of breaking according to Irribaren Number.

Table 2. Types of breaking (Source: Ergin, 2009)

Breaking Type	**Iribarren Number**
Spilling	ξ <0.5
Plunging	0.5 < ξ < 2.5
Collapsing	2.5 < ξ < 3.4
Surging	ξ < 3.4

The determination of the breaking wave characteristics in shallow water is very important and a difficult task for the engineering subjects. Therefore diagrams, for estimating the breaking water depth and the breaker height, have been compiled using extensive data obtained in the field and laboratory. One such diagram is presented in Figure 8.

Breaking types are shown in Figure 7.

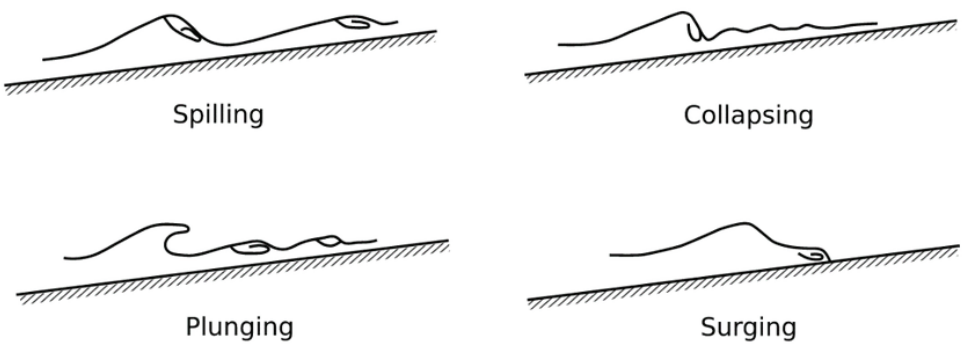

Figure 7. Breaking types (Source: https://www.researchgate.net/figure/Breaking-wave-types-FHWA-2008-The-type-of-wave-breaking-is-determined-by-the_fig)

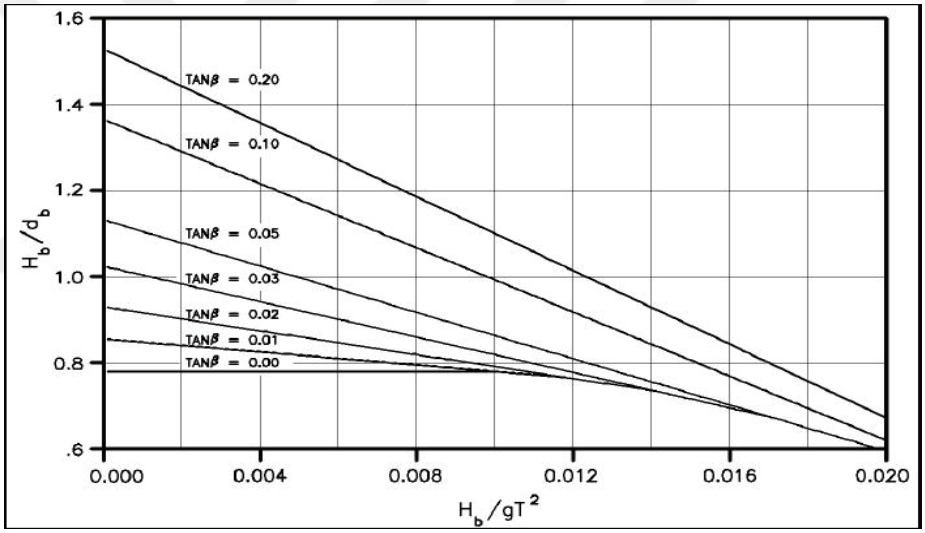

Figure 8. Breaker depth index as a function of (Hb/gT^2) (Source: http: // coastal engineeringmanual.tpub.com/Part-II-Chap4/Part-II-Chap407.htm)

2.4. Prediction of Wind Waves

Reliable information on wind waves is needed in various important coastal and sea activities. These include; design and execution of coastal and ocean development; coastal zone planning, design, construction, and management; harbor planning, design, construction, and management; coastal erosion control; fishery developments and fishing operations; tourism and recreation; protection of special coastal and marine

areas; wave forecasting; navigation; design and construction of sea vessels; wave energy development and so on (Ergin 2009).

The available wave prediction (either hindcasting or forecasting) methods may be classified into two classes. These are empirical and numerical methods. Empirical methods may be classified into two groups. Graphical and parametric which facilitates the computations of sea state parameters (significant wave height and period). The Sverdrup-Munk-Bretschneider (SMB) method is one of the most commonly used graphical methods. Energy Spectrum Methods, which assume a model for wave energy spectrum, and computes the values of spectral parameters for specific storm and then facilitate the computations of sea state parameters. Pierson-Moskowitz (PM) method is most commonly used in deep water (Alves, Banner, and Young 2003).

The numerical models compute the growth (or decay) and propagation of component waves (random wind waves). The concept of energy conservation is usually utilized in such models. Within these models, the physical process of wave generation, propagation, dissipation, and interaction are simulated to a certain practical degree of accuracy.

2.5. Numerical Models To Predict Wave Generation And Wave Transformation

The numerical wave models express the physical concepts of the phenomena. The performance of the numerical wave model depends on how best the phenomena are expressed into the numerical schemes, so that more accurate wave parameters could be estimated. The numerical wave models developed were based on the energy balance equation with various components of the source function as inputs.

The energy balance equation is given as,

$$\frac{dS(f,x,t,\theta)}{dT} = S = In + Nl + Dis \tag{16}$$

where; two-dimensional wave spectrum S (f, x, θ, t) is dependent on frequency f, propagation direction θ, and defined over the geographic coordinates x and time t. The left-hand side of Equation 22 is the full derivative of the spectrum with time and the

right-hand side is the source function S depending on both the wave spectrum and on the external wave-making factors such as local wind and local current.

It is generally used to distinguish three terms in the source function S, namely In = the mechanism of the energy exchange between the atmosphere and ocean waves, Nl= the energy conservative mechanism of nonlinear wave-wave interactions, and Dis = the dissipation, i.e., wave energy loss mechanism related to wave-breaking processes and interaction of waves with turbulence of the upper water layer.

Differences in the presentation of the above components of the source function determine general differences between various numerical wave models. Numerical wave models are mainly divided into three categories based on their mechanisms. They are the first, second, third-generation, wave models.

2.5.1. The First Generation Models

First-generation wave models developed in the 1960s and early 1970s avoided the problem of explicitly modeling the complete energy balance. Models are developed based on simple wind fields (In) and without dominating nonlinear interactions (Nl) and energy loss (Dis). Generation is simulated with simple empirical expressions, and dissipation (white capping) is simulated with an assumed universal upper limit of the spectral densities. In these models, it was assumed that the wave components suddenly stopped growing when they reached a universal saturation level. Thus, for growing wind seas, the prognostic region of the modeled spectrum was, in effect, limited to wave components in the neighborhood of the spectral peak. First-generation wave models exhibit basic quantitative shortcomings: they overestimated the wind input and underestimated the strength of the nonlinear transfer by almost order of magnitude (Hasselmann et al. 1988).

2.5.2. The Second Generation Models

In the 1970s, extensive JONSWAP wave growth experiments (Hasselmann et al. 1973) and direct measurements of the wind input to the waves (Snyder et al. 1981) fundamentally changed the view of the spectral energy balance on which the first-

generation models had been based, leading to the development of second-generation wave models.

The second-generation wave models are developed using varying wind fields and simplified nonlinear interactions. Here, the sea surface is defined as the sum of a large number of individual wave components, each wave propagating with constant frequency according to the linear wave theory. However, for these models also, restrictions resulting from the simplified nonlinear transfer parameterization effectively required the spectral shape of the wind sea spectrum to be prescribed for frequencies higher than the peak frequency. The specification of the spectral shape was introduced either at the outset in the formulation of the transport equation itself (parametrical or hybrid models) or as a side condition in the computation of the spectrum (discrete models). Although the adjustment to a quasi-universal spectral shape could be justified theoretically by two scaling arguments for typical synoptic-scale wind fields (Hasselmann et al. 1976), the second-generation models were unable to properly simulate complex wind seas generated by rapidly changing wind fields, for example, in hurricanes, intense, small-scale cyclones or fronts. The models also encountered basic difficulties in treating the transition between wind sea and swell.

2.5.3. The Third Generation Models

Although both the first and the second generation wave models can be tuned to provide useful results for certain classes of wind fields—and most models considered in the study had indeed proven their value in an operational framework—the study demonstrated that none of the existing wave models were applicable for all wind fields and that none were reliable for extreme situations for which wave forecasts are often most needed.

The third-generation wave models are developed for further improvement of the modeling process. These models use the energy balance equation for describing the time and space evolution of wave spectra. According to the first- and second-generation wave models, it was proposed that third-generation models should be developed, based on the techniques, in which the wave spectrum was computed alone by the integration of the basic spectral transport equation, without any prior restriction of the spectral shape (Mandal and Prabaharan 2010). To remove the restrictions on the spectral shape;

First, a parameterization of the exact nonlinear transfer source function is developed that contained the same number of degrees of freedom as the spectrum itself. For development, the Discrete Interaction approximation (DIA) of the quadruplet wave-wave interactions are formulated. Second, the energy balance is closed by specifying the unknown dissipation source function with the formulation of white capping by Komen et al. (1984).

The first implementation of a third-generation wave model is the WAM model of the Hasselmann et al. (1988). Other third-generation models are the WAVEWATCH model, the Program for Hindcasting of Waves in Deep, Intermediate and Shallow Water (PHIDIAS) model, the Telemac Based Operational Model Addressing Wave Action Computation (TOMAWAC) model, METU3 model and so on.

Waves at the surface of the deep ocean can be well predicted with third-generation wave models that are driven by predicted wind fields. These models cannot be realistically applied to coastal regions with horizontal scales less than 20–30 km and water depth less than 20–30 m (with estuaries, tidal inlets, barrier islands, tidal flats, channels, etc.), because (1) the shallow-water effects of depth-induced wave breaking and triad wave-wave interaction are not included and (2) the numerical techniques that are used are prohibitively expensive when applied to such small-scale, shallow-water regions. So that, for shallow water, the formulations for the deep-water processes need to be adapted and extended. This has been achieved, to some extent, in the above third-generation models with (1) the use of the shallow-water phase speed in the expressions of wind input, (2) a depth-dependent scaling of the quadruplet wave-wave interactions, (3) a reformulation of the white capping in terms of wavenumber rather than frequency, and (4) adding bottom dissipation. There is another 3rd generation model called SWAN (Simulating Wave Nearshore) was developed to capture the wave transformation effects. All those will be also used in the SWAN model and supplemented with formulations for (5) depth induced wave breaking and (6) triad wave-wave interactions that have been developed specifically for SWAN by Eldeberky and Battjes (1996) and Eldeberky (1996). Initially, the SWAN cycle 1 was formulated to be able to handle only stationary conditions on a rectangular grid. Later on, the SWAN cycle 2 model has been developed. This is considered as the second step in the development of SWAN models. Cycle 2 of SWAN is stationary and optionally nonstationary. It can compute the wave propagation not only on a regular rectangular grid but also on a curvilinear grid.

Literature survey on the predictions of third-generation numerical wave models

for both offshore and nearshore studies and results are explained below:

Booij, Ris, and Holthuijsen (1999) have been verified a third-generation spectral wave model (Simulating Waves Nearshore (SWAN)) in stationary mode with measurements for small-scale, coastal regions with shallow water, tidal flats, (barrier) island, local wind, and ambient currents in five real complex field case from the southern North Sea coast. The results of the SWAN computations and observed significant wave height, mean wave period, and mean wave direction are compared. In the computed significant wave height and mean wave period the average RMS error is 0.30 m and 0.7 s, respectively, which is 10% of the incident values for both. As a result, it is concluded that there is a need for more theoretical (e.g. regeneration of wave in case of low-frequency energy), modeling (e.g. atmospheric data for coastal regions), and real field (e.g. high-resolution depth data and tests) studies for the refinement of SWAN.

Ou et al. (2002) have been compared numerical calculations on the wave heights and periods during the transition of four representative typhoons, including Herb in 1996 (struck the northeastern coast of Taiwan and was classified as a super-strong typhoon), Amber in 1997 (originated from the northwest Pacific Ocean near the Philippines), Kent in 1995 (passed through the Bashi Straits in the southern coastal waters of Taiwan Island and landed on mainland China) and Zeb in 1998 (first generated in the ocean to the east of the Philippines that moved northwards), with the data measured from field wave stations on both the eastern and western coasts. The SWAN wave model is typically designed for wave simulations in the near-shore region and is therefore chosen to assess its applicability in the waves of typhoons in the coastal regions around Taiwan Island. To simulate the typhoon waves, the numerical far-field computational domain and the near-field nested computation domains (Hualien, Hsinchu, and Taishi at northern, Tungchi Tao at southern Taiwan) are used. For the far-field wave simulations the grid spacing is 12 km, time step of 15 min and for the coastal nested domains a grid size of 2 km and time step of 10 minutes, while in near-field nested domains, a grid size of 300 m and a time step of 5 minutes are adopted for numerical calculations. To derive the input cyclostrophic and gradient wind velocities, the modified Rankin vortex wind field model was adopted for the SWAN wave model computations. According to the results of comparisons of simulated waves and periods with measured data from wave stations on the east and west coastal waters it is seen that the model was delayed. In addition, the typhoon wave simulations were relatively well

matched to the measurements of both coastal waters of the island of Taiwan. However, for the eastern coastal waters better performance was achieved. It is considered that the central mountains of the island partially damage the cyclonic structures of typhoid that are partially passing through, caused the differences.

Van der Westhuysen, Zijlema, and Battjes (2007) investigates the effectiveness of a revised white capping source term in the spectral wind-wave model SWAN (Simulating Waves Nearshore) that is local in frequency space, nonlinear with respect to the variance density and weakly dependent on the wave age. This white capping expression is combined with an alternative wind input source term that is more accurate for young waves than the default expression. The shallow water source terms of bottom friction, depth-induced breaking and triad interaction are left unaltered. It is demonstrated that this alternative source term combination yields improved agreement with fetch- and depth-limited growth curves. Moreover, it is shown, by means of a field case over a shelf sea, that the investigated model corrects the erroneous over prediction of wind sea energy displayed by the default model under combined swell-sea conditions.

Rusu, Pilar, and Guedes Soares (2005) have been made a hindcast to approach the wave conditions for shallow water. The study area is the north of Portugal characterized by high traffic of ships, which includes coastal environment around the ports of Leixões, Viana do Castelo, Aveiro and Figueira da Foz. It was focused on a three-month period, between 1st of December 1993 and 28th February 1994 that was one of the most energetic periods on the Portuguese coast in the last 10 years. Additionally, the data obtained from four buoys are available for the focused time period to compare the simulation results. One of the buoys was located at a depth of 110 meters at the entrance of the port of Leixões and also the three other buoys were located in Figueira da Foz region at the depths of 93, 72 and 19.6 m, respectively, to the south of Leixões. For the simulations, WAM and SWAN models have been used. To gradually increase the resolution in the models, they were nested within themselves several times. A large SWAN area was nested into the WAM model to couple between the generation and the transformation models. The results obtained are acceptable in terms of significant wave heights, periods and are very good in terms of wave direction.

Moeini and Etemad-Shahidi (2009) have been studied with an aim of assessing the SWAN numerical model for white capping dissipation in a complex (the model of Hasselmann and Cumulative Steepness Method) and varying wind-wave climate by

comparing results with field measurements recorded in the year 2002 at Lake Erie. The data collected by three buoys at depth of 14.6 m, 22.0 m and 27.0 m, respectively. The significant wave height (Hs) and the peak wave period (Tp) were the parameters employed in the study and the BIAS parameter and scatter index methods were used for a quantitative inter-comparing of the results. The model was forced in a non-stationary mode (wind speed and direction in time and space), considering the linear and exponential growth from wind input, quadruplet wave-wave interaction, white-capping, and bottom friction. According to a result, it was seen that the model slightly overestimated significant wave height and underestimated the peak spectral period and the scatter indices were 19% and 23.15%, respectively which means that higher accuracy observed on significant wave height. Moreover, eliminate data with wave heights less than 0.5 meters reduced error about 3 percent for both parameters. And also using the cumulative steepness method for white-capping dissipation gives worse results for significant wave height and better results for peak spectral period estimation.

Akpinar et al. (2012) have been implemented and validated a wind-wave numerical model for the Black Sea to study the wave climate, perform extreme value analysis, and determine the wave energy potential in the region. SWAN model was selected and forced by the ERA-Interim dataset, which is the latest global atmospheric reanalysis produced by the ECMWF, reanalyzed u and v wind components at 10 m (six-hourly intervals). Wave data to verify the developed SWAN wind-wave model was obtained from three directional buoy stations located at Hopa, Sinop, and Gelendzhik. The 12-month wave dataset recorded in 1996 at Hopa and the 6-month datasets for the Sinop and Gelendzhik buoy stations. The bathymetry data were provided from the National Geophysical Data Center by the National Oceanic and Atmospheric Administration (NOAA) with the spatial resolution 0.0167° x 0.0167°. The SWAN model results were compared with these directional buoy measurements, parametric model results based on the JONSWAP growth relations, and the results of previous studies METU3 model for only a 1-month period and the WAM Cycle 4 model (Cherneva et al. 2008). For the simulation of the SWAN model, the linear and exponential growth from wind input, depth-induced wave breaking, bottom friction, white capping, four-wave (for deep-water) and triad-wave (for shallow water) nonlinear interactions have been activated and it was run non-stationary mode with spherical coordinates. The consequences of the SWAN model demonstrate that there is a good match between simulated and measured wave parameters (the peaks and troughs of the

temporal variations of significant wave height, average wave period and mean wave direction). However, it has less accurate estimates for the maximum values of both parameters. It is considered that; this underestimation of the peaks is probably due to temporal-spatial resolutions and low wind speeds fields caused by orographic effects in the ECMWF wind fields. Moreover, the accuracy of the SWAN model for all wave parameters is far better than that of the JONSWAP method and it is slightly more accurate than the results of the previous studies.

Siadatmousavi, Jose, and Stone (2012), were used two well-known third-generation wave models, SWAN and WAVEWATCH-III, with different assumptions for the high cut-off frequency to evaluate the interaction of low and high-frequency components in wave spectral evolution. For this a parallel implementation of unstructured SWAN and WAVEWATCH-III was used to simulating the waves in the Gulf of Mexico.To prepare the wind field, the velocity components were extracted from the North American Regional Re-analyzed (NARR) database from the National Center for Environmental Prediction (NCEP/NOAA) server. The data were combined with high-resolution H* wind data obtained from the Atlantic Oceanographic and Meteorological Laboratory (AOML/ NOAA) database to have a better spatial and temporal resolution as well as for avoiding underestimation during storms. For evaluating simulation results NDBC buoy data were used. The results showed that WAM cycle 3 formulation overestimates the energy content in the frequency band of 0.5–1 Hz for the Gulf of Mexico, which suggests using cut-off frequency close to 0.5 Hz rather than 1 Hz would improve the simulated bulk wave parameters. The evaluation of WAM cycle 4 and a newer nonlinear formulation implemented recently for white capping in SWAN showed a better performance of the wave model in oceanic scale.

Inghilesi et al. (2012) were implemented a coastal forecasting system to provide wind-wave forecasts over the whole Mediterranean Sea area, and with the added capability to focus on selected coastal areas. To analyze the large-scale, deep-sea propagation of waves the WAve Model (WAM) and to simulate waves in key coastal areas SWAN was used. The effect of the small-scale coastal processes on the propagation of waves towards the coasts was studied. The system was tested in three Italian coastal regions in order to optimize the numerical parameters. In shallow water, the coastal model gave better results than the regional model, mostly due to a more accurate representation of the bathymetry. It was observed that wind input-whitecapping performed well infinite and shallow water depth.

Valchev, Trifonova, and Andreeva (2012) have studied to assess trends in past and recent storminess in the western Black Sea. The analysis of storm climate is based on a continuous hindcast dataset covering a substantial historical time-span of 63 yr. (1948–2010). Eleven storminess proxies were analyzed and the most indicative appeared to be storm duration; integral, mean and specific storm wave energy; and wind velocity and direction, which were obtained for each storm season. The global sea level pressure reanalysis carried out by the European Centre for Medium-range Weather Forecast and complemented by the NCEP/NCAR was used in order to calculate the historical wind forcing for wave models. Wave conditions were modeled using a coupled system of third-generation spectral wave models. The WAM model was run on a regular spherical grid, covering the entire Black Sea basin and deep-water settings were applied with a source. SWAN was set up for wave simulations in the western shelf zone. Results showed a shortening of the average duration of storms.

Rusu, Bernardino, and Soares (2014) have been studied for better understanding of the wind and wave conditions in the vicinity of the major ports and shipping routes of the Black Sea, by considering multiple datasets, to highlight the spatial and temporal variability of the wind and wave climate as resulting from the analysis of various datasets and to perform a comparative analysis of the datasets along the main shipping routes. Hence, the results are analyzed for the sites located close to the main harbors and also along the major trading routes. The reanalysis data provided by NCEP-CFSR (U.S. National Centers for Environmental Prediction-Climate Forecast System Reanalysis) and the hindcast results given by a Regional Climate Model (RCM) that were retrieved from EURO-CORDEX (European Domain-Coordinated Regional Climate Downscaling Experiment) are the two different datasets to evaluate the wind condition. SWAN model forced with the data sets above and the results are considered for the waves. The results show the best correlation between the two datasets for both wind and waves at the offshore sites. Moreover, except for the points located in the southern part of the Black Sea, there is a good agreement between the average values of the wind data that are provided by the different datasets for near-shore sites and also for the extreme values. Finally, it can be concluded that the results obtained in this study are useful for the evaluation of the wind and wave climate in the Black Sea. Also, they give a more comprehensive picture of how well the wind field provided by the Regional Climate Model, and the wave model forced with this wind, can represent the features of a complex marine environment as the Black Sea is.

Umesh et al. (2017) have been made an application of numerical ocean wave prediction, the validation of ocean waves spectra for the east coast of India. ECMWF ERA-Interim winds and QuikSCAT-NCEP blended winds are forced by using the SWAN model and their impact on results and also their impact in predicting extreme wave events were studied. The study signifies a good correlation between model wave spectra and in-situ observations. The blended winds are more suitable in comparison with the ECMWF ERA-Interim winds for modeling both normal and extreme events in the coastal Puducherry location.

Mahmoudof et al. (2018) have been studied to evaluate the validity and performance of the formulations for depth-induced wave breaking and its corresponding dissipation term in the wave action balance equation. Simulating WAves Nearshore (SWAN) model was forced in predicting significant wave height and spectral peak energy content for swell waves in very shallow water at Southern Coast of Caspian Sea with different configurations for breaking term introduced by Battjes and Janssen (1979), hereafter referred to as BJ78, Nelson (1987) (NEL87), Ruessink et al. (2003) (RUE03), Thornton and Guza (1983) (TG83), Salmon et al. (2015) (BKD). The model results were compared with field measurements at five nearshore stations, located in the west of Nowshahr Port. According to results of some breaker index formulations were successful for significant wave height prediction in surf zones and the formulation by Ruessink et al. (2003) represented the most accurate results. However, it was observed an overestimation in predicting the spectral peak energy content and an incorrect shape of the energy spectrum specifically in very shallow stations. All of the embedded depth-induced wave breaking formulations in SWAN were applied, leading to the conclusion with an averaged relative error of 30% as the most successful in predicting near spectral peak energy content. It is considered that this inconsistency can be interpreted as the current SWAN version (41.01) not being able to transfer energy content from peak frequency to lower and higher frequencies in case of wave breaking. Finally, it was concluded that decreasing the breaker index with shoreward depth reduction was the most accurate option in the study area and two separated breaker index formulations were a need to predict the significant wave height and spectral peak energy. Therefore, the Ruessink et al. (2003) formulation was modified.

As a result literature study shows that SWAN has many advantages like modeling in stationary and non-stationary modes, including triad and quadruplet non-linear wave interactions and it is user –friendly and widely used all around the world.

CHAPTER 3

RESEARCH METHODOLOGY: DATA

3.1. Project Site and In-situ Measurement Data

In this study, Filyos coasts in the Western Black Sea region of Turkey was chosen to make nearshore wave modeling. Because one of the limited numbers of nearshore wave measurement campaigns in the Southern Black Sea was carried out in Filyos. It was carried by the Turkish Ministry of Transport, Maritime Affairs and Communications, General Directorate of Infrastructure Investments which is responsible for the design and construction of ports and harbors in Turkey. The measurement was necessary to design a new and one of the biggest ports in Filyos. With the help of the new Filyos Port project, the cargo handling capacity of the region will increase considerably. A self-recording pressure type instrument demonstrated in Figure9 was used to conduct the wave measurements. The instrument was mounted with the help of a case shown in Figure 9 on the 1.0m high concrete base placed on the seabed.

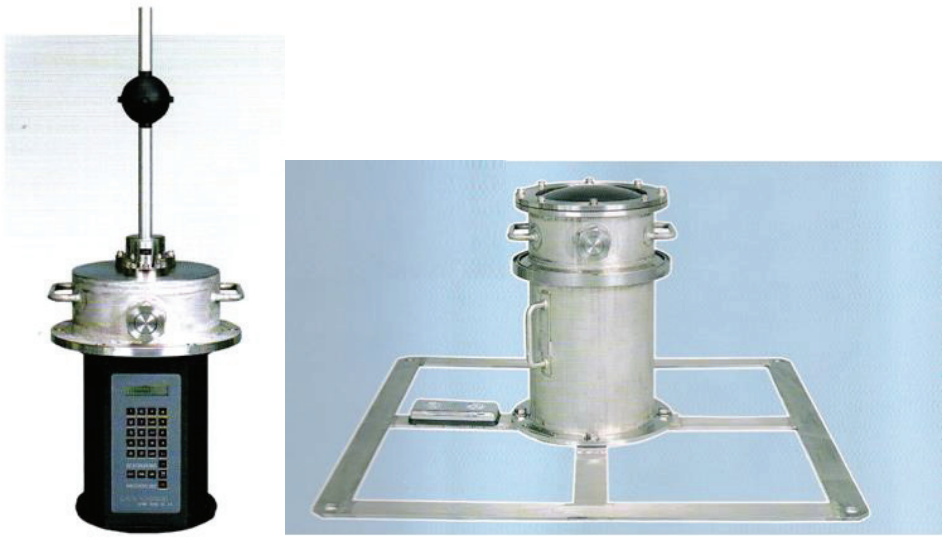

Figure 9. The self-recording pressure type instrument and its case (Source: Bilyay, Ozbahceci, and Yalciner 2011)

The gauge is located at 41 degrees 35 minutes North, 32 degrees 04 minutes East coordinates. Considering the breakwater construction depth and the steep bottom slope in front of the project area, the measurement depth was determined as 12.5 m. The location of the Filyos region, study area, and the measurement point are given in Figure10.

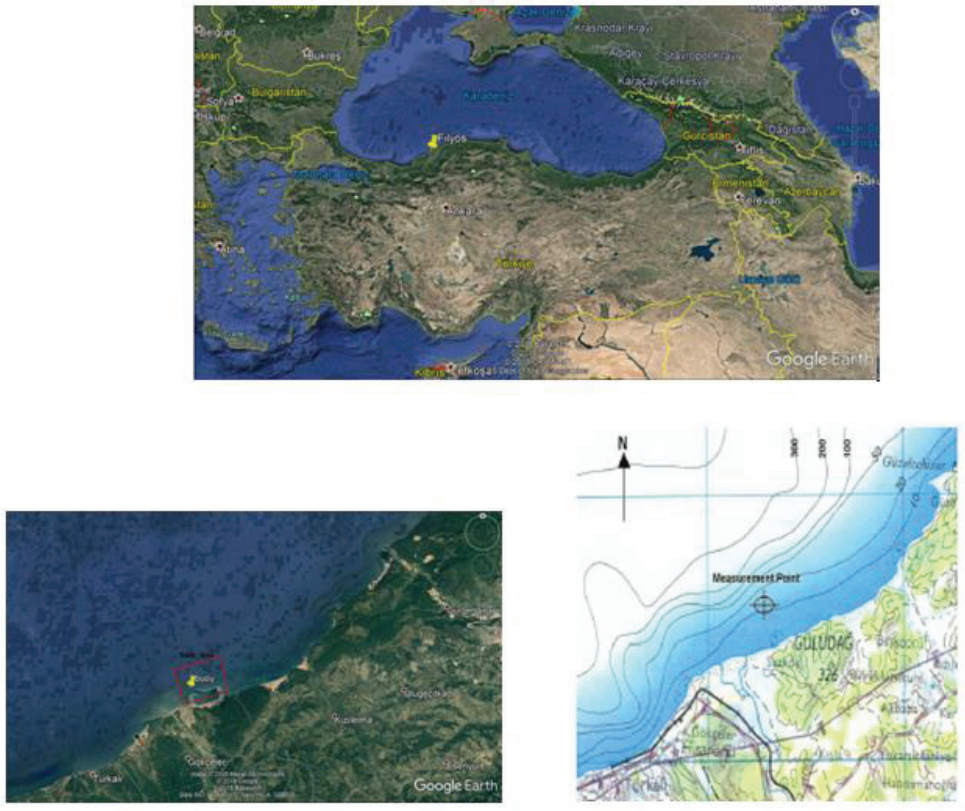

Figure 10. Project site and location of gauge

Wave data were sampled every two hours with a sample length of 20 min and a sampling frequency of 2 Hz. The wave measurement project at Filyos lasted for a period of two years, 1994–1996. During this measurement period, 7949 records could be obtained on account of the losses during battery and memory cassette changes. Surface elevation records are obtained from subsurface pressure records by using the following formula according to linear wave theory:

$$\eta = \frac{N(P+\gamma)}{\gamma K_p} \tag{17}$$

where; P is the pressure, γ=unit weight of seawater, N is the correction factor.

$$Kp = \frac{Cosh(k(z+d))}{Cosh(kd)} \tag{18}$$

Directional information of both waves and currents was determined by means of a two-axis electromagnetic current meter which yielded current velocity components in two Cartesian coordinates. Nagata's method was used to calculate the mean wave propagation angle for the record. Wave and current roses and the number of occurrences of the significant wave height H_s and the mean wave period T_m for all the records are given in Bilyay, Ozbahceci, and Yalciner (2011). They concluded that almost half of the records have a significant wave height H_s less than 0.5m and the mean wave period T_m is mostly between 5 sec. and 7 sec.

Significant wave height H_s and the mean wave period T_m recorded by the pressure gauge for two years (December 1994-1996) are given in Figures 11 and 12.

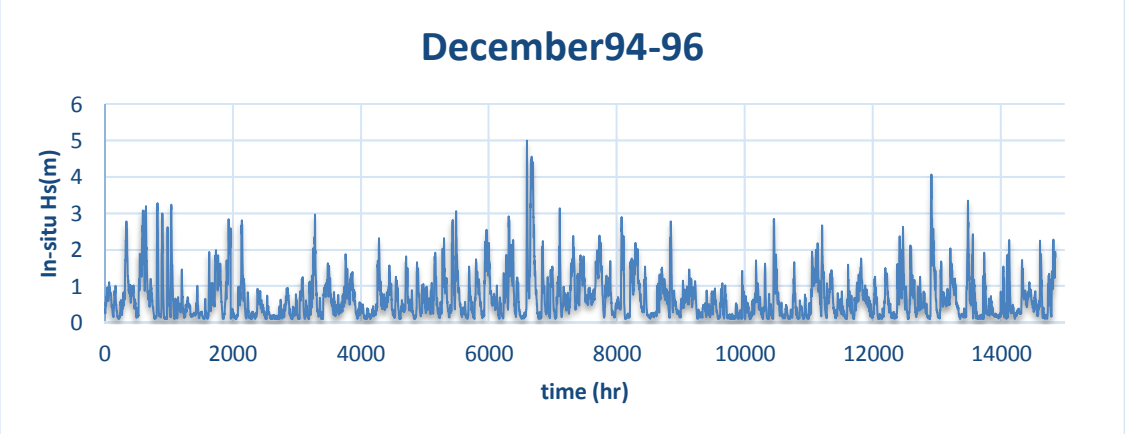

Figure 11. Significant wave height record in Filyos for two years (december 1994-december 1996)

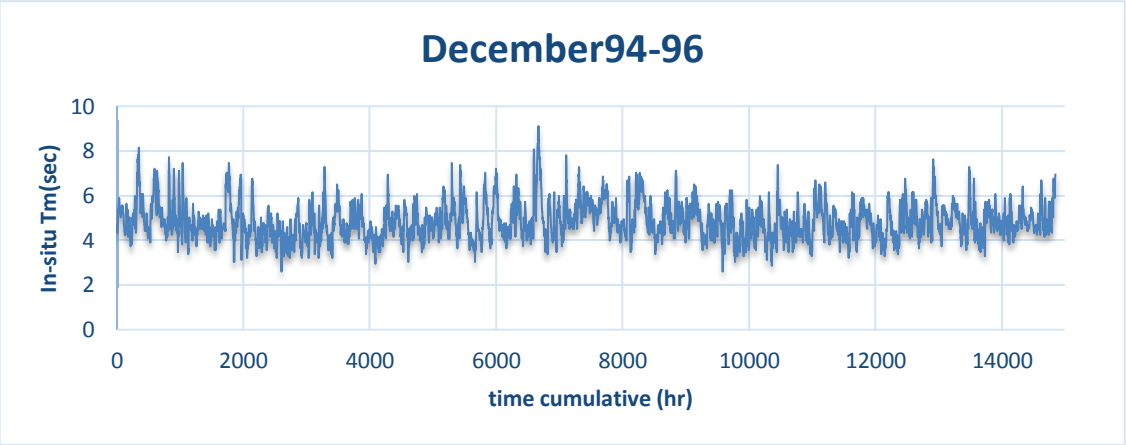

Figure 12. Mean wave period record in Filyos for two years (december 1994-december 1996)

Figure 11 shows that the maximum Hs is equal to 5m. The longest Tm is 9 sec as can be seen in Figure12. Mean wave direction distribution is presented as a wave rose given in Figure 13.

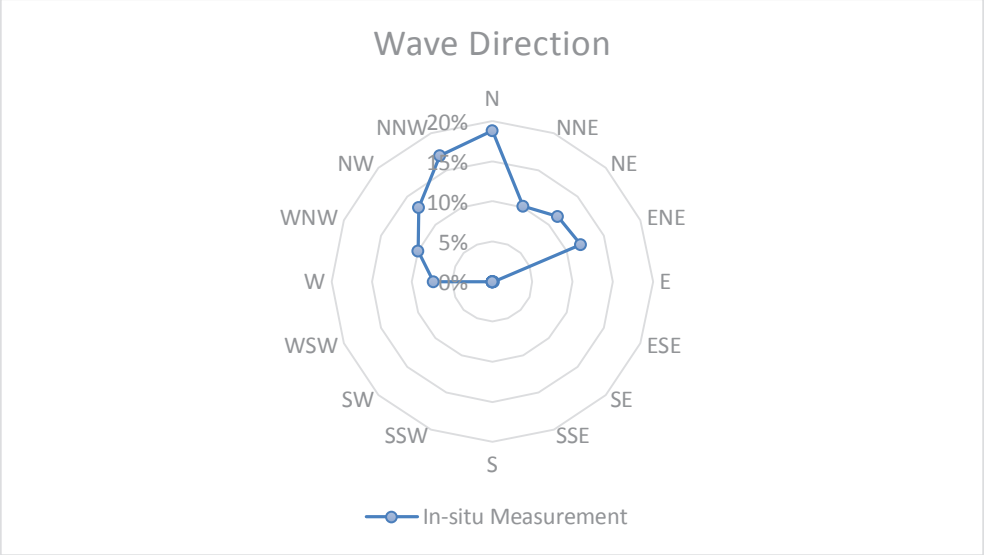

Figure 13. Wave rose diagram for wave direction as a percentage

As is seen in Figure 13, most of the waves come from the north to west directions.

3.2. Bathymetry Data

The numerical model requires bathymetry data. In this study, actual measurement bathymetry data are obtained through personal communication with the design company of the project. Bathymetry data are important for the accuracy of the model estimation result. Therefore, the finer the resolution of the bathymetry data, the more successful the model results will be. The raw bathymetry file of the model area is in XYZ format as a text file. The file was converted to a regular bathymetry grid file for the Swan model to read the data. For that conversion, raw bathymetry was first opened in a program called Blue Keneu and triangulated. Then the starting point (grid in the lower-left corner), the number of nodes in X and Y directions, the angle of the field with the horizontal is entered and prepared for the first use. When defining a regular grid, it was desirable to prepare high-resolution bathymetry data, so the distance between the grids was taken as 10 meters. Finally, raw bathymetry was interpolated from a regular grid. To interpolate, the triangulated file was drag into the defined regular grid file and computed. Thus, missing data points are assigned by interpolation. The resulting bathymetry file was saved in '2D Rect Scalar (ASC2 Single Frame) (*. R2s)' format. Raw bathymetry in XYZ format is shown in Figure 14. In the Blue Keneu program, raw bathymetry, triangulated bathymetry, and regular gridded bathymetry files are shown in the Figures 15-16-17.

The regular gridded bathymetry file, which has been prepared, has been imported into the AutoCAD program to better view the model working area, the position of the port in the model working area, and the position of the pressure type gauge used to record the wave data in regular gridded bathymetry. It is shown in Figures 18-19. The model workspace is 3100 m in horizontal and 2490 m in vertical.

3.3. Wave Data

In the modeling study for the Filyos region, wave data were used as the boundary input and are undoubtedly the most important input for the study.

X	Y	Z
423379.716	4609141.527	-160
423406.017	4609058.672	-145
423026.834	4608931.096	-145
423379.851	4609130.327	-155
422329.1353	4608672.7797	-140
422496.6406	4608742.3858	-140
422975.2911	4608835.3288	-140
423541.4135	4608944.8110	-140
423534.2256	4608986.0911	-145
422313.9155	4608734.8205	-150
422164.0588	4608494.3448	-60
422172.0510	4608568.0182	-90
422234.5413	4608579.0310	-120
423578.5271	4608830.9846	-110
422986.8532	4608695.2654	-110
422385.2349	4608538.0296	-110
422372.8156	4608580.7960	-120
422949.8769	4608759.6571	-120
423565.1495	4608882.5457	-120
423378.7005	4608505.4408	-25
423650.4337	4608587.0909	-25
423621.5769	4608683.1498	-50
423595.1249	4608769.6026	-100
420469.440	4608072.908	-320
421926.0385	4607445.2345	-20
421917.4027	4607536.6461	-20
422049.7549	4607733.5332	-20
422156.4152	4607893.6399	-20
422379.2314	4608102.3117	-20

Figure 14. Raw bathymetry in XYZ format

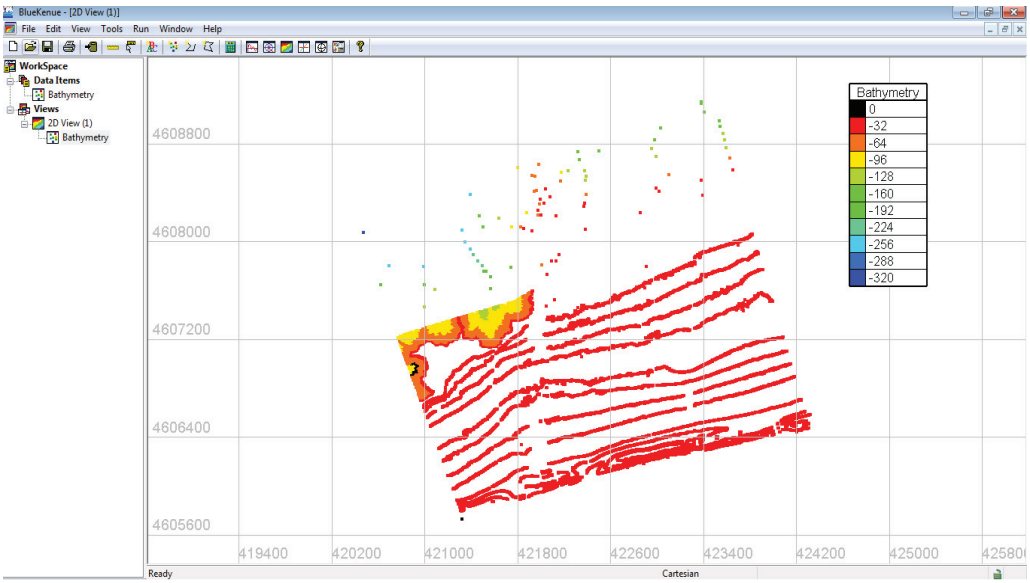

Figure 15. Raw bathymetry data in Blue Kenue

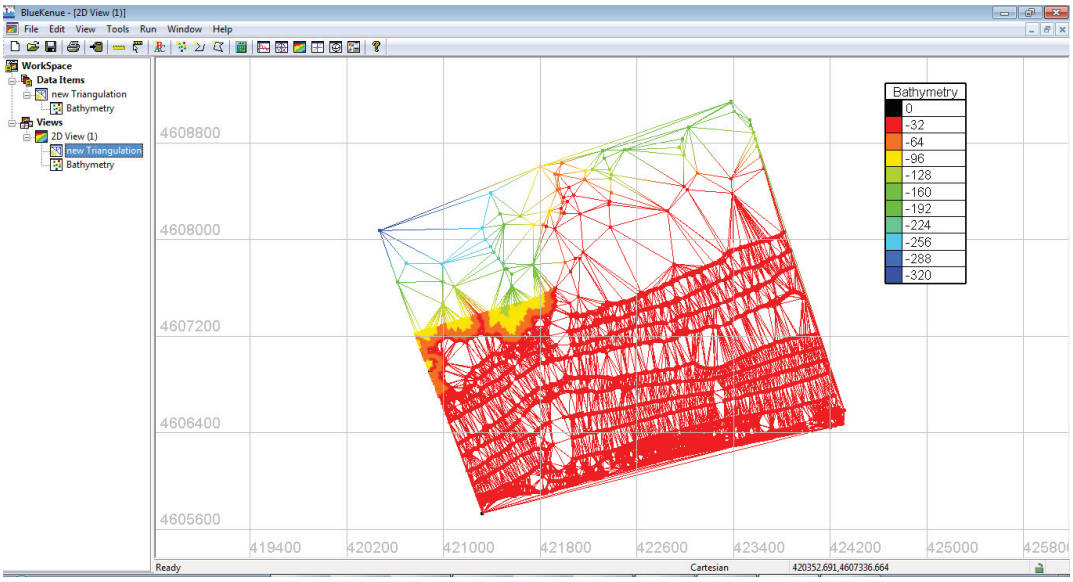

Figure 16. Triangulated bathymetry data

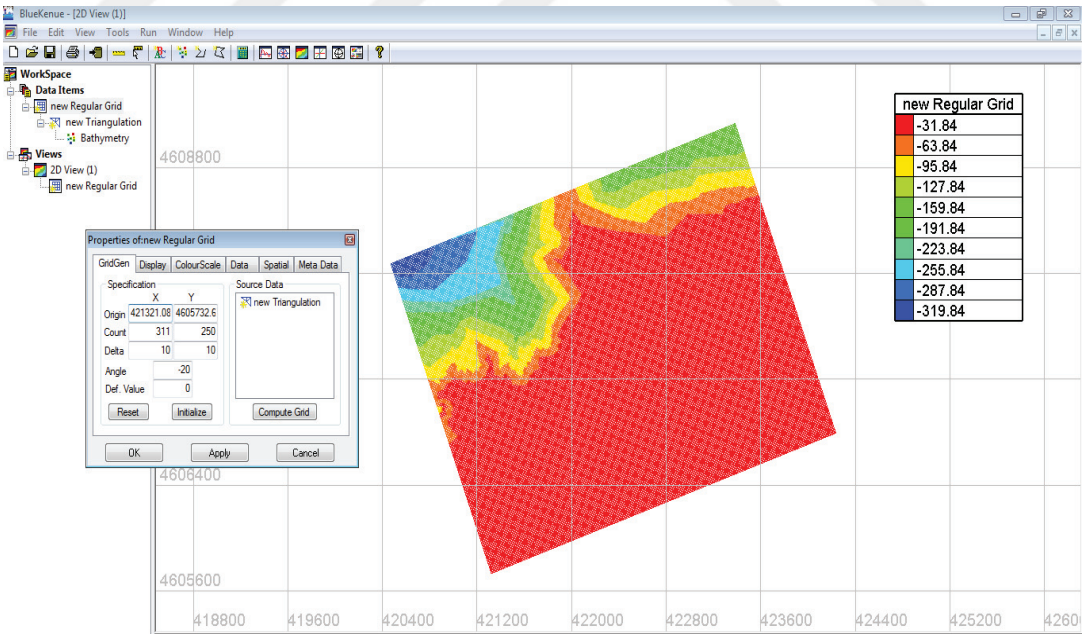

Figure 17. Regular grid bathymetry

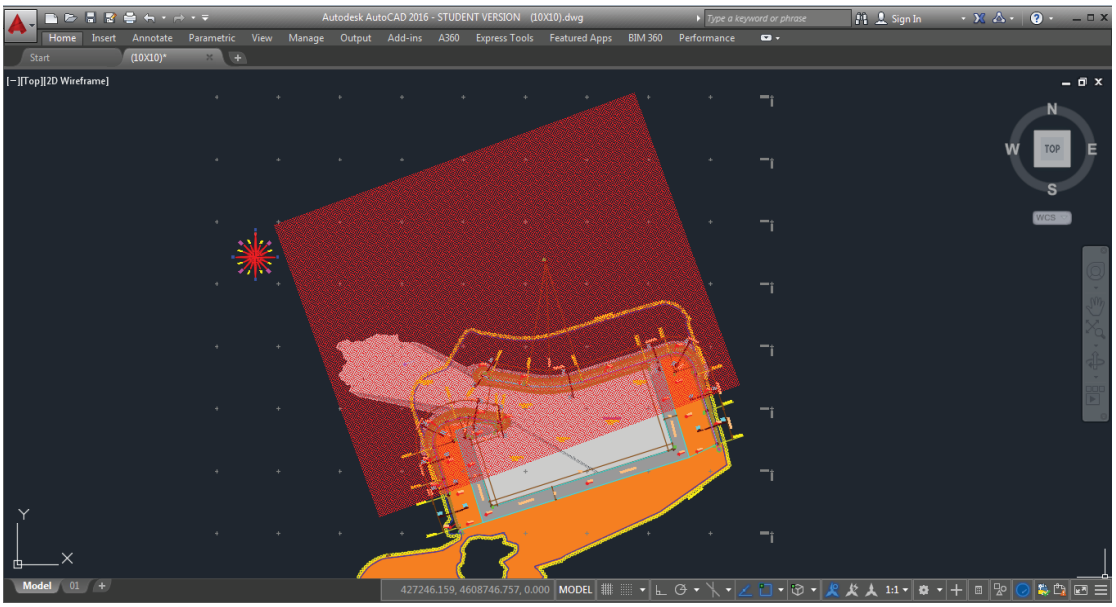

Figure 18. Model study area with a regular grid and Filyos port

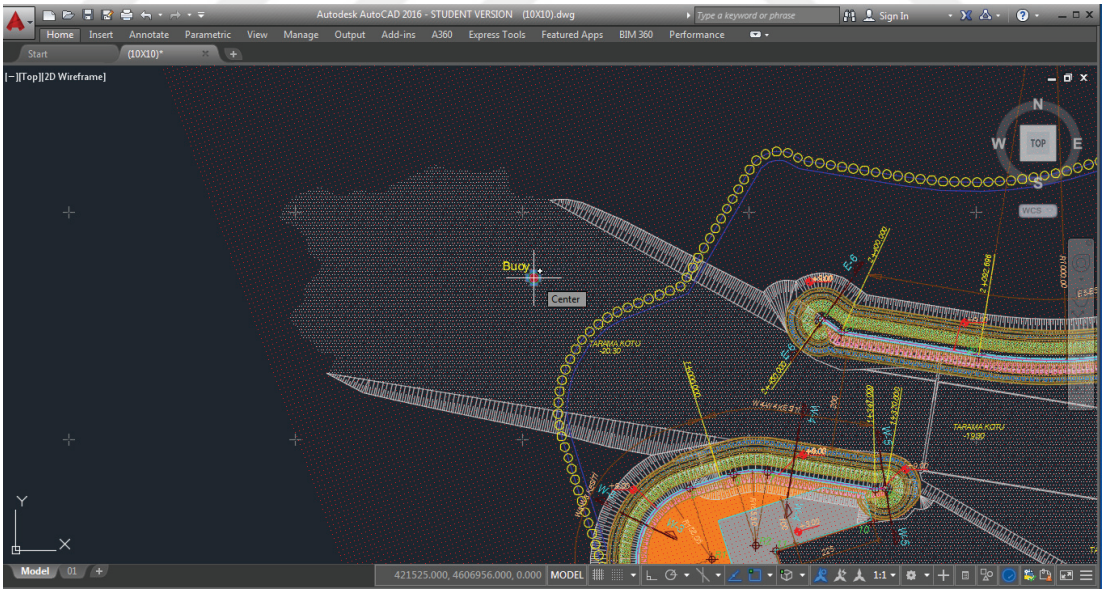

Figure 19. Location of the pressure gauge on regular gridded bathymetry

Various meteorological agencies in the world produce the models to forecast and the hind-cast the wave data. It is possible to obtain wave data from various meteorological agencies with historical re-analysis data sets and future operational forecasts. One of these agencies is the European Center for Medium-Range Forecast (ECMWF). In the study, ERA5 was chosen as the most recent data set from ECMWF reanalysis data sets (e.g. ERA-interim, Cera20C) and covering the period 1979 to present. Era 5 is recognized as an ERA-Interim Reanalysis system and ERA5 is being developed through the Copernicus Climate Change Service (C3S). It offers the chance to make hourly forecasts from the terrain surface to the movements of the atmosphere, to the ocean waves. Data processing for ERA5 is carried out by ECMWF. The steps for downloading data are shown in Figure 20.

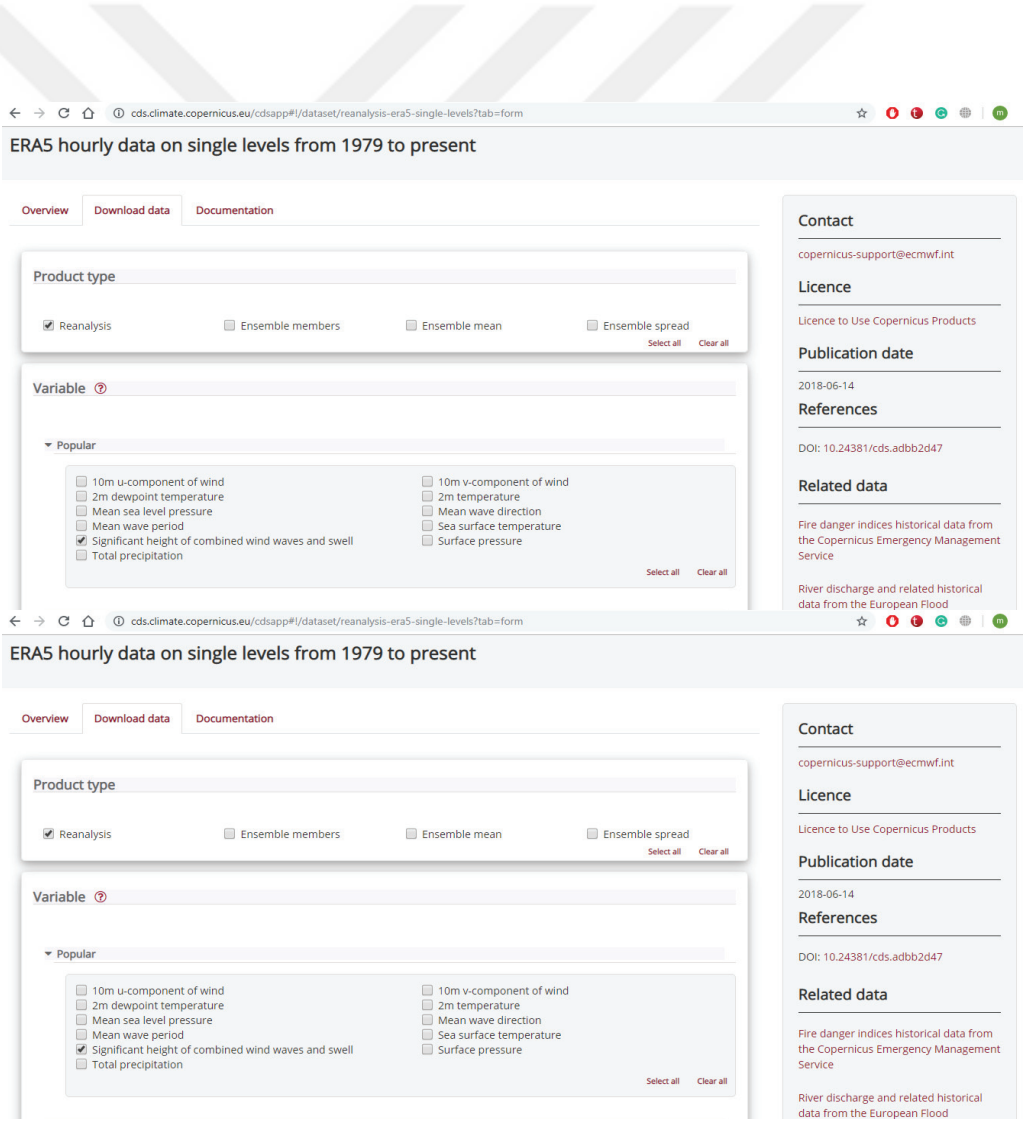

Figure 20. (Cont. on next page)

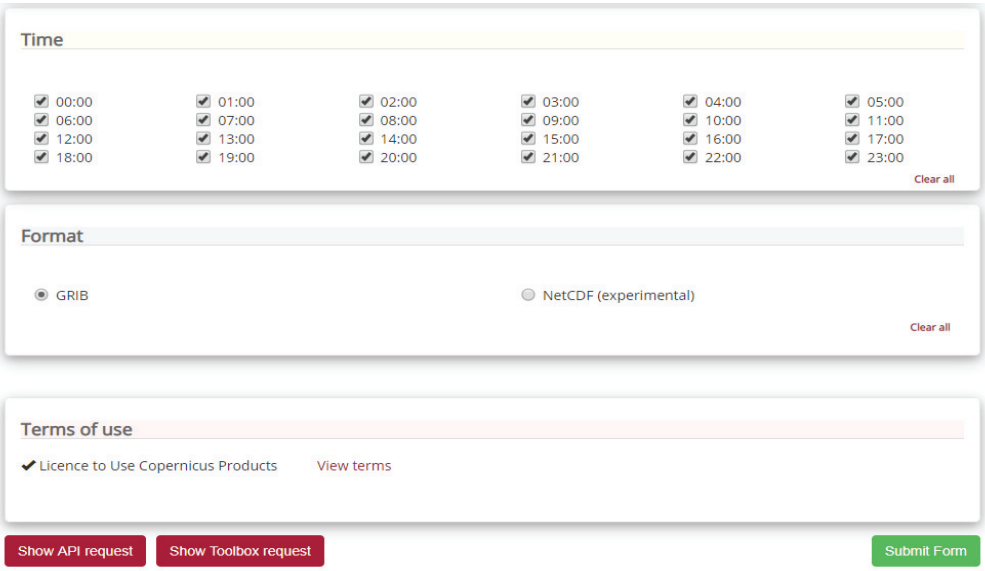

Figure 20. C3s public datasets web interface (Cont.)

Era5 significant wave height (Hs), mean wave period (Tm) and mean wave direction (θm) data were downloaded as GRIB file format in default mode for all over the world because it is not possible to download the data at the desired coordinate, as shown in Figure 20. Since GRIB files cannot be read directly by the SWAN model, all GRIB files are converted to the desired format by SWAN using software called Panoply. Then, the data at the coordinate 42.0, 32.0, which are the closest point to the model study area, were retrieved from the whole data set using a MATLAB script for each time step. Era5 re-analysis data as a graph and position of the desired data are shown in the Figures 21-22-23-24.

3.3.1. Calibration of ERA5 Wave Data

Before downloaded ERA5 wave data for two years are used as input data in the SWAN model, they were compared with in-situ measurement data to determine whether the data should be calibrated or not. The comparison study was carried out for significant wave height, Hs, the mean period, Tm parameters. The comparison is performed by scatter plots to see the agreement between the ERA5 and the in-situ data.

Figure 21. Coordinate of the downloaded ERA5

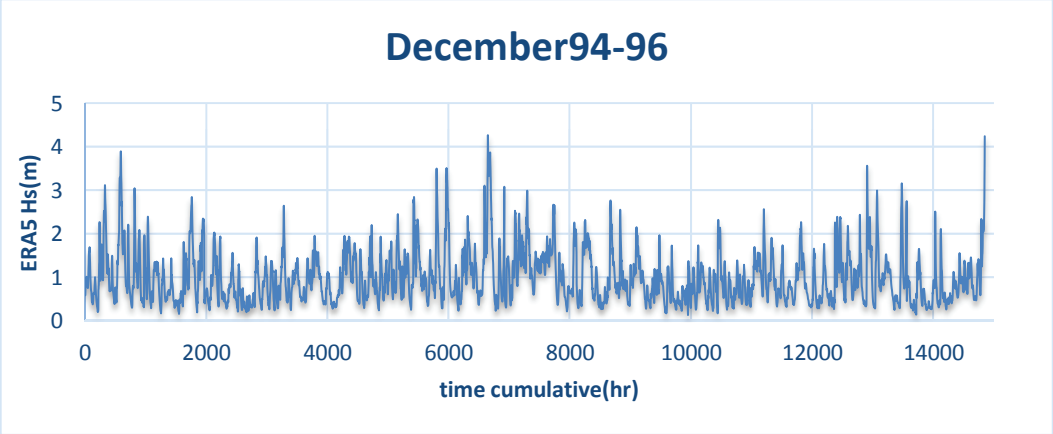

Figure 22. Significant wave height of ERA5

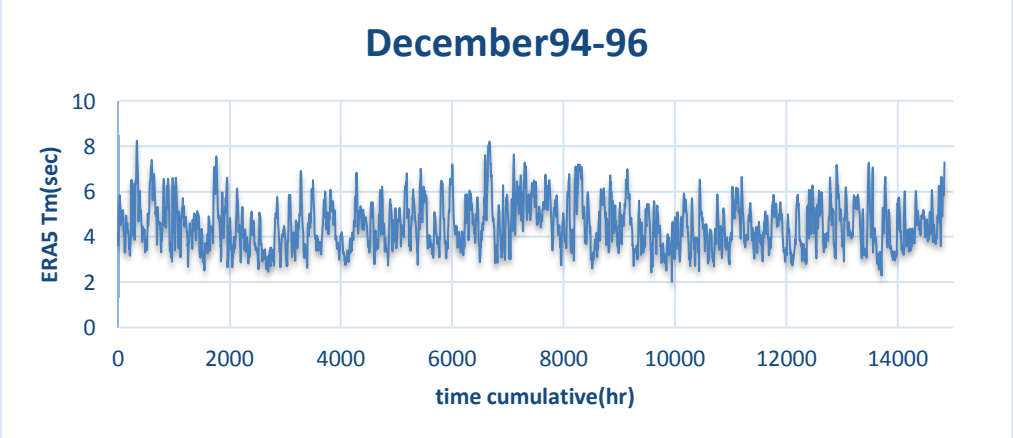

Figure 23. Mean wave period of ERA5

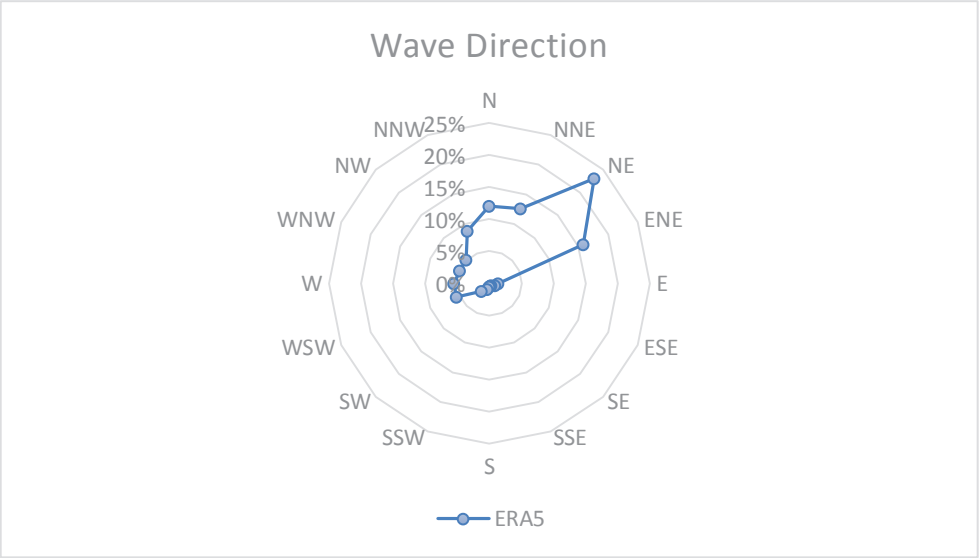

Figure 24. Wave rose diagram, mean wave direction of ERA5

Scatter plots of in-situ data of Hs and Tm in Filyos versus ERA5 Hs and Tm data together with the line y = x are shown in Figures 25-26.

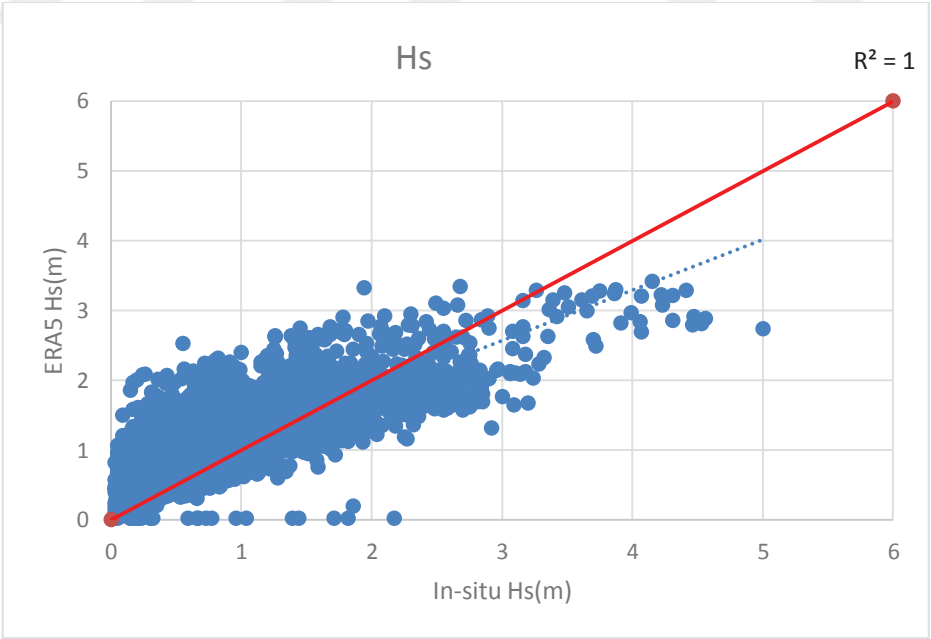

Figure 25. ERA5 Hs vs. in-situ Hs

As it is seen in Figure 25, higher waves are underestimated by ERA5 data even the smaller waves are higher than the in-situ Hs. Since ERA5 wave data is deep water

data it is expected that Hs estimates of ERA5 should be higher than the in-situ data recorded in 12.5 m due to wave transformation. Therefore, it is considered that Era5 significant wave height data should be calibrated before use them in the model.

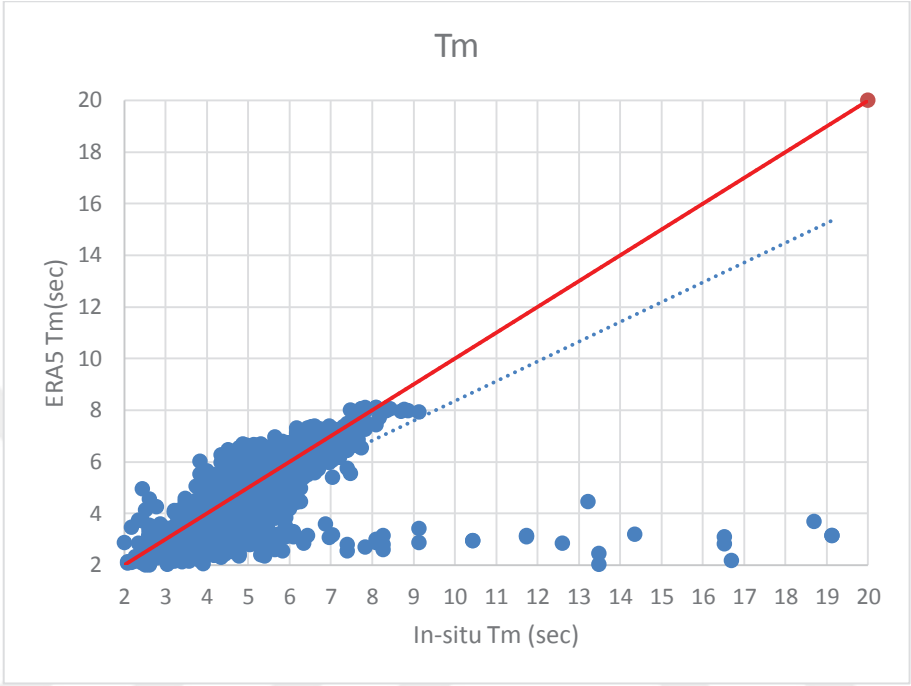

Figure 26. ERA5 Tm vs. in-situ Tm

As can be seen in Figure 26, ERA5 Tm data have much better agreement with the in-situ Tm data compared to the agreement in the Hs of ERA5 and the in-situ data. Therefore, it may not be necessary to calibrate. In addition, there are some in-situ data with longer wave periods and smaller wave height (Hs<0.1m). Those are swell data that are out of the scope of this study. In order to eliminate swell waves, it was decided to filter the data with a wave height of less than 0.1 m. The scatter plot for the filtered data is plotted and shown in Figures 27-28.

The comparison study shows that Era5 significant wave height data should be calibrated before using them in the numerical model. For calibration, it is decided to use the satellite data. Satellite data are reliable data (Abdalla and Yilmaz 2015) and can be used for the calibration. Radar Altimeter (RA), Synthetic Aperture Radar (SAR) and Scatter meter are used to provide wave height and sea surface wind speed data. The satellite RA data used for calibration were obtained from Turgut (2019). The RA data

were downloaded from the RADS (Radar Altimeter Database System) developed by Delft University of Technology. The data obtained were checked and filtered for extremely large and small data that caused irregularity and error. Details can be found in Turgut (2019).

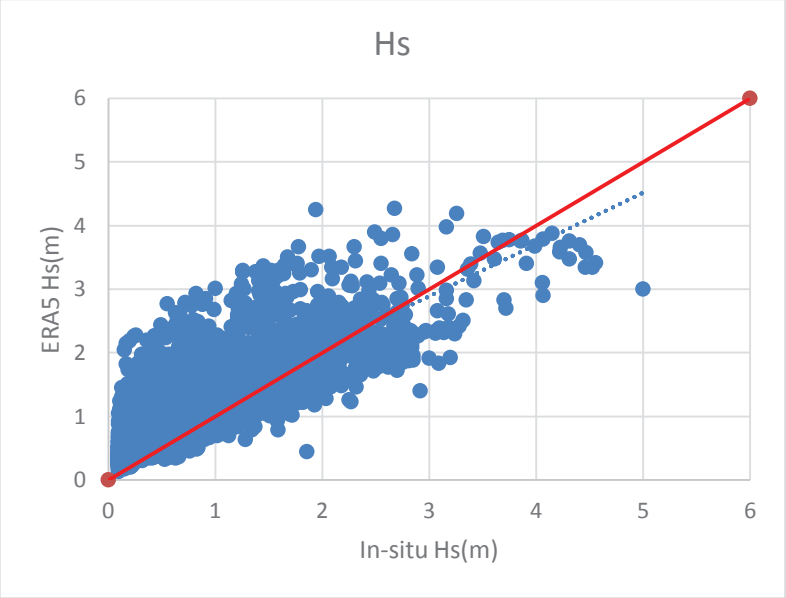

Figure 27. Filtered ERA5 Hs vs in-situ Hs

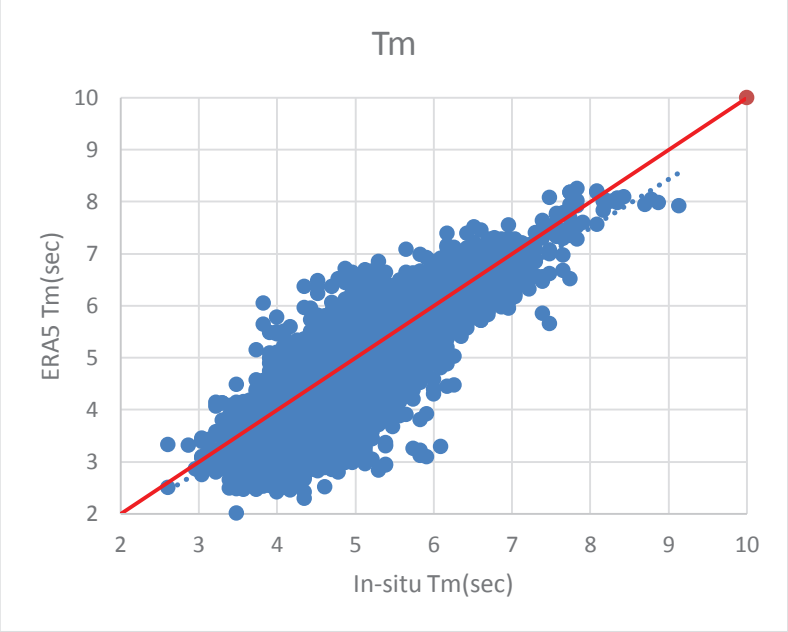

Figure 28. Filtered ERA5 Tm vs in-situ Tm

A comparison between Hs of the satellite RA data and ERA5 data is shown in Figure 29.

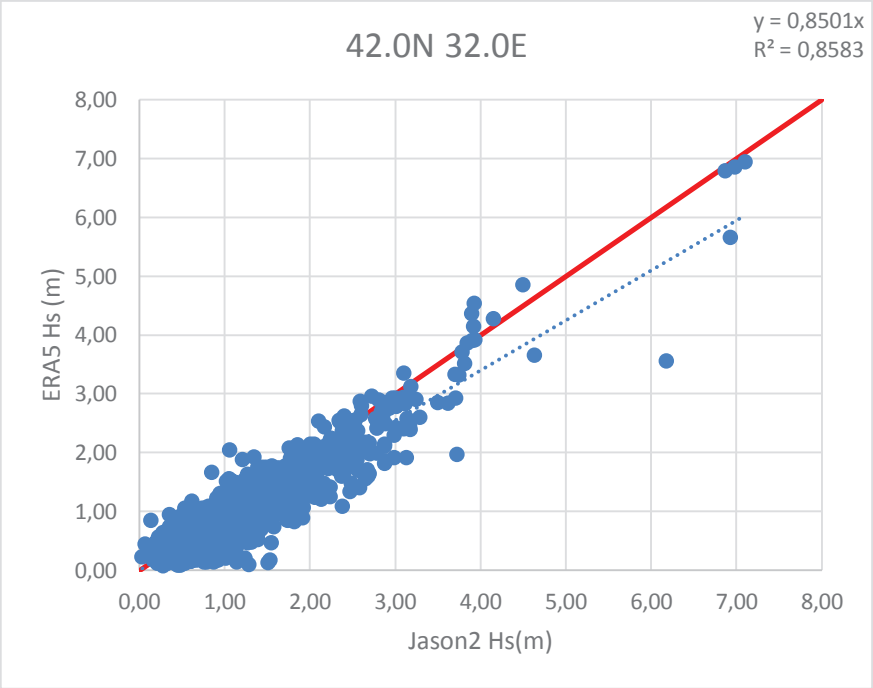

Figure 29. Comparison for Hs bw. ERA5 and Jason2 satellite RA data

In the Figure it is seen that the satellite data are larger than Era5 data. The regression coefficient, A (y=Ax) was calculated as 0.85. Therefore, ERA5 data were calibrated by dividing it to 0.85.

CHAPTER 4

NUMERICAL MODELING BY SWAN

4.1. Swan Model General Formulation

Over the past two decades, a number of advanced spectral wind-wave models, known as third-generation models, has been developed such as WAM (Hasselmann et al. 1988), WAVEWATCH III (Tolman, 1991), TOMAWAC (Benoit, Marcos, and Becq 1996) and SWAN (Booij, Ris, and Holthuijsen 1999). These models solve the spectral action balance equation without any a priori restrictions on the spectrum for the evolution of wave growth. This equation with sources and sink represents the effects of spatial propagation, refraction, shoaling, generation, dissipation, and nonlinear wave-wave interactions. SWAN (an acronym for Simulating WAves Nearshore) is an extension of the deep-water third-generation wave models. It incorporates state-of-the-art formulations for the deep-water processes of wave generation, dissipation and the quadruplet wave-wave interactions and also formulations for dissipation due to bottom friction, triad wave-wave interactions, and depth induced breaking in shallow water.

4.1.1. Spectral Balance Equation

All information about the sea surface is contained in the wave variance spectrum or energy density E (σ, θ), distributing wave energy over (radian) frequencies σ (as observed in a frame of reference moving with current velocity) and propagation directions θ (the direction normal to the wave crest of each spectral component). Usually, wave models determine the evolution of the action density N ($\vec{x}$, t, σ, θ) in space $\vec{x}$ and time t. The action density is defined as $N = E/\sigma$ and is conserved during propagation in the presence of ambient current, whereas energy density E is not. The evolution of the wave spectrum is described by the spectral action balance equation,

which, for Cartesian coordinates, is (e.g., Hasselmann et al. 1973).

$$\frac{\partial}{\partial t}N + \frac{\partial}{\partial x}c_x N + \frac{\partial}{\partial y}c_y N + \frac{\partial}{\partial \sigma}c_\sigma N + \frac{\partial}{\partial \theta}c_\theta N = \frac{S}{\sigma} \quad (19)$$

The first term on the left-hand side of (1) represents the local rate of change of action density in time, the second and third term represent the propagation of action in geographical space (with propagation velocities c_x and c_y in x and y space, respectively). The fourth term represents the shifting of the relative frequency due to variations in depths and currents (with propagation velocity c_σ in σ space). The fifth term represents depth-induced and current-induced refraction (with propagation velocity c_θ in θ space). The term S [=S(σ,θ)] at the right-hand side of the action balance equation is the source/sink term in terms of energy density, representing the effects of generation, dissipation, and nonlinear wave-wave interactions.

4.1.2. Sources and Sink

In shallow water, six processes contribute to S_{tot}:

$$S_{tot} = S_{in} + S_{ds,b} + S_{ds,br} + S_{ds,w} + S_{nl3} + S_{nl4} \quad (20)$$

These terms denote, respectively, wave growth by the wind, nonlinear transfer of wave energy through three-wave and four-wave interactions and wave decay due to White-capping, bottom friction, and depth-induced wave breaking.

Wind input

Transfer of wind energy to the waves is described with a resonance mechanism and a feedback mechanism. Based on the two wave growth mechanisms, wave growth due to wind commonly described as the sum of linear and exponential growth term of a wave component:

$$S_{in}(\sigma,\theta) = A + BE(\sigma,\theta) \quad (21)$$

in which A and B depend on wave frequency and direction, and wind speed and direction. The effects of currents are accounted for by using the apparent local wind speed and direction. The expression for the term A is due to Cavaleri and Malanotte-Rizzoli (1981) with a filter to avoid growth at frequencies lower than the Pierson-Moskowitz frequency (Tolman 1992a). Two optional expressions for coefficient B are used in the SWAN model. The first is taken from an early version of the WAM Cycle 3 model. It is due to Snyder et al. (1981), rescaled in terms of friction velocity U_* by Komen et al. (1984). The drag coefficient to relate U_* to the driving wind speed at 10 m elevation U_{10} is taken from either Wu (1982) or Zijlema et al. (2012). The second expression for B in SWAN is taken from the WAM Cycle 4 model (Komen et al. 1994).

Dissipation

The dissipation term of wave energy is represented by the summation of three different contributions: white-capping $S_{ds,w}$, bottom friction $S_{ds,b}$ and depth-induced breaking $S_{ds,br}$. White-capping is primarily controlled by the steepness of the waves. In presently operating third-generation wave models, the white-capping formulations are based on a pulse-based model (Hasselmann 1974).

$$S_{ds,w}(\sigma,\theta) = -\Gamma\bar{\sigma}\frac{k}{\bar{k}}E(\sigma,\theta) \quad (22)$$

where Γ is a steepness dependent coefficient, k is wave number and $\bar{\sigma}$and $\bar{k}$ denote a mean frequency and a mean wave number, respectively (cf. the WAMDI group, 1988). Komen et al. (1984) estimated the value of Γ by closing the energy balance of the waves in fully developed conditions. This implies that this value depends on the wind input formulation that is used. Since two expressions are used for the wind input in SWAN, also two values for Γ are used. The first is due to Komen et al. (1984), as in WAM Cycle 3. The second expression is an adaptation of this expression based on Janssen (1991), as in WAM Cycle 4 (see Janssen 1991b; Günther et al. 1992).

A number of alternative white-capping expressions have been proposed to improve the accuracy of SWAN. This alternative is proposed by Mulligan et al. (2007),

based on the white-capping expression of Alves and Banner (2003). This expression is based on experimental findings that white capping dissipation appears to be related to the nonlinear hydrodynamics within wave groups. White- capping expression proposed by Alves and Banner (2003) features additional dependencies on the spectral mean wavenumber and steepness, which is problematic in situations of the mixed sea and swell often encountered in the nearshore. Therefore, their white-capping expression is applied in Van der Westhuysen (2007) without these mean spectral dependencies. This adapted white-capping expression is used together with a wind input term that is based on that of Yan (1987).

$S_{ds,b}$ is the energy dissipation caused by bottom friction.

$$S_{ds,b} = -C_b \frac{\sigma^2}{g^2 \operatorname{Sin} h^2(k\, d)} E(\sigma, \theta) \tag{23}$$

in which C_b is a bottom friction coefficient. There are 3 options in Swan to calculate dissipation caused by bottom friction.

- The empirical JONSWAP model of Hasselmann et al. (1973),
- The drag law model of Collins (1972)
- The eddy-viscosity model of Madsen et al. (1988).

When waves propagate towards the shore, shoaling leads to an increase in wave height. When the ratio of wave height over water depth exceeds a certain limit, waves start to break, thereby dissipating energy rapidly. In extremely shallow water (surf zone), this process becomes dominant over all other processes. The process of depth-induced wave breaking is still poorly understood and little is known about its spectral modeling. In contrast to this, the total dissipation (i.e. integrated over the spectral space) due to this type of wave breaking can be well modeled with the dissipation of a bore applied to the breaking waves in a random field (Battjes and Janssen 1978; Thornton and Guza 1983).

$$S_{ds,br}(\sigma, \theta) = \frac{D_{tot}}{E_{tot}} E(\sigma, \theta) \tag{24}$$

in which E_{tot} is the total wave energy and $D_{tot} < 0$ is the rate of dissipation of the total energy due to wave breaking according to Battjes and Janssen (1978). The value of D_{tot}

depends critically on the breaker parameter $\gamma = H_{max}/d$ (in which H_{max} is the maximum possible individual wave height in the local water depth d). In SWAN, both a constant value and a variable value are available. Examples of a variable breaker parameter can be found in Nelson (1987) and Ruessink et al. (2003). (Both are implemented in SWAN.) The constant value is $\gamma = 0.73$ found as the mean value of the data set of Battjes and Stive (1985).

Nonlinear wave-wave interactions

The physical meaning of the interactions is that resonant sets of wave components exchange energy, redistributing energy over the spectrum. In deep and intermediate water, four-wave interactions (so-called quadruplets) are important, whereas in shallow water three-wave interactions (so-called triads) become important.

In deep water, quadruplet wave-wave interactions dominate the evolution of the spectrum. They transfer wave energy from the spectral peak to lower frequencies (thus moving the peak frequency to lower values) and to higher frequencies (where the energy is dissipated by white-capping). A full computation of the quadruplet wave-wave interactions is extremely time-consuming. A number of techniques, based on parametric methods and approximations have been proposed to improve the computational speed of computing quadruplets. In SWAN, the computations are carried out with the Discrete Interaction Approximation (DIA).

In very shallow water, triad wave interactions become important for steep waves. It transfers energy to higher frequencies, resulting in higher harmonics. The energy transfer in this process can take place over a relatively short distance and can dramatically change single peaked spectra into multiple peaked spectra. To describe triad wave-wave interactions in terms of a spectral energy source term Lumped Triad Approximation (LTA) technique is employed in SWAN. This Lumped Triad Approximation (LTA) technique is adapted based on a discrete triad approximation (DTA).

SWAN can run in several modes, indicating the level of parameterization. SWAN can operate in the first-, second and third-generation mode. An overview of the options is given in Table 3.

The default SWAN mode and coefficient values are as follows unless they are changed or disabled by the user:

- The option GEN3 is a default which indicates that SWAN should run in the third-generation mode for wind input, quadruplet interactions, and white-capping. Triads, bottom friction, and depth induced breaking are not activated by this command.
- The linear wave growth term is activated by the "AGROW" command. Normally it is disabled.
- White-capping according to Komen et al. (1984) is the default. The coefficient for determining the rate of white-capping dissipation (=C_{ds}) is 2.36e-5, the value of the wave steepness for a Pierson-Moskowitz spectrum is 3.02e-3.
- For Quadruplet wave-wave interactions DIA approximation is used. DIA is usually updated per sweep, either semi-implicit or explicit. Fully explicit computation of the nonlinear transfer with DIA per sweep is the default.
    - Coefficient for quadruplet configuration, $\Lambda = 0.25$
    - Proportionality coefficient for quadruplet interactions, $C_{nl4} = 3\ x\ 10{-}7$
    - The coefficient for shallow water scaling, $C_{sn1} = 5.5$
    - The coefficient for shallow water scaling, $C_{sn2} = 0.833333$
    - The coefficient for shallow water scaling, $C_{sn3} = -1.25$
- Breaking term is another physical process defined in Swan. The default breaker index, i.e. the ratio of maximum individual wave height over depth(γ) is 0.73.
- In SWAN four different formulations are available, i.e., that of Hasselmann et al. (1973), JONSWAP, Collins (1972), Madsen et al. (1988) and Smith et al. (2011) for dissipation due to bottom friction. The default option is JONSWAP with a constant friction coefficient. The recommended value for typical sandy bottoms is 0.038 m^2s^{-3}
- For triad wave-wave interactions the LTA method is the default.

4.2. Model Simulation Process

In order to measure the model performance, the dates 94-96 December are preferred. Thus, it was determined how successful the model was in this period. Era5 re-analysis data of this period were downloaded in GRIB format and prepared as SWAN boundary input with the TPAR file. TPAR file contains nonstationary wave parameters. It has a string TPAR on the first line of a file and a number of lines that contain each

5 numbers, sequentially; Time (ISO-notation), Hs, Period, Direction and directional spread. Additionally, the file must have a.DAT format to be read in SWAN. Figure 30 shows the TPAR file used as the deep-water boundary input in SWAN.

Table 3. Overview of physical processes and generation mode in SWAN. (Source: SWAN, 2013a)

process	authors	generation mode		
		1st	2nd	3rd
Linear wind growth	Cavaleri and Malanotte-Rizzoli (1981) (modified)	×	×	
	Cavaleri and Malanotte-Rizzoli (1981)			×
Exponential wind growth	Snyder *et al.* (1981) (modified)	×	×	
	Snyder *et al.* (1981)			×
	Janssen (1989, 1991)			×
	Yan (1987) (modified)			×
Whitecapping	Holthuijsen and De Boer (1988)	×	×	
	Komen *et al.* (1984)			×
	Janssen (1991)			×
	Alves and Banner (2003)			×
Quadruplets	Hasselmann *et al.* (1985)			×
Triads	Eldeberky (1996)	×	×	×
Depth-induced breaking	Battjes and Janssen (1978)	×	×	×
Bottom friction	JONSWAP (1973)	×	×	×
	Collins (1972)	×	×	×
	Madsen *et al.* (1988)	×	×	×
Obstacle transmission	Seelig (1979), d'Angremond (1996)	×	×	×
Wave-induced set-up		×	×	×
Vegetation dissipation	Dalrymple (1984)	×	×	×
Mud dissipation	Ng (2000)	×	×	×
Turbulence dissipation		×	×	×

The wave coming from a boundary that not specified in SWAN is assumed to be zero and when generated waves move through that boundary it is assumed that waves go out of the specified area. Since the southern part of the Filyos model study area is part of the land, the boundary condition for the North, East and West directions is specified.

For wind and wave direction both the Cartesian and *a* nautical convention can be used. Directions and spherical coordinates are in degrees and not in radians. Users can define the geographic location, size, resolution, and orientation of the computational

grid in the problem coordinate system in case of a uniform, rectilinear computational grid, a curvilinear grid or unstructured mesh. The uniform computational grid is default and chosen for this study. It is recommended to use spatial resolution Δx, $\Delta y = 50-1000$ m, for direction resolution for wind sea $\Delta\theta = 15^{o}-10^{o}$, direction resolution for swell $\Delta\theta = 5^{o}-2^{o}$ and frequency range $0.04 \leq f \leq 1.00$ Hz. Swan (2013a) for coastal areas.

TPAR

19951101.000000	0.23561	3.41018	332.81564	2.00000
19951101.010000	0.22817	3.37215	333.43777	2.00000
19951101.020000	0.22767	3.24029	334.95920	2.00000
19951101.030000	0.23832	3.00495	342.31406	2.00000
19951101.040000	0.23671	2.94288	345.82648	2.00000
19951101.050000	0.23930	2.89794	351.54208	2.00000
19951101.060000	0.24852	2.89542	358.84070	2.00000
19951101.070000	0.26350	2.95564	4.22026	2.00000
19951101.080000	0.28052	3.10972	4.18657	2.00000
19951101.090000	0.31061	3.26000	5.15282	2.00000
19951101.100000	0.35871	3.36484	13.29860	2.00000
19951101.110000	0.43518	3.36579	17.72522	2.00000
19951101.120000	0.52594	3.35398	22.51990	2.00000
19951101.130000	0.62162	3.37805	26.47548	2.00000
19951101.140000	0.71329	3.42691	30.20365	2.00000
19951101.150000	0.79596	3.48959	34.23734	2.00000
19951101.160000	0.86394	3.56330	37.83130	2.00000
19951101.170000	0.91589	3.64343	40.50801	2.00000
19951101.180000	0.94899	3.72835	42.25214	2.00000
19951101.190000	0.96029	3.81077	43.36143	2.00000
19951101.200000	0.99142	3.94762	44.33384	2.00000
19951101.210000	0.97049	4.01621	45.20225	2.00000
19951101.220000	0.92930	4.07844	45.67274	2.00000
19951101.230000	0.87599	4.13327	44.95342	2.00000
19951102.000000	0.82320	4.17813	43.66902	2.00000
19951102.010000	0.77596	4.21301	42.23887	2.00000
19951102.020000	0.73526	4.23109	40.91437	2.00000
19951102.030000	0.69947	4.24063	39.74391	2.00000
19951102.040000	0.66898	4.23419	38.81740	2.00000
19951102.050000	0.64250	4.21772	38.24210	2.00000
19951102.060000	0.61811	4.20308	37.91526	2.00000
19951102.070000	0.59613	4.18439	37.70411	2.00000
19951102.080000	0.57553	4.17325	37.66702	2.00000
19951102.090000	0.55552	4.17111	37.81452	2.00000
19951102.100000	0.53128	4.22181	37.97792	2.00000
19951102.110000	0.51635	4.20960	38.51717	2.00000
19951102.120000	0.50515	4.17059	38.94146	2.00000

Figure 30. Example of TPAR file

SWAN can be run either stationary or nonstationary and one dimensional (1D-mode) or two-dimensional (2D-mode). In the 1D-mode length of the computational grid in the y−direction (in m) is zero. In the stationary model, it is accepted that boundary conditions and source expressions do not change over time and remain constant. For very small areas on the nearby shore, it is preferable to save time if previous sea condition information is unnecessary. For this reason, the model is run in the 3rd generation GEN3 default mode KOMen source with nonstationary mode (time step).

When model physics is examined, triad wave interactions, bottom friction and wave breaking gain importance in shallow water. Triad wave interactions transfer energy from low frequencies to high frequencies. Waves approaching the shore are under the effect of bottom friction and wave breaking is effective at the wave height in shallow water. Therefore, first, it was decided that these parameters would be activated in order to improve nearshore wave performance. Then, in order to obtain better results, the sensitivity analysis was performed by changing the coefficients of these parameters for November 95 before the 2-year data were run. After determining the most appropriate coefficients, 2-year data were run in Swan and the results were obtained. In addition, for Filyos, ambient current and tide were considered and 0.3 meters were taken for SWAN input. Finally, from the results of the 2-year model, a detailed analysis of the stormy days occurring in this process was conducted and the accuracy of the model was examined during the stormy days.

SWAN Cycle 3 version 40.91A software was run on 64 cores with the Microsoft Windows operating system. In order to save calculation time, iteration was requested 1 hour and results were taken 1 hour in 2 hours. The results were requested at 1 in 2 hours because the in-situ data to be verified was measured at 1 in 2 hours. Due to the large size of the output file, the data was run month by month, and the calculation time of the model for 1 month was approximately 3 hours. Figure 31 shows how to run the SWAN Cycle 3 version 40.91A in Microsoft Windows operating system.

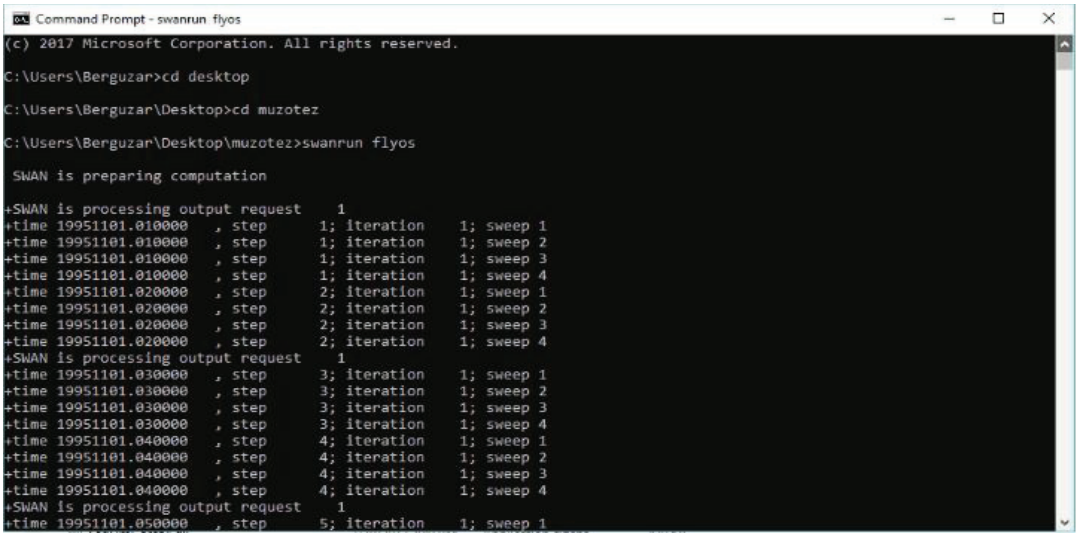

Figure 31. Model run with Microsoft windows operation system

4.3. Sensitivity Analysis

Significant wave height is the most frequently used and the most important parameter in engineering studies. For this reason, a sensitivity analysis was performed for Hs. For this analysis, November 1995, which includes a stormy period, was preferred. The analysis was performed by changing the coefficients of white-capping, wave breaking, bottom friction, triad wave interaction of model physics. While the other variables were kept constant, the coefficient that it is wanted to see the effect on the result was changed (these coefficients are shown in the model physics section and the wave properties section). The following error parameters were calculated for the sensitivity analysis.

Root Mean Square Error (RMSE)

The square root of the sum of the squares of the difference between the model results and the in-situ data. Formula,

$$RMSE = \left[\frac{1}{N}\sum_{i=1}^{N}(P_i - O_i)^2\right]^{\frac{1}{2}} \quad (25)$$

Here, the P_i is model results correspond to the measured values O_i.

Scatter Index (SI)

The formula SI is as follows. The closer the RMSE and SI parameters are to zero, the better the model performance. $\overline{O}$ in the formula corresponds to the average of the measured values.

$$SI = \frac{RMSE}{\overline{O}} \quad (26)$$

Correlation Coefficient (R)

The correlation coefficient is a statistical calculation showing the strength of the relationship between the two variables.

KOMen and JANSen, two different sources for the white-capping term, have

tested. Different values of the coefficient for determining the rate of white-capping dissipation (C_{ds}) was run in the model. A different constant breaker index (gamma, the ratio of maximum individual wave height over depth) was used for breaking term. A different constant JONSWAP bottom friction coefficient (which indicates that the semi-empirical expression derived from the JONSWAP results for bottom friction dissipation) was tried. Finally, different LTA approximation method of Eldeberky (1996) proportionally coefficient [trfac] was tried for triad wave-wave interaction. The error parameters were shown in the following Table 4, as well as graphs of the RMSE values in Figure 32.

The values in the parameters were selected taking as a reference to other studies. When the results of sensitivity analysis were examined, it was observed that different parameters did not cause much change in the model result. However, the least error coefficients were chosen and the model was run for 2 years.

By looking at the Table 4;

- White-capping Janssen C_{ds}=0.25
- Breaking Constant Gamma=0.9
- Friction Jonswap cfjon=0.019
- Triad trfac=0.8

Coefficients were found to be the least error coefficients. These coefficients are used in model physics.

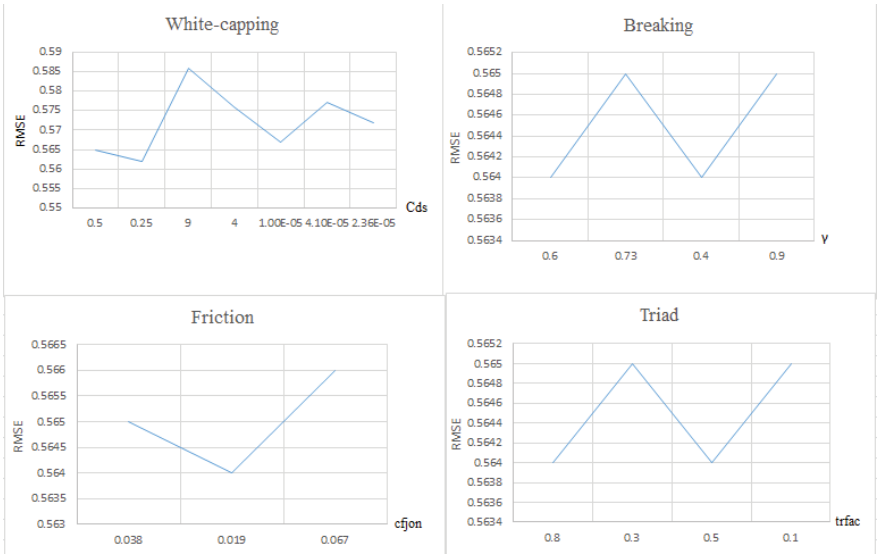

Figure 32. RMSE for different parameters with different coefficient

Table 4. Error parameters of sensitivity analysis

Cds=	0.5	0.25	9.0	4.0	1.0E-05	4.1E-05	2.36E-05
RMSE	0.565	0.562	0.586	0.576	0.567	0.577	0.572
SI	0.584	0.581	0.606	0.595	0.586	0.597	0.591
R	0.916	0.916	0.92	0.919	0.917	0.919	0.918
γ=	0.6	0.73	0.4	0.9			
RMSE	0.565	0.565	0.572	0.564			
SI	0.584	0.584	0.591	0.583			
R	0.916	0.916	0.916	0.916			
cfjon=	0.038	0.019	0.067				
RMSE	0.565	0.564	0.566				
SI	0.584	0.583	0.585				
R	0.916	0.916	0.916				
trfac=	0.8	0.3	0.5	0.1			
RMSE	0.564	0.565	0.564	0.565			
SI	0.583	0.583	0.583	0.584			
R	0.916	0.916	0.916	0.916			

CHAPTER 5

VERIFICATION STUDY

5.1. Verification with All Data

The model physics parameters were decided by sensitivity analysis and the model was ready to run for 2 years. The model input file is shown and it is explained in detail in Figure 34.

Chapter 3 describes how to create a regular gridded bathymetry file. The model calculation resolution is the same as the bathymetry resolution (311x250). It means that the model gives output at 77750 grid points for each successive time step. In order to perform model verification, model output data is requested at the point where the in-situ measurement gauge is located. It is at a 33650th grid point from the bottom left corner. The data at this point were requested using MATLAB software. The requested data were saved in excel format. Figure 33 shows the model output file.

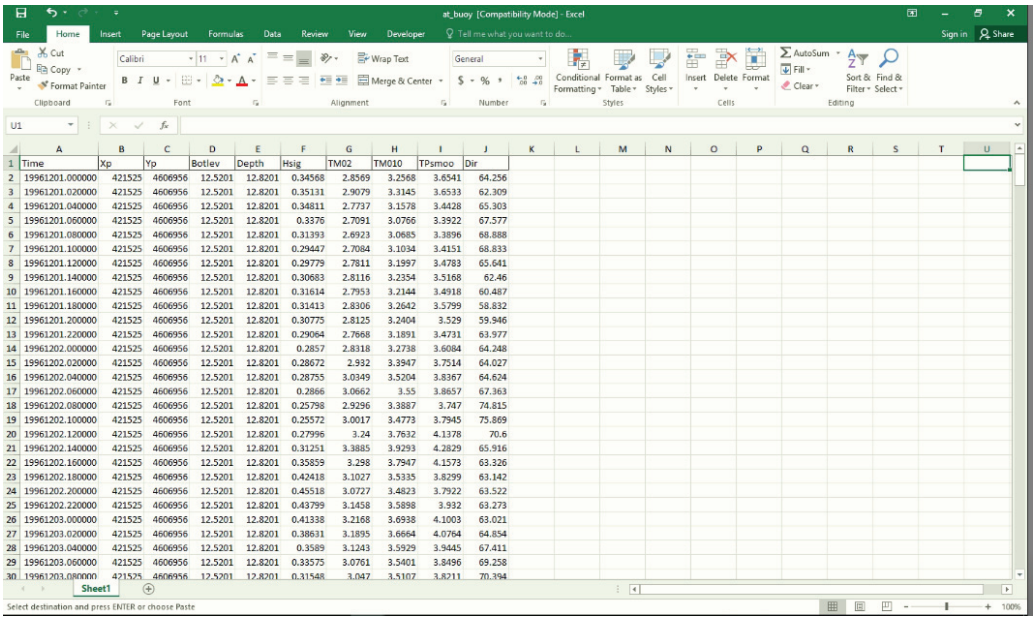

Time	Xp	Yp	Botlev	Depth	Hsig	TM02	TM010	TPsmoo	Dir
19961201.000000	421525	4606956	12.5201	12.8201	0.34568	2.8569	3.2568	3.6541	64.256
19961201.020000	421525	4606956	12.5201	12.8201	0.35131	2.9079	3.3145	3.6533	62.309
19961201.040000	421525	4606956	12.5201	12.8201	0.34811	2.7737	3.1578	3.4428	65.303
19961201.060000	421525	4606956	12.5201	12.8201	0.3376	2.7091	3.0766	3.3922	67.577
19961201.080000	421525	4606956	12.5201	12.8201	0.31393	2.6923	3.0685	3.3896	68.888
19961201.100000	421525	4606956	12.5201	12.8201	0.29447	2.7084	3.1034	3.4151	68.833
19961201.120000	421525	4606956	12.5201	12.8201	0.29779	2.7811	3.1997	3.4783	65.641
19961201.140000	421525	4606956	12.5201	12.8201	0.30683	2.8116	3.2354	3.5168	62.46
19961201.160000	421525	4606956	12.5201	12.8201	0.31614	2.7953	3.2144	3.4918	60.487
19961201.180000	421525	4606956	12.5201	12.8201	0.31413	2.8306	3.2642	3.5799	58.832
19961201.200000	421525	4606956	12.5201	12.8201	0.30775	2.8125	3.2404	3.529	59.946
19961201.220000	421525	4606956	12.5201	12.8201	0.29064	2.7668	3.1891	3.4731	63.977
19961202.000000	421525	4606956	12.5201	12.8201	0.2857	2.8318	3.2738	3.6084	64.248
19961202.020000	421525	4606956	12.5201	12.8201	0.28672	2.932	3.3947	3.7514	64.027
19961202.040000	421525	4606956	12.5201	12.8201	0.28755	3.0349	3.5204	3.8367	64.624
19961202.060000	421525	4606956	12.5201	12.8201	0.2866	3.0662	3.55	3.8657	67.363
19961202.080000	421525	4606956	12.5201	12.8201	0.25798	2.9296	3.3887	3.747	74.815
19961202.100000	421525	4606956	12.5201	12.8201	0.25572	3.0017	3.4773	3.7945	75.869
19961202.120000	421525	4606956	12.5201	12.8201	0.27996	3.24	3.7632	4.1378	70.6
19961202.140000	421525	4606956	12.5201	12.8201	0.31251	3.3885	3.9293	4.2829	65.916
19961202.160000	421525	4606956	12.5201	12.8201	0.35859	3.298	3.7947	4.1573	63.326
19961202.180000	421525	4606956	12.5201	12.8201	0.42418	3.1027	3.5335	3.8299	63.142
19961202.200000	421525	4606956	12.5201	12.8201	0.45518	3.0727	3.4823	3.7922	63.522
19961202.220000	421525	4606956	12.5201	12.8201	0.43799	3.1458	3.5898	3.932	63.273
19961203.000000	421525	4606956	12.5201	12.8201	0.41338	3.2168	3.6938	4.1003	63.021
19961203.020000	421525	4606956	12.5201	12.8201	0.38631	3.1895	3.6664	4.0764	64.854
19961203.040000	421525	4606956	12.5201	12.8201	0.3589	3.1243	3.5929	3.9445	67.411
19961203.060000	421525	4606956	12.5201	12.8201	0.33575	3.0761	3.5401	3.8496	69.258
19961203.080000	421525	4606956	12.5201	12.8201	0.31548	3.047	3.5107	3.8211	70.394

Figure 33. Output file saved as excel format

Figure 34. (Cont. on next page)

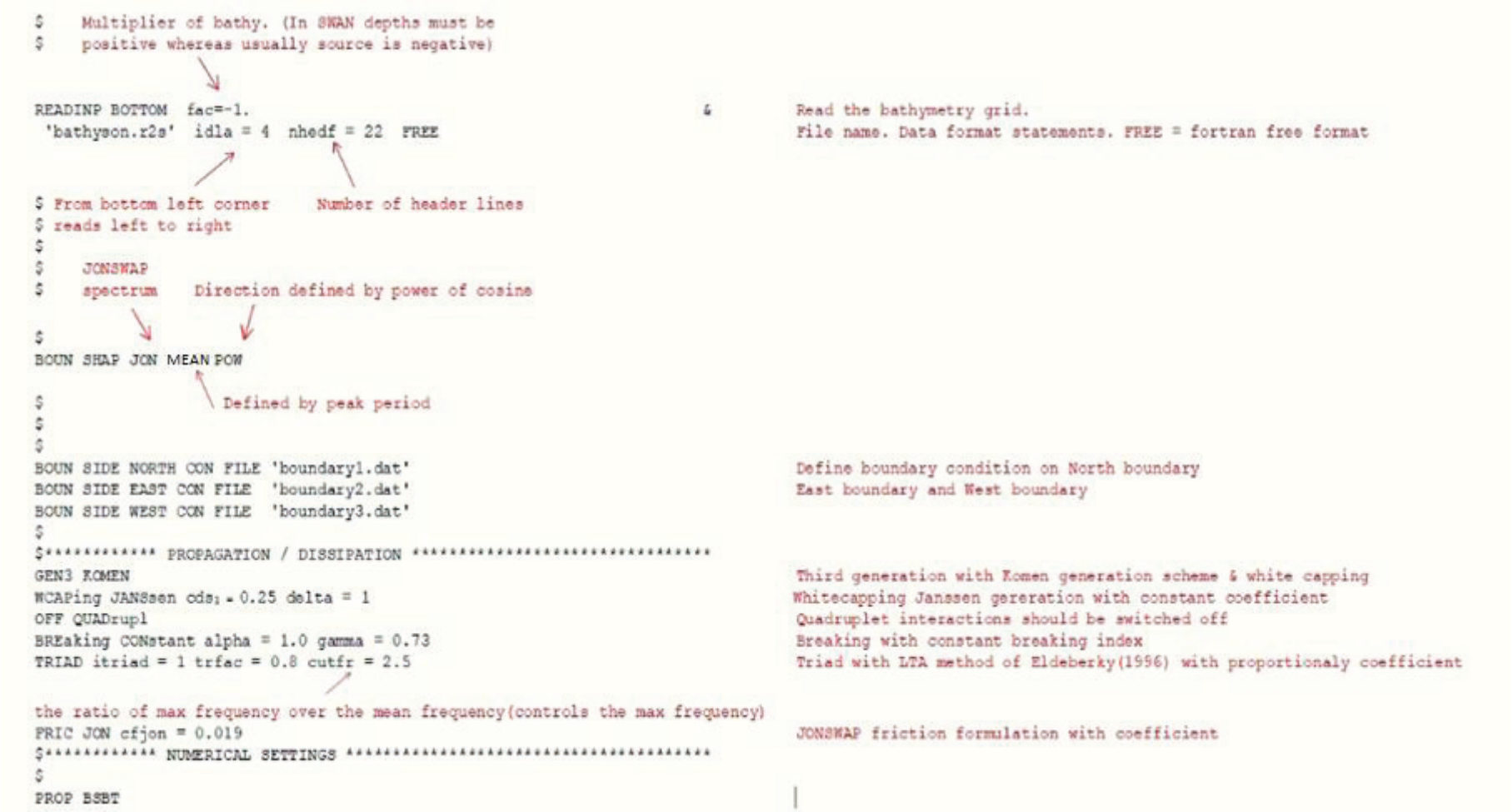

Figure 34. (Cont. on next page)

```
$
NUM STOPC drel = 0.01  curvat = 0.01                                    &        Based on relative change of Hs and curvature
    npnts = 98.  STAT mxitst = 40
                                          Maximum number of iterations
$   Percentage of nodes over
$   which criteria must apply
$
$************ OUTPUT REQUESTS ****************************************
$
$ Other outputs ---------------------------------------------------
$
TABLE 'COMPGRID' HEADER 'resim.out' TIME XP YP BOTLEV DEP HSIGN   &             Output results
           TM02 TMM10 TPS DIR                                    &
          OUTPUT tbegtbl = 19951101.000000 delttbl = 2 HR                     Starting time when model starts writing out file
$
COMPUTE NONST tbegc = 19951101.000000 deltc = 1 HR                  &         Compute nonstationary time dependent with starting and ending time of
$             tendc = 19951130.230000                                           computations

STOP
```

Figure 34. Swan input file used in the modeling (Cont.)

As shown in Figure 33, the model was asked to print the results for Time, X and Y coordinates, bottom elevation, water depth, significant wave height, wave periods Tm_{02}, Tm_{010}, T_p and wave direction parameters. The coordinate of the pressure type gauge in regular gridded bathymetry is (421525, 4606956) and the depth is 12.5 meters. Significant wave height is the average of the highest 1/3 of the waves in the measured time. Tm_{02} is the mean wave period obtained from the zeroth and second spectral moments, Tm_{010} is the wave energy period and T_p is the peak wave period corresponding to spectral peak.

In order to visualize the model result in the whole study area as an example, one-hour data including the largest wave height of the two years measurement (21st of November, 1995) were selected the model was run in stationary mode. The inputs were Hs = 3.87572 Tm = 7.85375 dir= 341.47556. The file format was changed. r2s, r2v files by using SWANMangler_v3.1 software to open the result file in BlueKeneu64. SWANMangler_v3.1 software is shown in Figure 35. Period, wave height, bottom elevation and direction results visualized by Blue Keneu software are shown in Figures 36-37-38 respectively.

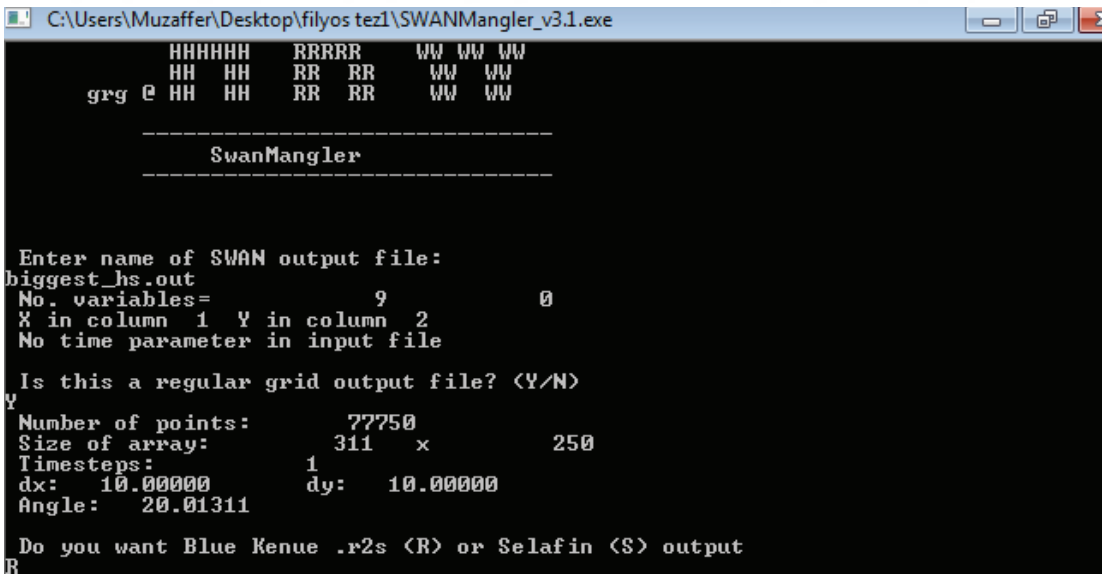

Figure 35. SWANMangler_v3.1 software

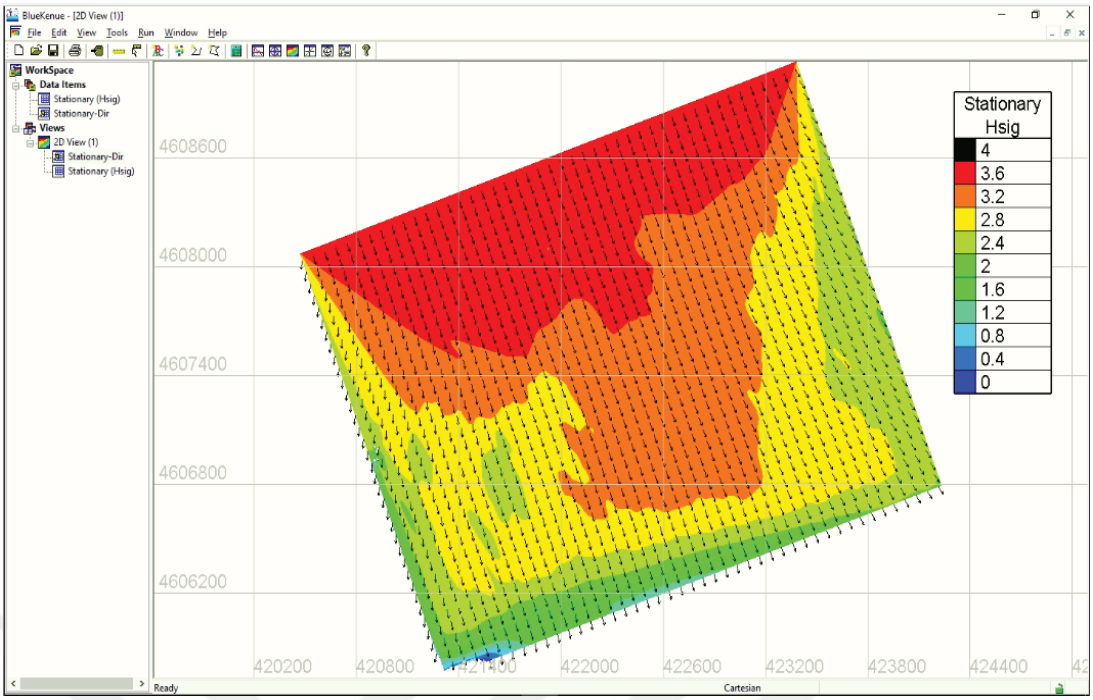

Figure 36. 21.11.1995 20:00 Significant Wave Height and Wave Direction

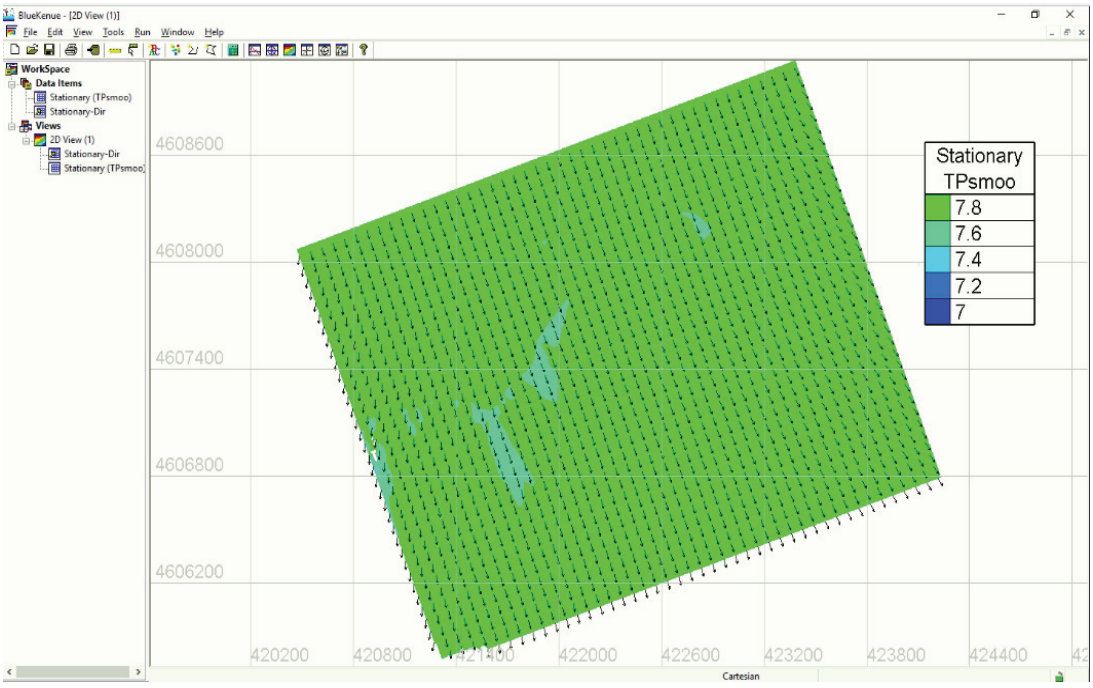

Figure 37. 21.11.1995 20:00 Peak Wave Period and Wave Direction

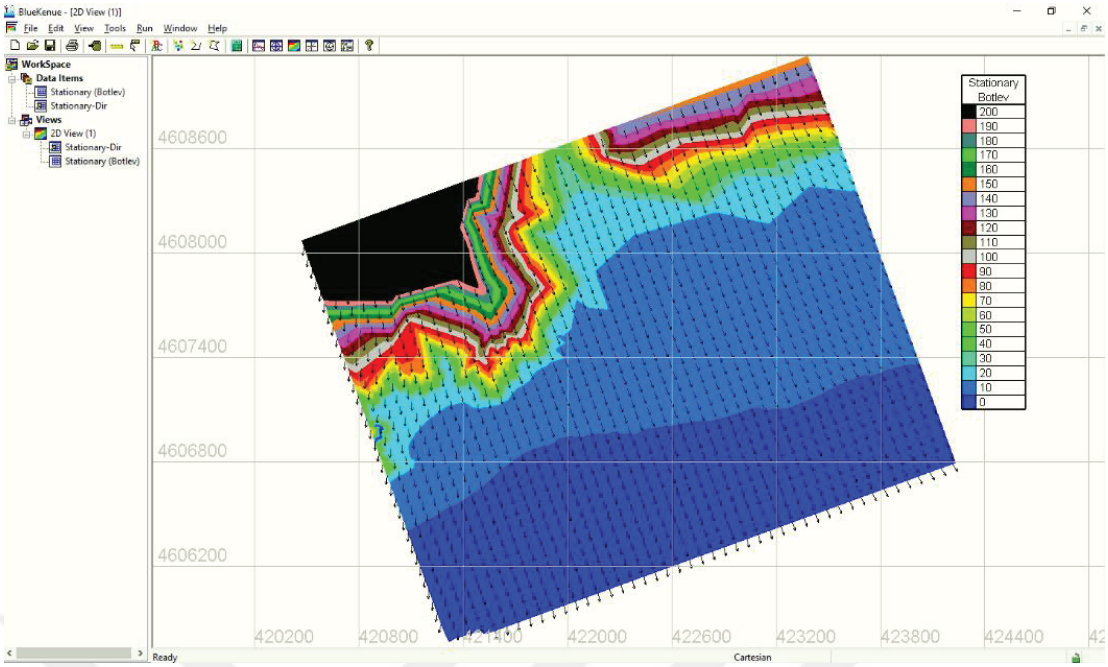

Figure 38. 21.11.1995 20:00 Bottom Elevation and Peak Wave Direction

Similar runs were performed for two years of data, arranged in chronological order and model validation study was performed. For this purpose, the model results were compared with the in-situ data, and the various error parameters were calculated to assess the error. These are RMSE (Eq.25), SI(Eq.26), bias, mean absolute value (MAE), correlation coefficient and regression coefficient. Definitions of bias, MAE and regression coefficient are given below:

Mean of Predict Error Parameter (Bias)

Bias is the difference between the model results and the average of the measured values. When the bias is 0 it is named as objectivity.

$$\text{Bias} = \sum_{i=1}^{N} \frac{1}{N} (P_i - O_I) \qquad (27)$$

Mean Absolute Error (Mae)

It is the average of the absolute differences between model out and measured data.

$$\text{Mae} = \sum_{i=1}^{N} \frac{1}{N} \left(\left| P_i - O_i \right| \right) \quad (28)$$

Regression Coefficient

The Regression Coefficient is the coefficient A in the linear regression equation (y=Ax).

In addition, the ERA5 deep-water input data were also compared with the in-situ measurement data to examine the difference between model results and ERA5 deep water data. Calculated error parameters are presented in Table 5.

Table 5. Error assessment for the Hs and Tm of SWAN output and ERA5 deep water data against In-situ Measurements

Hs	RMSE	SI	R	BIAS	MAE	A
Swan_out	0.4111	0.6239	0.8128	0.2260	0.3123	0.7914
ERA5 deep-water	0.4963	0.7533	0.9869	0.3294	0.3794	0.6999

Tm	RMSE	SI	R	BIAS	MAE	A
Swan_out	0.6741	0.1388	0.8445	-0.3868	0.5350	1.0652
ERA5 deep-water	0.6342	0.1306	0.8540	-0.3254	0.5071	1.0514

Table 5 shows that the error in the SWAN model is less than the error in input ERA5 data. It is an expected result because the in-situ measurement is at near-shore but input wave data belongs to the deep water condition.

For the wave direction comparison, a parameter, Delta, was first calculated to measure the wave direction error statistics. Delta is the shortest distance between two different wave directions.

$$\Delta = 180 - \left| 180 - |\theta_1 - \theta_2| \right| \quad (29)$$

Following error parameters were used to examine wave direction performance:

$$MAE_\theta = BIAS_\theta = \frac{1}{N} \sum_{i=1}^{N} \Delta_i \quad (30)$$

$$RMSE_\theta = \sqrt{\frac{1}{N}\sum_{i=1}^{N}\Delta_i^2} \quad (31)$$

Calculated error parameters for the wave direction are given in Table 6.

Table 6. Error assessment for the wave direction of SWAN output and ERA5 deep water data against In-situ Measurements

Direction	RMSE	MAE
Swan_output	67.853	54.968
ERA5 Deepwater	72.518	59.088

The Hs, Tm and direction results were also compared with the previous studies in terms of error statistics and it is shown in Table 7.

For the significant wave height parameter, as it is seen in Table 7 that the error statistics of the previous studies and the current study are similar, and the error parameters in the Filyos course grid study of Bingölbali et al. (2019) are almost the same. In addition, it was observed that the model gives better results than ERA5 deep-water boundary data as expected. It is also seen in the time series comparison given in Figure 39, the model result and the in-situ data fits well. All in all, it can be said that the model performance is good for the significant wave height parameter.

When the average wave period parameter is taken into consideration, it can be said that the results are much better compared to the previous studies and the performance of the model is very good.

When Table 7 is examined for the wave direction, it is observed that the error statistics are higher than the previous studies. However, the model result is slightly better than the model inputs with respect to in-situ measurements.

For Hs and mean wave period time series were also plotted for the comparison of the SWAN model and the in-situ measurements and the plots are shown in Figures 39 and 40. A wave rose diagram was plotted for the comparison of wave direction between the SWAN model and the in-situ measurements as shown in Figure 41.

Table 7. Statistical error parameters for the Hs, Tm, and direction of the current study and the previous studies against the in-situ measurements

Hs	Location	Depth(m)	RMSE	SI	R	BIAS	MAE
Current Study	Filyos	12.5	0.411	0.624	0.813	0.226	0.31
Liliana Rusu et al.(2005)	Figueira da Foz Portugal	19.5	0.659	0.188	0.873	-0.153	-
Amarouche,Khalid et al.(2019)	Azzefoun(Algeria)-Default Swan	30	0.47	0.43	0.92	-0.3	0.33
	-Calibrated KJ	30	0.34	0.31	0.92	0.09	0.32
	Marseille(France)-Default Swan	32	0.44	0.4	0.96	-0.26	0.29
	-Calibrated KJ	32	0.3	0.28	0.96	-0.06	0.21
Bilal Bingölbali et al.(2019)	Karaburun (Fine Grid)	16	0.53	0.53	0.65	-0.11	0.4
	Filyos(Fine Grid)	12.5	0.38	0.58	0.82	-0.09	0.28
	Karaburun (Coarse Grid)	16	0.29	0.38	0.84	-0.02	0.2
	Filyos(Coarse Grid)	12.5	0.42	0.68	0.74	-0.13	0.28

Tm	Location	Depth(m)	RMSE	SI	R	BIAS	MAE
Current Study	Filyos	12.5	0.674	0.139	0.844	-0.387	0.535
Liliana Rusu et al.(2005)	Figueira da Foz Portugal	19.5	2.471	0.187	0.541	-1.317	-
Amarouche,Khalid et al.(2019)	Azzefoun(Algeria)-Default Swan	30	1.21	0.26	0.78	-0.45	0.97
	-Calibrated KJ	30	0.95	0.21	0.78	-0.03	0.73
	Marseille(France)-Default Swan	32	1.46	0.33	0.83	-1.11	1.21
	-Calibrated KJ	32	1.29	0.29	0.84	-0.92	1.04
Bilal Bingölbali et al.(2019)	Filyos(Sub Grid)	12.5	1.11	0.2	0.67	-0.01	0.84
	Filyos(Coarse Grid)	12.5	1.21	0.22	0.62	-0.37	0.92

(Cont. on next page)

Table 7 . (Cont.)

Wave Direction	Location	Depth(m)	RMSE	MAE
Current Study	Filyos	12.5	67.8	54.9
Liliana Rusu et al.(2005)	Figueira da Foz Portugal	19.5	14.9	-
Amarouche, Khalid et al. (2019)	Palos(Spain)-Default Swan	230	49	31
	-Calibrated KJ	230	51	33
	Nice(France)-Default Swan	270	36	26
	-Calibrated KJ	270	27	19

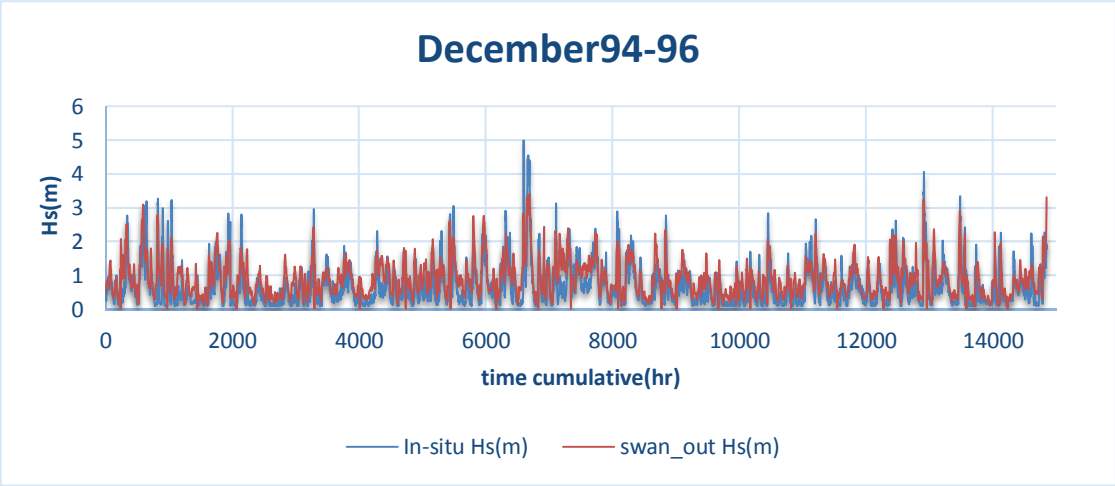

Figure 39. Time-series comparison of SWAN model and in-situ measurements for Hs

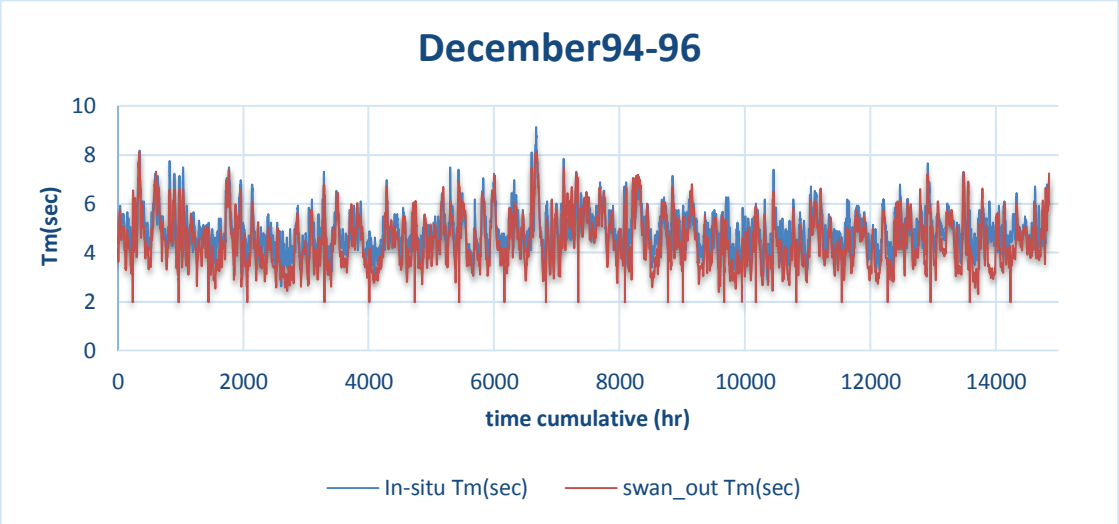

Figure 40. Time-series comparison of SWAN model and in-situ measurements for Tm

Time-series comparison shows that wave height and period of the model and the in-situ measurement are in phase. As can be seen in Figure 41, while the dominant wave direction is North-East (NE) according to the SWAN model results, it is North for the in-situ measurements. To check the direction discrepancy between the model and in-situ measurements, wind direction data are gathered from the State Meteorological Organization. There is not any station on the sea near Filyos. However, there are three land-based meteorological stations that the wind direction is measured close to the

Filyos region. Those are Amasra, Bartın and Zonguldak stations. Amasra data are selected since the station location is close to the sea

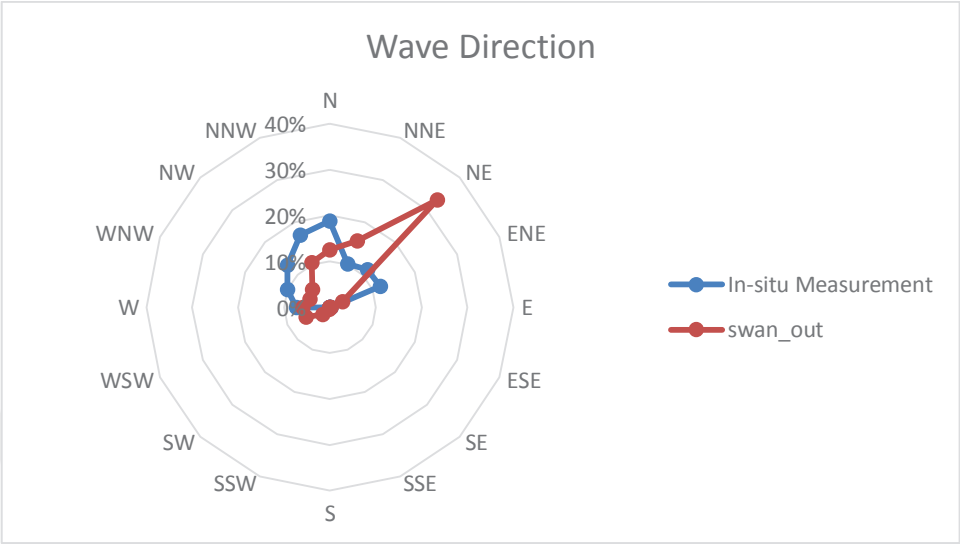

Figure 41. Comparison of SWAN model and in-situ measurements for the wave direction by wave roses.

For the year 1995, wind direction and wave direction was compared in terms of time series plot. It is given in Figure 42.

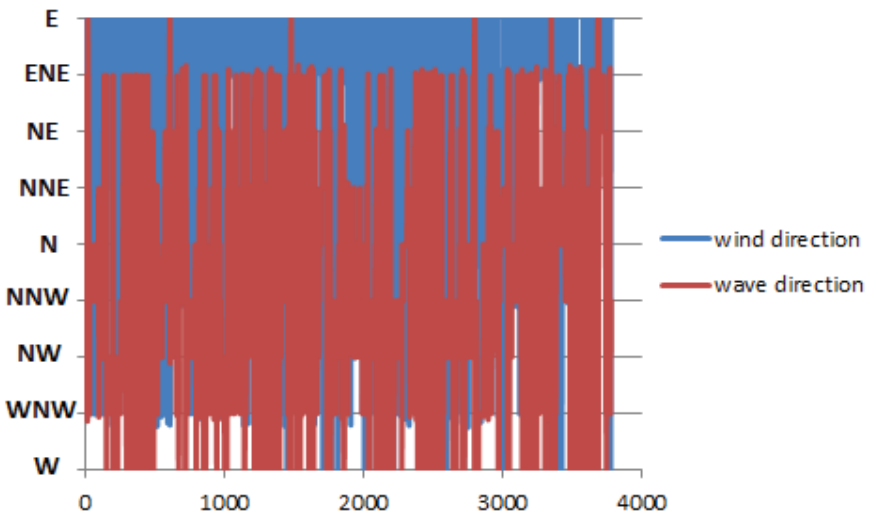

Figure 42. Comparison of wind and wave direction

Figure 42 shows that one to one correspondence between wind and wave direction does not fit well. Moreover, occurrence probabilities of wind and wave for each direction were calculated and wind and wave roses were plotted together with the SWAN model result. The plot is given in Fig. 43.

Figure 43 indicates that waves due to eastern winds that are measured in the in-situ station and having the longer fetches comparing to the western fetches were estimated better by the SWAN model. However, those waves cannot be seen in in-situ wave records. It may be the explanation of the high error in the estimation of the wave direction.

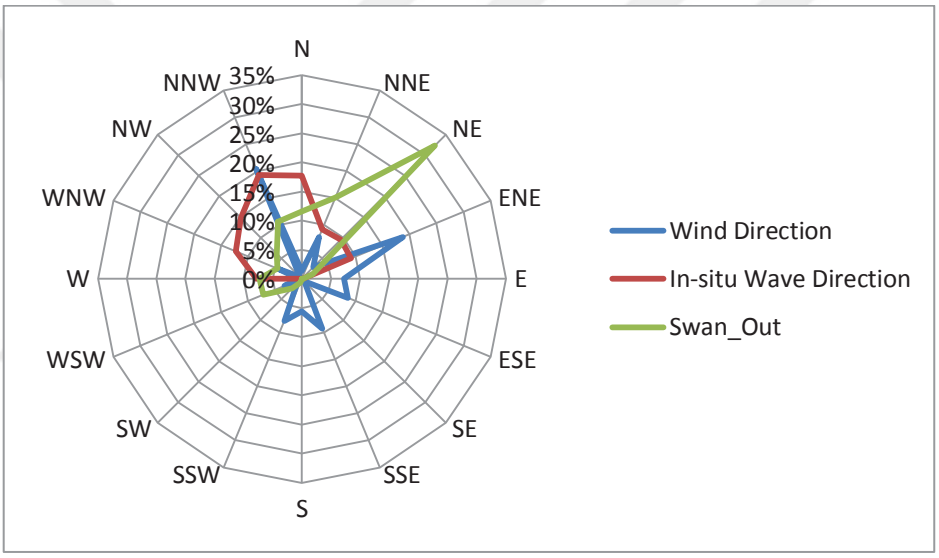

Figure 43. Directional distribution of wind, in-situ wave and SWAN model

5.2. Comparison of the Selected Storms

In Section 5.1, the numerical estimates were compared with the in-situ measurements for the whole data. However, it may be interesting to check the agreement in stormy times. Therefore, 14 storms are selected to analyze the make comparison. The storms are selected according to the following criteria:

I. During the storm, significant wave height must be at least 2.0 m.

II. Storm must be as independent as possible.

III. The duration of a storm must be at least 6 hrs.

Multi-peaked storms are excluded from this preliminary study to avoid and possible distortion of the results. A list of the selected storms for this study is given in Table 8.

Table 8. Stormy days in two years period

Storm No.,name	Date	Duration (hrs)	No.of waves
1, 95011	01.25-01.26.1995	24	2271
2, 95012	01.28-01.29.1995	24	2346
3, 95021	02.01-02.02.1995	28	2834
4, 95022	02.04-02.05.1995	30	2893
5, 95051	05.03-05.05.1995	50	4211
6, 95091	09.30-10.01.1995	38	3754
7, 95101	10.02-10.04.1995	42	5256
8, 95111	11.19-11.20.1995	34	1924
9, 95121	12.21-12.22.1995	28	2752
10, 96031	03.03-03.04.1996	32	3069
11, 96061	06.15-06.16.1996	28	2791
12, 96091	09.28-09-29.1996	30	2671
13, 96101	10.22-10.24.1996	51	5090
14, 96111	11.25-11.26.1996	22	2479

5.2.1. Time Series Analysis

The results of the stormy period were separated from the whole data set of the two-year model result, and the time series were plotted for the Hs, Tm and Direction parameter of the model result and in-situ measurement data for each storm. An example comparison plot is given for the storm with the largest Hs in the two years measurement in Figure 44.

Figure 44 indicates that although the model cannot capture the highest wave height, there is good agreement between the SWAN model and the in-situ measurement for the storm, especially for the mean wave period. There is still a discrepancy in the wave direction as it is in the case of the comparison for all of the waves.

The rest of the plots for the other storms are shown in Appendix A.

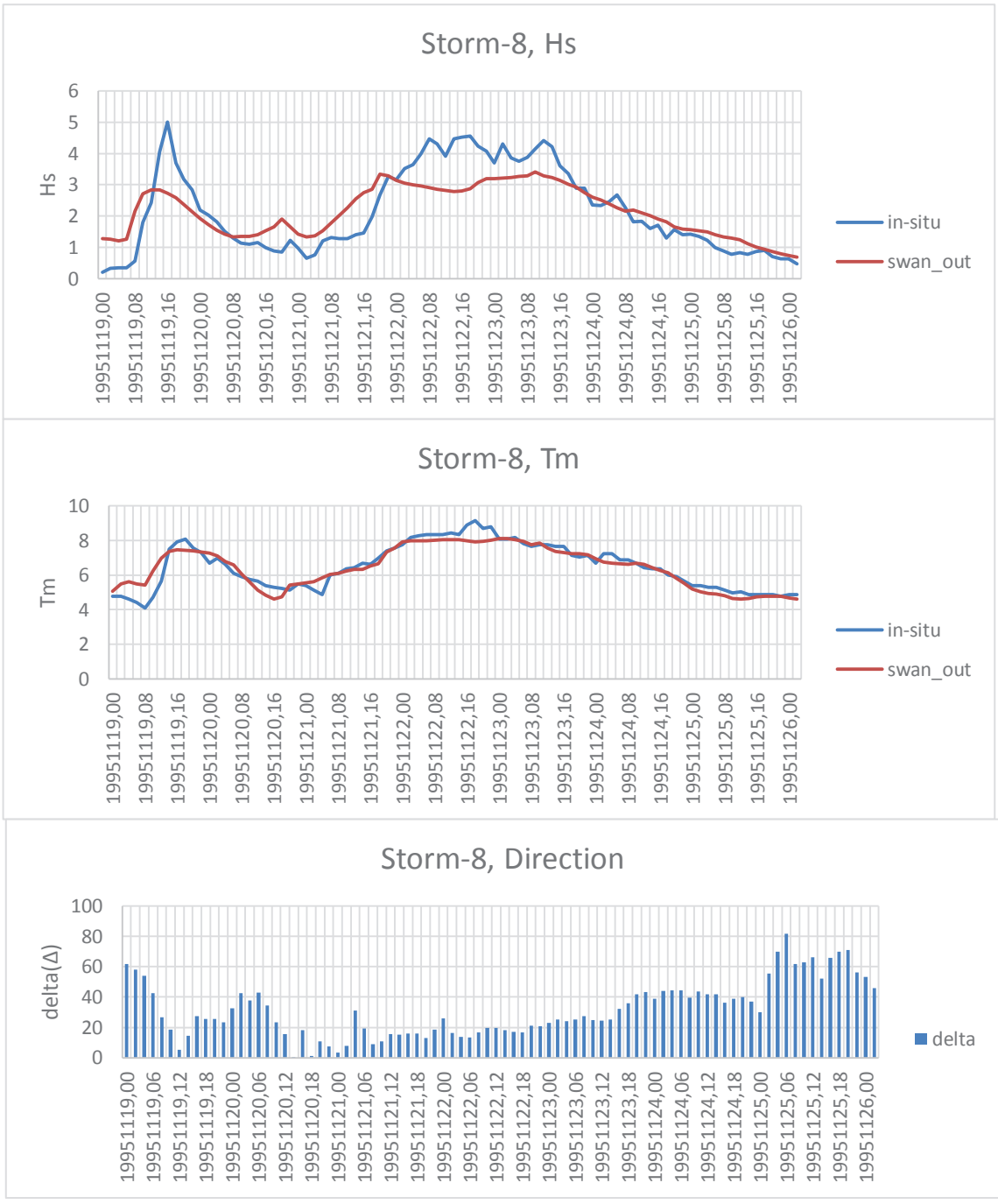

Figure 44. Comparison for Hs, Tm and the direction of in-situ Measurement and Swan-out for the Storm-8 (Cont.)

When the time series comparison of the significant wave height is examined, it is seen that there is a time agreement between the model and the in-situ data, especially the storm3-4, storm8, storm12, and storm13, they fit very well. When Storm10 is examined, it is seen that the stormy period of the model result lasts shorter than the measured values and there is a slight deviation in the peak values of the model result in

storm1 and storm5. To summarize, it was observed that the model results almost catch the peak values in stormy days, Comparison plots for the mean wave period of the model and in-situ data indicate that the agreement is for each of the storms. There is no deviation and model estimations catch the peak values .

Error parameters were also calculated for the storms. The calculated error parameters are presented in Table 9.

Table 9. Error Parameters for Hs, Tm, and Direction of SWAN model against the in-situ measurements for the storms

Stormy Dates	RMSE	MAE	SI	R	BIAS	A
Hs	0.602	0.451911	0.394	0.821	0.049	1.016
Tm	0.578	0.449	0.10	0.873	-0.160	1.026
Dir	65.4	50.1				

When the error statistics given in Table 9 are compared with those of Tables 5-6 which shows the comparison for the whole data, it is seen while RMSE and MAE of the error parameters in Hs increase, SI and bias decrease, and the correlation coefficient are better in storms. RMSE and MAE are high because of the higher average values. SI is independent from the average value therefore it shows the nominal decrease in the error. In addition, it is seen that all of the error parameters of Tm are getting smaller in the storm base comparison. The average delta for the stormy period was calculated as 50 and RMSE as 65 degrees. When only the stormy period is considered, it is seen that the model result is better than all the data.

5.2.2. Spectral Analysis

In order to make spectral analysis, the recorded subsurface pressure data (raw data) are converted into the corresponding surface profile data. The surface profile data then undergo to the spectral analysis. In order to convert the subsurface pressure data into surface profile data, the method developed by Hashimoto et al. (1997) based on weakly nonlinear directional wave theory is used.

The standard Fast Fourier Transform (FFT) technique is used to estimate the frequency spectrum from the data of surface profiles, called the observed spectrum hereafter. It is also possible to obtain the frequency spectrum of the wave modeled by SWAN. Figure 45 shows the comparison of observed and the model spectrum for the 3rd storm given in Table 8.

Figure 45 shows that agreement between the observed and the model spectrum is well except the peak of the spectrum (01.02.1995, 21:00). Since the peak value is underestimated by the model, spectrum density values are also lower.

Observed and the model spectrum are also compared in terms of the parameters calculated using spectral moments. These parameters are the peak frequency, fp, spectrum wave height, Hm0, spectrum peakedness parameter, Qp and, spectral width parameter ε. Qp and ε are defined as (Goda, 2010):

$$\varepsilon = \left[1 - m_2^2 / (m_0 m_4)\right]^{1/2} \tag{32}$$

$$Q_p = \frac{2\int_0^\infty f S^2(f) df}{m_0^2} \tag{33}$$

Spectral width parameter, ε takes a value between 0 and 1. And as it becomes close to 1.0, it means that the spectrum becomes broader. Table 10 presents the spectral parameters calculated from the observed and the model spectrum.

As can be seen in Table 10, spectral wave height, peak frequency, and spectral width and peakedness parameters of the observed and the model spectrum are close to each other. It shows that the SWAN model is successful to predict the wave spectrum. Spectral widths are between 0.6-0.76 indicating that the spectrum is not narrow as expected in nature.

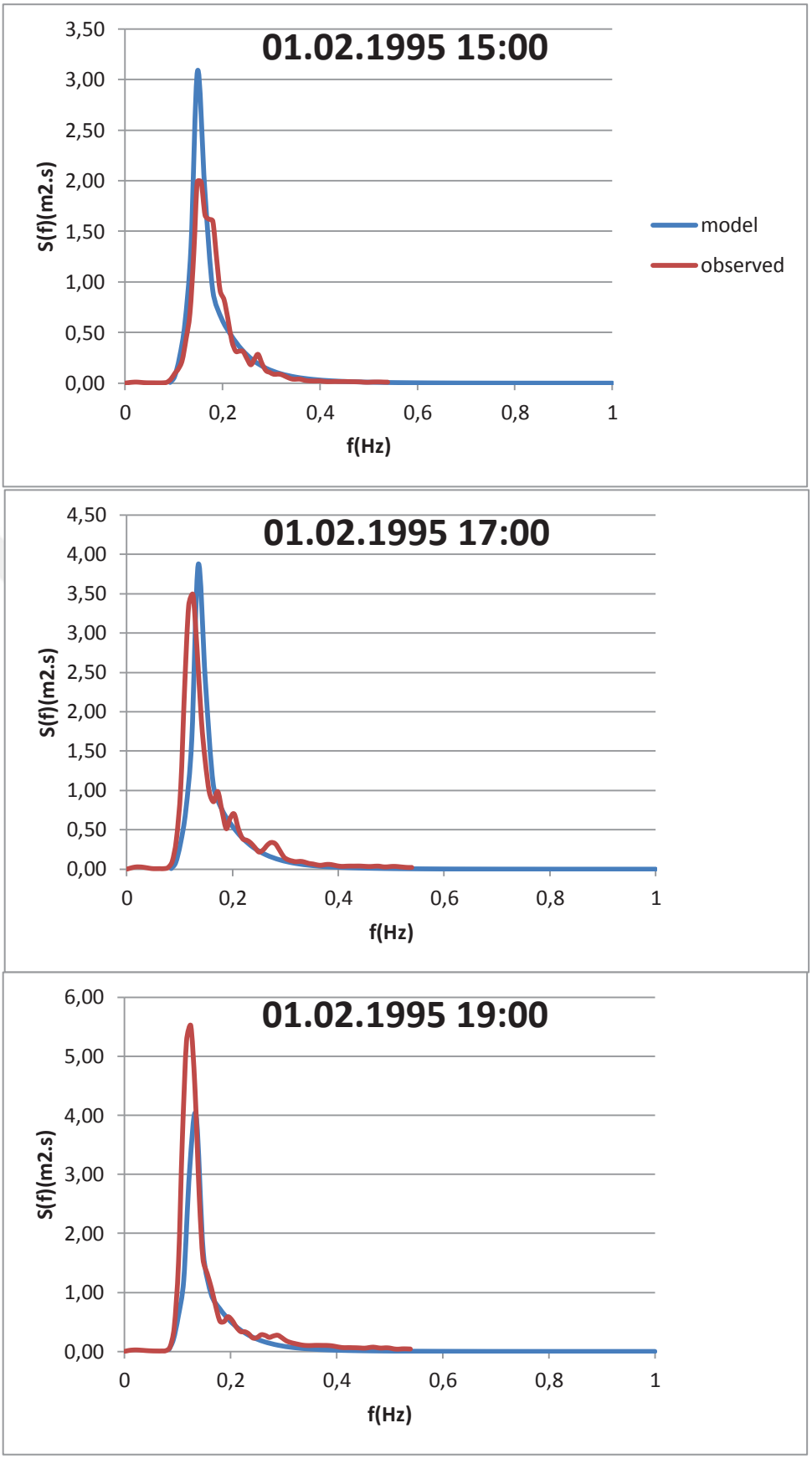

Figure 45. (Cont. on next page)

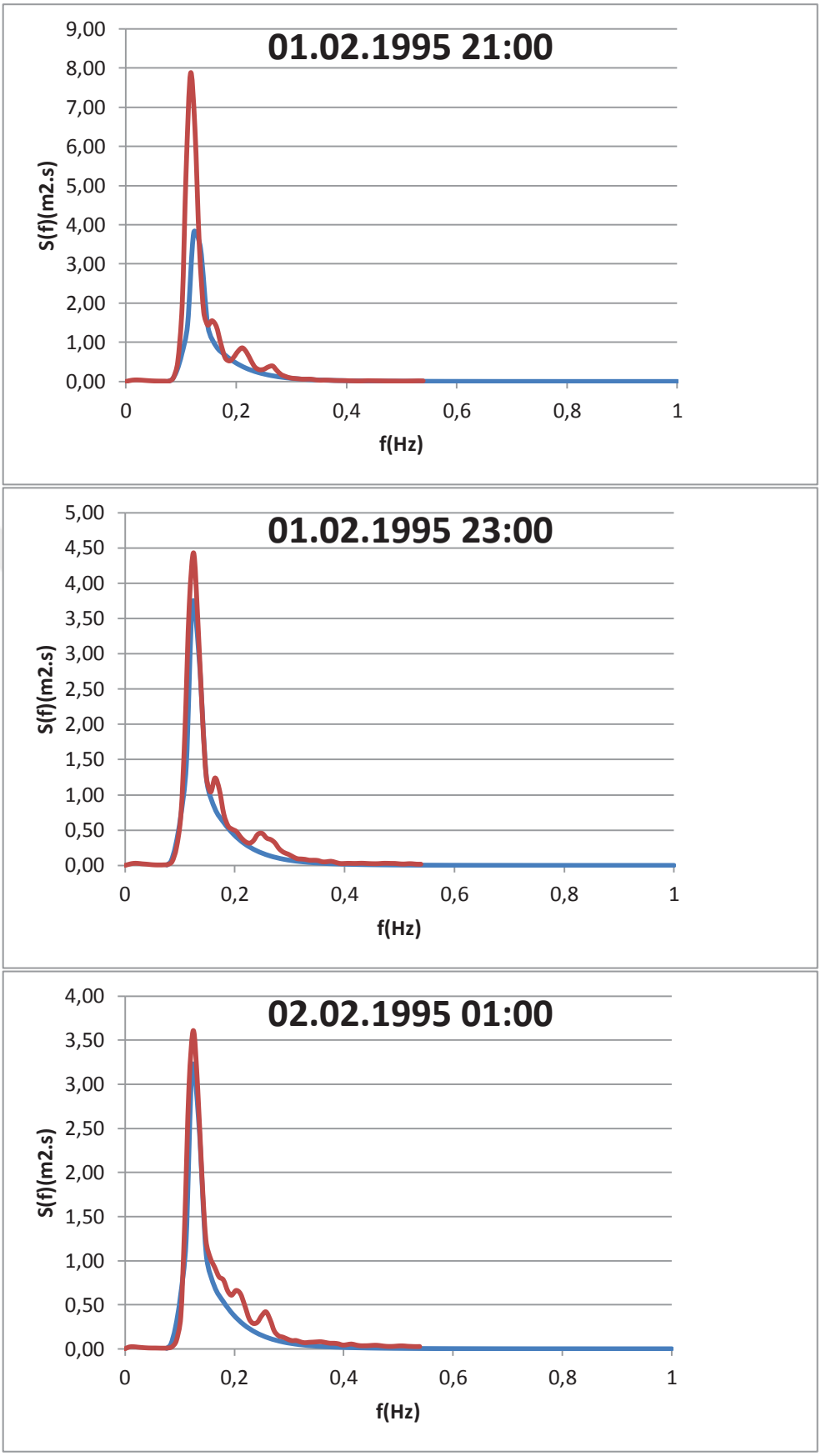

Figure 45. Comparison of the observed and the model spectra (storm 3)(Cont.)

Table 10. Spectral parameters calculated from the observed and the model spectrum.

	Hm0		fp		Qp		spectral width,ε	
TIME	in-situ	model	in-situ	model	in-situ	model	in-situ	model
02.01,15	1.558	1.624	0.156	0.151	2.604	2.912	0.602	0.717
17	1.862	1.719	0.125	0.137	2.122	2.947	0.741	0.733
19	2.150	1.772	0.125	0.133	2.600	2.905	0.778	0.740
21	2.266	1.756	0.117	0.127	2.993	2.891	0.691	0.746
23	1.910	1.683	0.125	0.126	2.438	2.894	0.722	0.751
02.02,01	1.794	1.570	0.125	0.126	2.285	2.872	0.732	0.755
5	1.401	1.308	0.133	0.132	2.896	2.812	0.648	0.760
7	1.309	1.185	0.141	0.135	2.733	2.840	0.686	0.760
9	1.129	1.075	0.141	0.137	2.876	2.858	0.660	0.765
11	0.933	1.072	0.148	0.135	2.667	2.827	0.636	0.761
13	0.913	0.971	0.156	0.139	2.952	2.784	0.663	0.755
17	0.813	0.868	0.164	0.165	2.528	2.875	0.573	0.710

CHAPTER 6

CONCLUSIONS

In this study, nearshore waves along the Filyos, north-western coasts of Turkey were numerically modeled. Widely used 3rd generation wave model, SWAN was used for this purpose. A bathymetry data with a spatial resolution of 10m was used. Era5 re-analysis wave data provided by ECMWF with a time resolution of one hour was inputted as a deep-water boundary. After all necessary files were prepared, the model was run for 2 years (December 1994-December 1996). After the simulation process, results (for wave direction, significant wave height, and mean wave period parameters) were compared with in situ wave data measured in a campaign organized by the Turkish Ministry of Transport for the design of a new port in Filyos. Various error parameters of the square root of the mean square error (RMSE), scattering index (SI), bias, Mean Absolute Error, (MAE), correlation coefficient (R) were calculated for the error assessment study. The comparison study was performed for not only whole data but also for the selected storms with higher waves.

As a result of the performed studies, the following conclusions were drawn:

For the significant wave height parameter, it is seen that the error statistics of the previous studies and the current study are similar. Bingölbali et al. (2019) also found similar error parameters in their study for Filyos. In addition, it was observed that the model gives better results than ERA5 deep-water boundary data as expected. It is also seen in the time series comparison, the model result and the in-situ data fits well. All in all, it can be said that the model performance is good for the significant wave height parameter.

When the average wave period parameter is taken into consideration, it can be said that the results are much better compared to the previous studies and the performance of the model is very good.

For the wave direction comparison, a parameter, Delta, the shortest distance between two different wave directions was calculated to measure the wave direction error statistics. Wave direction comparison shows that the error statistics are higher than

the previous studies. However, model results are slightly better than the model inputs with respect to in-situ measurements. The simulation result shows that the dominant wave direction is North-East (NE) while for in-situ measurements it is North.

A comparison study in the storm base indicates that although the model cannot capture the highest wave height, there is a good agreement between the SWAN model and the in-situ measurement for the storm, especially for the mean wave period. There is still a discrepancy in the wave direction as it is in the case of the comparison for all of the waves. Error assessment for the stormy period shows that the error is small compared to the error values calculated for the whole data.

It is possible to produce different models by changing the options and coefficients in Swan. In order to obtain a better result, appropriate model physics coefficients were determined by sensitivity analysis, thus increasing the model performance for Filyos, the SWAN study area.

The SWAN (Simulating Wave Nearshore) wave prediction model developed by Delft University has been found to be suitable for the Filyos study area using high-resolution bathymetry data, Era5 wave data and with appropriate coefficients.

We can list improvement suggestions for the future wave modeling studies with regular grid method as follows:

1. For the location of where in-situ data are recorded, a higher resolution can be created and focused on that area,
2. The bottom structure can be determined and the friction coefficient can be selected accordingly and
3. Wind data can be used instead of wave data as input in the model.

REFERENCES

Abdalla, Saleh, & Yilmaz, N. 2015. "Suitability of ECMWF ERA-20C for wind and wave climate in the Black Sea. "*12th International Conference on the Mediterranean Coastal Environment, MEDCOAST 2015*, *2*(October), 6–10.

Akpinar, Adem, Gerbrant Ph van Vledder, Murat Ihsan Kömürcü, and Mehmet Özger. 2012. "Evaluation of the Numerical Wave Model (SWAN) for Wave Simulation in the Black Sea." *Continental Shelf Research* 50–51: 80–99. https://doi.org/10.1016/j.csr.2012.09.012.

Akpınar, Adem, Mehmet Ozger, Serkan Bekiroglu, and Murat Ihsan Komurcu. 2014. "Performance Evaluation of Parametric Models in the Hindcasting of Wave Parameters along the South Coast of Black Sea." *Indıan Journal of Geo-Marine Siences* 43 (June): 905-920.

Alves, Jose Henrique G.M., Michael L. Banner, and Ian R. Young. 2003. "Revisiting the Pierson-Moskowitz Asymptotic Limits for Fully Developed Wind Waves." *Journal of Physical Oceanography* 33 (7): 1301–23. https://doi.org/10.1175/1520-0485(2003)033<1301:RTPALF>2.0.CO;2.

Alves, Jose Henrique G.M., and Michael L. Banner. 2003. "Performance of a Saturation-Based Dissipation-Rate Source Term in Modeling the Fetch-Limited Evolution of Wind Waves." *Journal of Physical Oceanography* 33 (6): 1274–98. https://doi.org/10.1175/1520-0485(2003)033<1274:POASDS>2.0.CO;2.

Amarouche, Khalid, Adem Akpınar, Nour El Islam Bachari, Recep Emre Çakmak, and Fouzia Houma. 2019. "Evaluation of a High-Resolution Wave Hindcast Model SWAN for the West Mediterranean Basin." *Applied Ocean Research* 84 (January): 225–41. https://doi.org/10.1016/j.apor.2019.01.014.

Battjes, J. A., and J. P.F.M. Janssen. 1979. "Energy Loss and Set-Up Due To Breaking of Random Waves." *Proceedings of the Coastal Engineering Conference* 1 (August 1978): 569–87. https://doi.org/10.9753/icce.v16.32.

Benoit, M, F Marcos, and F Becq. 1996. "CHAPTER 37 DEVELOPMENT OF A THIRD GENERATION SHALLOW-WATER WAVE MODEL WITH UNSTRUCTURED SPATIAL MESHING Michel BENOIT ', Frederic MARCOS \ Franchise BECQ 2." *Coastal Engineering*, 465–78. https://doi.org/10.9753/ICCE.V25.%P.

Bilyay, E., B. O. Ozbahceci, and A. C. Yalciner. 2011. "Extreme Waves at Filyos, Southern Black Sea." *Natural Hazards and Earth System Science* 11 (3): 659–66. https://doi.org/10.5194/nhess-11-659-2011.

Bingölbali, Bilal, Adem Akpınar, Halid Jafali, and Gerbrant Ph Van Vledder. 2019. "Downscaling of Wave Climate in the Western Black Sea." *Ocean Engineering* 172 (November 2018): 31–45. https://doi.org/10.1016/j.oceaneng.2018.11.042.

Booij, N., R. C. Ris, and L. H. Holthuijsen. 1999. “A Third-Generation Wave Model for Coastal Regions 1. Model Description and Validation.” *Journal of Geophysical Research: Oceans* 104 (C4): 7649–66. https://doi.org/10.1029/98JC02622.

Cherneva, Z., N. Andreeva, P. Pilar, N. Valchev, P. Petrova, and C. Guedes Soares. 2008. “Validation of the WAMC4 Wave Model for the Black Sea.” *Coastal Engineering* 55 (11): 881–93. https://doi.org/10.1016/j.coastaleng.2008.02.028.

J. Ian Collins. 1972. “Prediction of shallow water spectra.” *Journal of Geophysıcal Research* 77 (15) **:** 2693- 2707.

ECMWF. (n.d.). ERA 5. Retrieved from https://www.ecmwf.int/en/forecasts/datasets/reanalysis-datasets/era5

Eldeberky, Y. 1996. “Nonlinear Transformation of Wave Spectra in the Nearshore Zone.” *Communications on Hydraulic and Geotechnical Engineering - Delft University of Technology* 96 (4): 200.

Eldeberky, Yasser, and Jurjen A. Battjes. 1996. “Spectral Modeling of Wave Breaking: Application to Boussinesq Equations.” *Journal of Geophysical Research C: Oceans* 101 (C1): 1253–64. https://doi.org/10.1029/95JC03219.

Engin, Ayşen. 2009. “ Coastal Engineering.”*Middle East Technical University Development Foundation, METU press.*(p.365).

Goda, Y. 2010. "Random Seas and Design of Maritime Structures. "In *Advanced Series on Ocean Engineering* (3rd ed., p. 732).

Günther, H., S. Hasselman, and P.A.E.M. Jansen. 1992. “The WAM Model Cycle 4.” *Technical Report 4, DKRZ* 1992 (4).

Hashimoto, Noriaki, Sidney W. Thurston and Masao Mitsui. 1998. “Surface Wave Recovery from Subsurface Pressure Records on the Basis of Weakly Nonlinear Directional Wave Theory.” *Proceedings of the 1997 3rd International Symposium on Ocean Wave Measurement and Analysis, WAVES - Virginia Beach, VA, USA* (January) : 869-882.

Hasselmann, K., T. P. Barnett, E. Bouws, H. Carlson, D. E. Cartwright, K. Eake, J. A. Euring, et al. 1973. “Measurements of Wind-Wave Growth and Swell Decay during the Joint North Sea Wave Project (JONSWAP).,” no. July 2015.

Hasselmann, K., W. Sell, D.B. Ross, and P. Müller. 1976. “A Parametric Wave Prediction Model. ” *J. Phys. Oceanogr.,* **6**, 200–228. https://doi.org/10.1175/1520-0485(1976)006<0200:APWPM>2.0.CO;2.

Hasselmann, S., K. Hasselmann, J. H. Allender, and T. P. Barnett. 1985. “Computations and Parameterizations of the Nonlinear Energy Transfer in a Gravity-Wave Spectrum. Part II: Parameterizations of the Nonlinear Energy Transfer for Application in Wave Models.” *J. Phys. Oceanogr.* https://doi.org/10.1175/1520-0485(1985)015<1378:capotn>2.0.co;2.

Hasselmann, Klaus, S. Hasselmann, E. Bauer, P. A.E.M. Janssen, G. J. Komen, L. Bertotti, P. Lionello, et al. 1988. “The WAM Model - a Third Generation Ocean

Wave Prediction Model." *J. Phys. Oceanogr.* https://doi.org/10.1175/1520-0485(1988)018<1775:twmtgo>2.0.co;2.

Inghilesi, R., F. Catini, G. Bellotti, L. Franco, A. Orasi, and S. Corsini. 2012. "Implementation and Validation of a Coastal Forecasting System for Wind Waves in the Mediterranean Sea." *Natural Hazards and Earth System Science* 12 (2): 485–94. https://doi.org/10.5194/nhess-12-485-2012.

Ippen, Arthur T. 1966. "Estuary and Coastline Hydrodynamics." *Engineering Societies Monographs* (1st ed.,p. 744).

Janssen, P. A.E.M. 1991a. "Quasi-Linear Theory of Wind-Wave Generation Applied to Wave Forecasting." *J. PHYSICAL OCEANOGRAPHY* 21 (11): 1631–42. https://doi.org/10.1175/1520-0485(1991)021<1631:QLTOWW>2.0.CO;2.

Janssen, P.A.E.M. 1991b. " Consequences of the effect of surface gravity waves on the mean air flow" *Int. Union of Theor. and Appl. Mech*. (IUTAM), Sydney, Australia : 193-198.

Komen, G. J., S. Hasselmann, and K. Hasselmann. 1984. "On the Existence of a Fully Developed Wind-Sea Spectrum." *J. Phys. Oceanogr.* 14 (8, Aug. 1984): 1271–85. https://doi.org/10.1175/1520-0485(1984)014<1271:oteoaf>2.0.co;2.

Komen, G.J., L. Cavaleri, M. Donelan, K. Hasselmann, S. Hasselmann, and P.A.E.M. Janssen. n.d. 1994. "Dynamics and Modelling of Ocean Waves." *Earth Science Reviews*, 111–13.

Kutupoğlu, Volkan, Recep Emre Çakmak, Adem Akpınar, and Gerbrant Ph van Vledder. 2018. "Setup and Evaluation of a SWAN Wind Wave Model for the Sea of Marmara." *Ocean Engineering*165(July): 450–64. https://doi. org/10.1016/j. oceaneng.2018.07.053.

Luigi Cavaleri, Paola Malanotte Rizzoli. 1981. "Wind wave prediction in shallo water: Theory and applications." *Journal of Geophysical Research: Oceans* 86(C11) (November): 10961-10973.

Madsen, Ole Secher, and Moises Michel Rosengaus. 1988. "Spectral Wave Attenuation by Bottom Friction: Experiments," no. November: 849–57. https://doi.org/10.9753/icce.v21.63.

Mahmoudof, Seyed Masoud, Peyman Badiei, Seyed Mostafa Siadatmousavi, and Vahid Chegini. 2018. "Spectral Wave Modeling in Very Shallow Water at Southern Coast of Caspian Sea." *Journal of Marine Science and Application* 17 (1): 140–51. https://doi.org/10.1007/s11804-018-0011-y.

Mandal, S., and N. Prabaharan. 2010. "Ocean Wave Prediction Using Numerical and Neural Network Models." *The Open Ocean Engineering Journal* 3 (1): 12–17. https://doi.org/10.2174/1874835x01003010012.

Moeini, M. H., and A. Etemad-Shahidi. 2009. "Wave Parameter Hindcasting in a Lake Using the SWAN Model." *Scientia Iranica* 16 (2 A): 156–64.

Mulligan, R. P., A. J. Bowen, A. E. Hay, A. J. Van Der Westhuysen, and J. A. Battjes.

2007. “Whitecapping and Wave Field Evolution in a Coastal Bay.” *Journal of Geophysical Research: Oceans* 113 (3). https://doi.org/10.1029/2007JC004382.

Nelson, Richard Carroll. 1987. “Design wave heights on very mild slopes — an experimental study.” *Civil. Eng. Trans., Inst. Eng.* 29(Agus): 157-161.

Ou, Shan Hwei, Jian Ming Liau, Tai Wen Hsu, and Shiaw Yih Tzang. 2002. “Simulating Typhoon Waves by SWAN Wave Model in Coastal Waters of Taiwan.” *Ocean Engineering* 29 (8): 947–71. https://doi.org/10.1016/S0029-8018(01)00049-X.

Ozbahceci B.O.2019. “Extreme value statistics of wind speed and wave height of the Marmara Sea based on combined radar altimeter data.” *Advances in Space Research, in press,* https://doi.org/10.1016/j.asr.2019.08.025.

Ozhan, E. ve Abdalla, S. 1999. “Turkish Coast Wind and Deep Water Wave Atlas, Applied Project Report.” *Middle East Technical University, Civil Engineering Department, Ocean Engineering Research Center*, Ankara, Turkey.

Ruessink, B. G., D. J.R. Walstra, and H. N. Southgate. 2003. “Calibration and Verification of a Parametric Wave Model on Barred Beaches.” *Coastal Engineering* 48 (3): 139–49. https://doi.org/10.1016/S0378-3839(03)00023-1.

Rusu, L, P Pilar, and C Guedes Soares. 2005. “Hindcasts of the Wave Conditions in Approaches to Ports of the North of Portugal,” no. May 2014.

Rusu, L., M. Bernardino, and C. Guedes Soares. 2014. “Wind and Wave Modelling in the Black Sea.” *Journal of Operational Oceanography* 7 (1): 5–20. https://doi.org/10.1080/1755876X.2014.11020149.

Salmon, J. E., L. H. Holthuijsen, M. Zijlema, G. Ph van Vledder, and J. D. Pietrzak. 2015. “Scaling Depth-Induced Wave-Breaking in Two-Dimensional Spectral Wave Models.” *Ocean Modelling* 87: 30–47. https://doi.org/10.1016/j.ocemod.2014.12.011.

Snyder, R. L., F. W. Dobson, J. A. Elliott, and R. B. Long. 1981. “Array Measurements of Atmospheric Pressure Fluctuations above Surface Gravity Waves.” Journal of Fluid Mechanics 102. Cambridge University Press: 1–59. doi:10.1017/S0022112081002528

Siadatmousavi, S. Mostafa, F. Jose, and G. W. Stone. 2012. “On the Importance of High Frequency Tail in Third Generation Wave Models.” *Coastal Engineering* 60 (1): 248–60. https://doi.org/10.1016/j.coastaleng.2011.10.007.

SWAN 2013a. SWAN Cycle III Version 40.91AB User Manual *SWAN Team, Delft University of Technology, Netherlands*.

SWAN 2013b. SWAN Cycle III Version 40.91AB Scientific And Technical Thornton, E.B. and R.T. Guza.1983. Transformation of wave height distribution, *J. Geophys. Res.* 88, C10:5925-5938.

Tolman, Hendrik L. 1991. “A Third-Generation Model for Wind Waves on Slowly Varying, Unsteady and Inhomogeneous Depths and Currents.” *Journal of Physical*

Oceanography 21 (6): 782–97.

Thornton, E. B., and R. T. Guza. 1983. "Transformation of Wave Height Distribution." *Journal of Geophysical Research* 88 (C10): 5925–38. https://doi.org/10.1029/JC088iC10p05925.

Turgut, Ahmet. 2019. " Derivation of Century-Based Wave Climate and Extreme Wave Analysıs Along Turkish Coasts ." Izmir Institute Of Technology (July, p. 103).

Umesh, P. A., Prasad K. Bhaskaran, K. G. Sandhya, and T. M. Balakrishnan Nair. 2017. "An Assessment on the Impact of Wind Forcing on Simulation and Validation of Wave Spectra at Coastal Puducherry, East Coast of India." *Ocean Engineering* 139 (September): 14–32. https://doi.org/10.1016/j.oceaneng.2017.04.043.

Valchev, N. N., E. V. Trifonova, and N. K. Andreeva. 2012. "Past and Recent Trends in the Western Black Sea Storminess." *Natural Hazards and Earth System Science* 12 (4): 961–77. https://doi.org/10.5194/nhess-12-961-2012.

Westhuysen, André J. van der, Marcel Zijlema, and Jurjen A. Battjes. 2007. "Nonlinear Saturation-Based Whitecapping Dissipation in SWAN for Deep and Shallow Water." *Coastal Engineering* 54 (2): 151–70. https://doi.org/10.1016/j.coastaleng.2006.08.006.

Wu, Jin. 1982. "Wind-stress coefficients over sea surface from breeze to hurricane." *J. Geophys. Res*. 87, C12 :9704-9706.

Yan, L. 1987. "An Improved Wind Input Source Term for Third Generation Ocean Wave Modelling." http://publicaties.minienm.nl/documenten/an-improved-wind-input-source-term-for-third-generation-ocean-wa%0Apapers2://publication/uuid/3D3F948F-8ED5-4866-9E0A-743D454BA05C.

Zijlema, M., G. Ph Van Vledder, and L. H. Holthuijsen. 2012. "Bottom Friction and Wind Drag for Wave Models." *Coastal Engineering* 65: 19–26. https://doi.org/10.1016/j.coastaleng.2012.03.002.

APPENDIX A

TIME SERIES COMPARISON

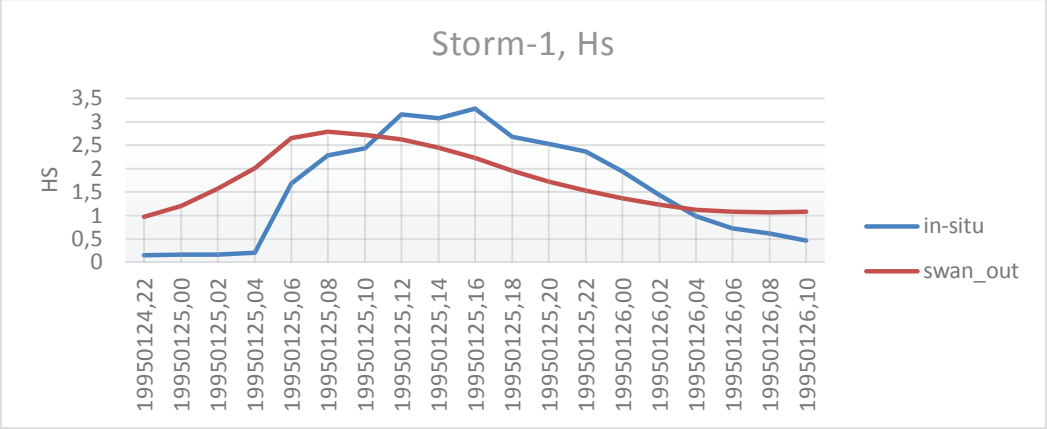

Figure 46. Time-series comparison for Hs of in-situ measurement and SWAN-out for the storm-1,

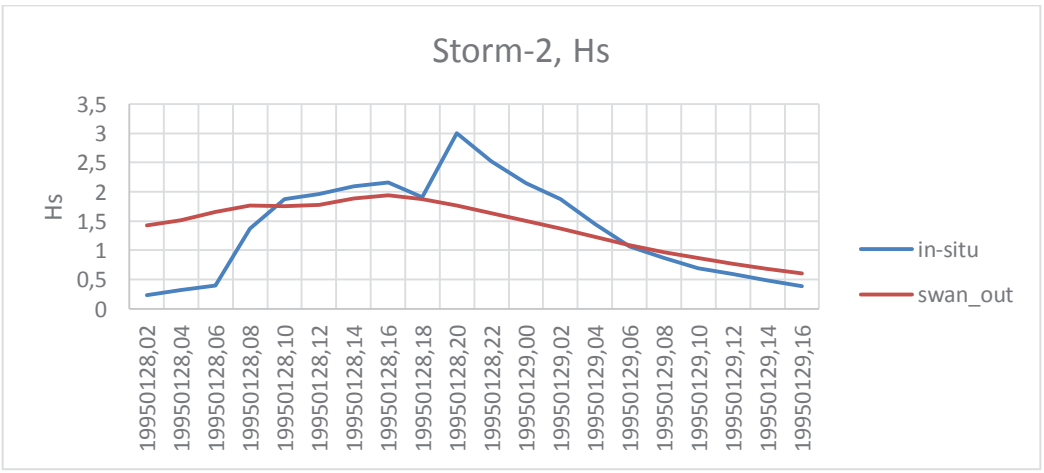

Figure 47. Time-series comparison for Hs of in-situ measurement and SWAN-out for the storm-2,

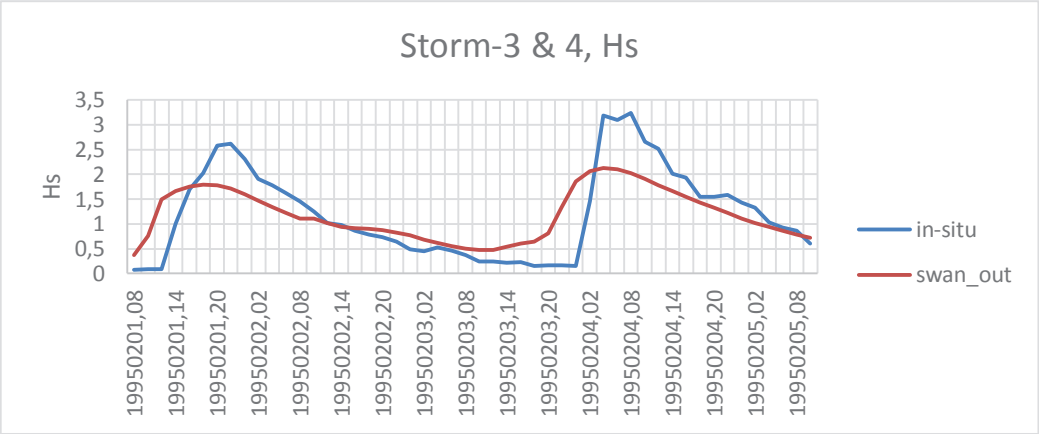

Figure 48 .Time-series comparison for Hs of in-situ measurement and SWAN-out for the storm-3-4,

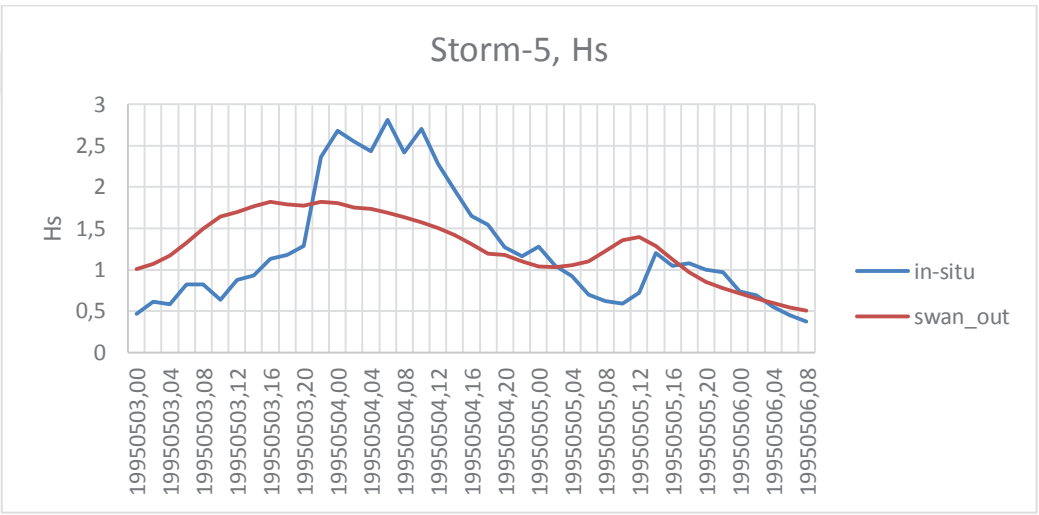

Figure 49. Time-series comparison for Hs of in-situ measurement and SWAN-out for the storm-5,

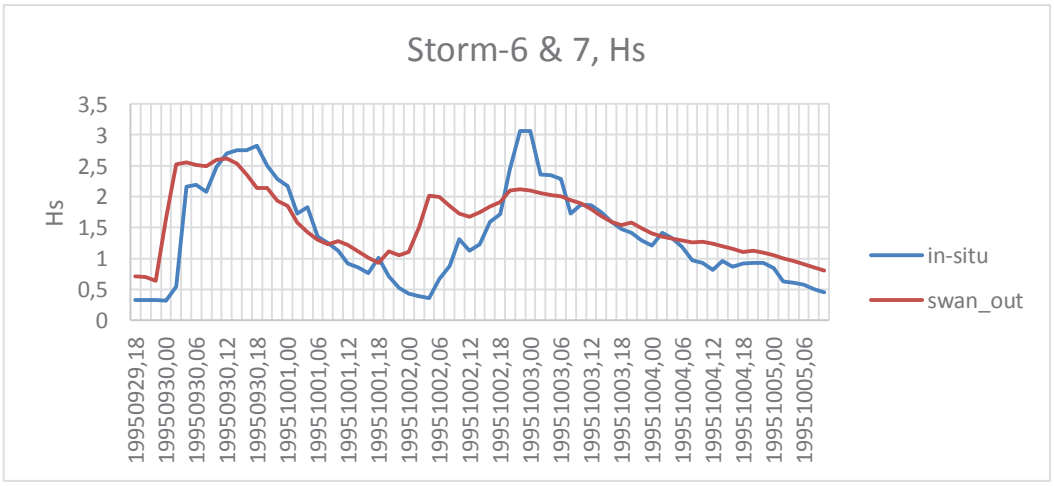

Figure 50. Time-series comparison for Hs of in-situ measurement and SWAN-out for the storm6-7,

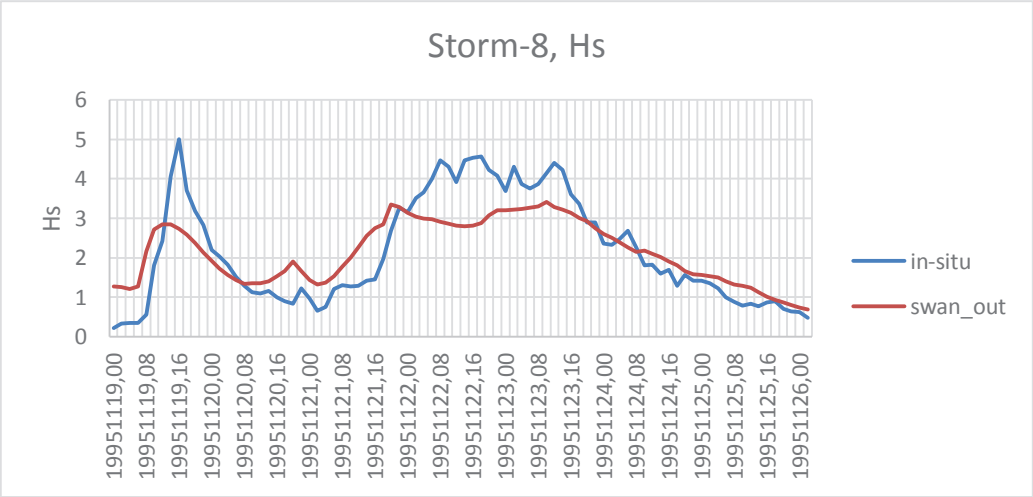

Figure 51. Time-series comparison for Hs of in-situ measurement and SWAN-out for the storm-8,

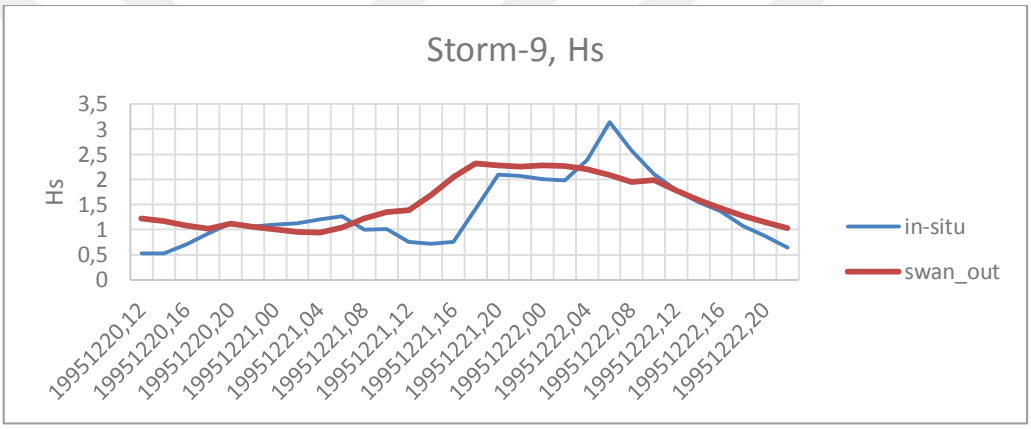

Figure 52. Time-series comparison for Hs of in-situ measurement and SWAN-out for the storm-9,

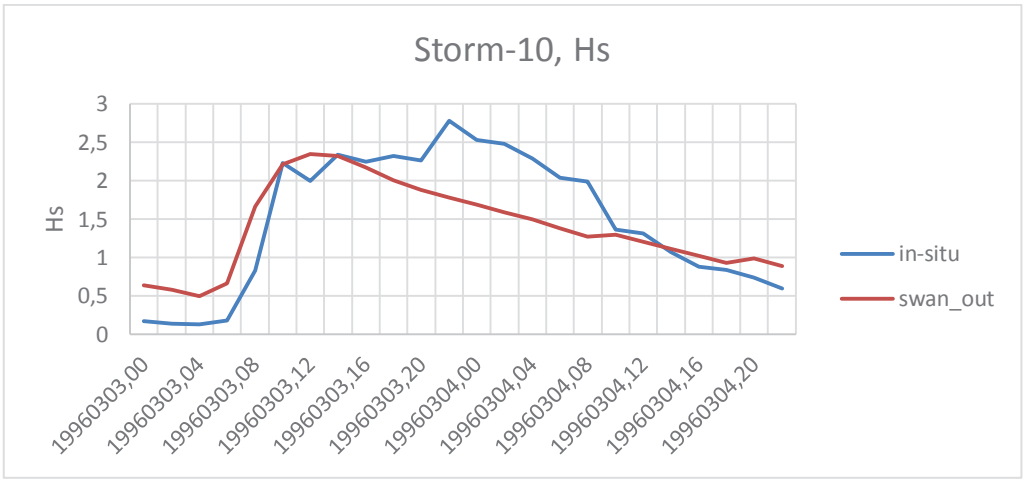

Figure 53. Time-series comparison for Hs of in-situ measurement and SWAN-out for the storm-10,

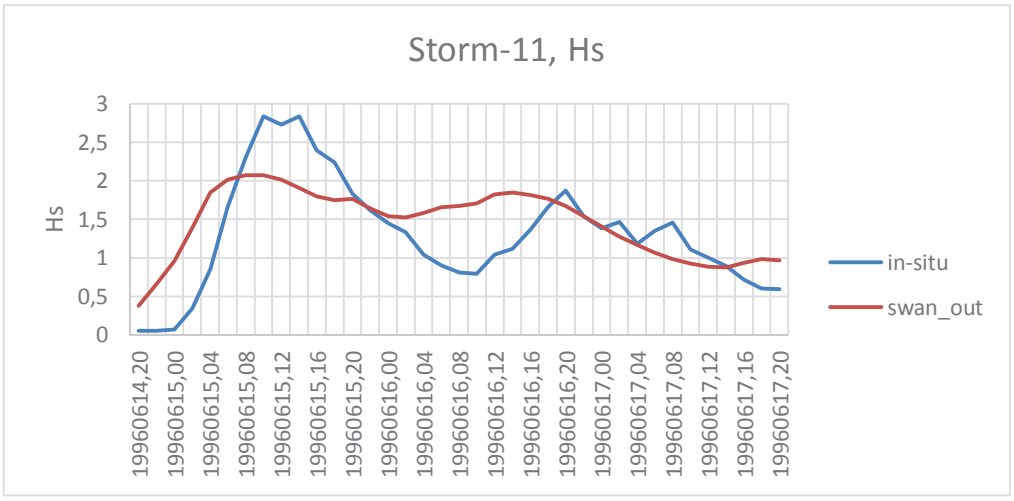

Figure 54.Time-series comparison for Hs of in-situ measurement and SWAN-out for the storm-11,

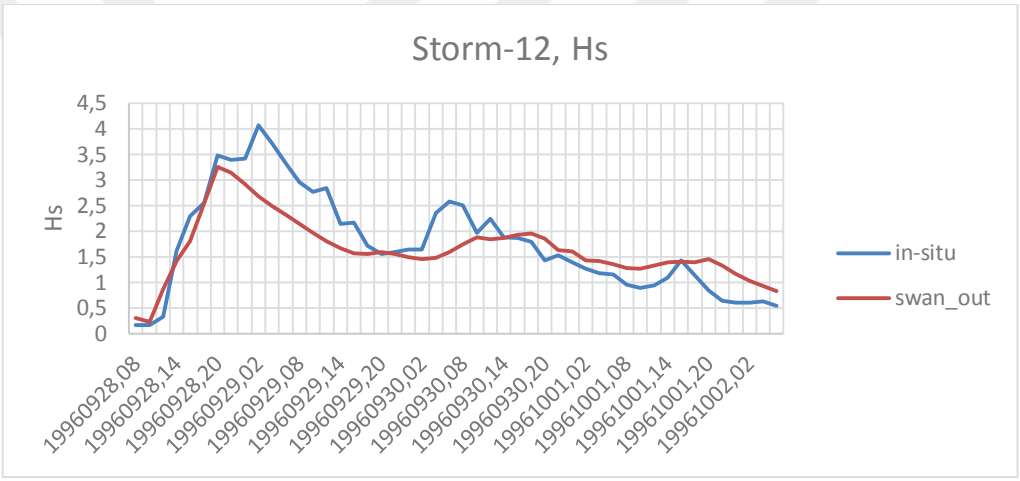

Figure 55.Time-series comparison for Hs of in-situ measurement and SWAN-out for the storm-12,

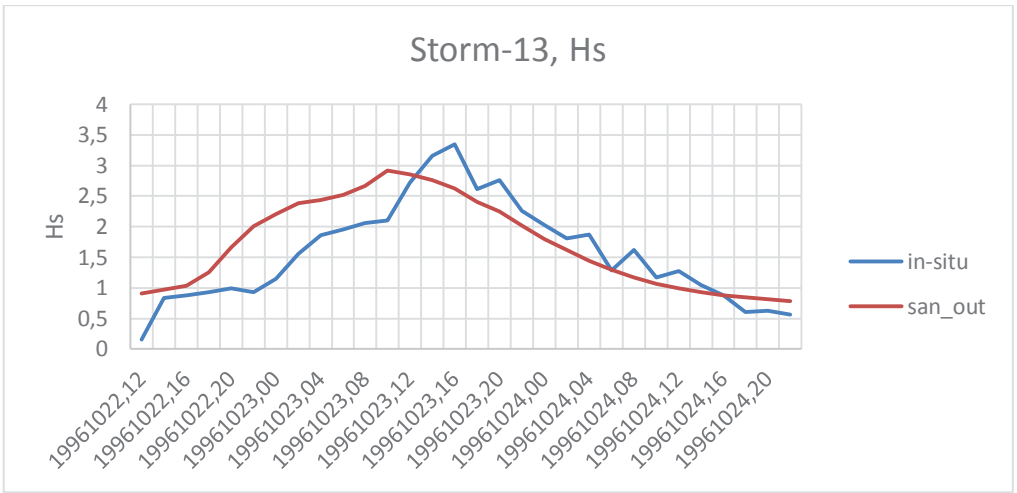

Figure 56.Time-series comparison for Hs of in-situ measurement and SWAN-out for the storm-13,

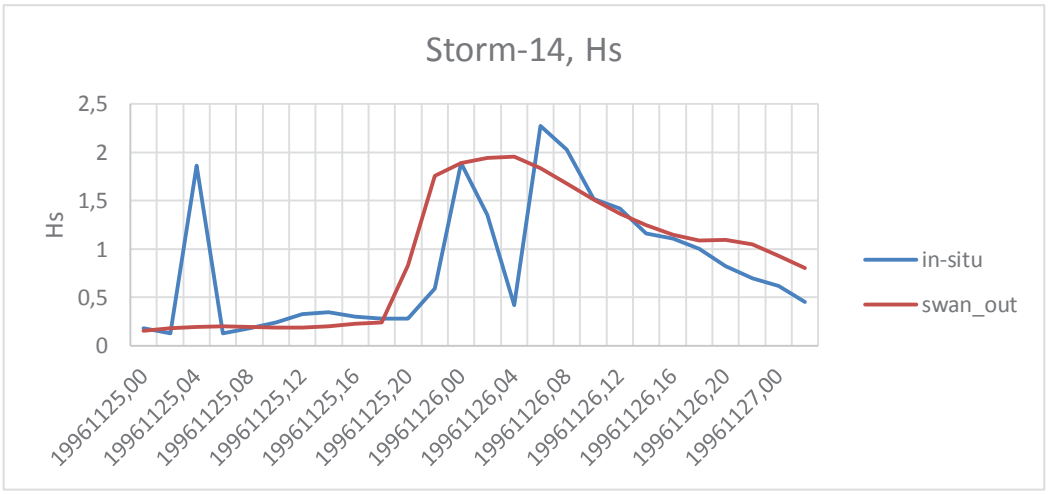

Figure 57.Time-series comparison for Hs of in-situ measurement and SWAN-out for the storm-14,

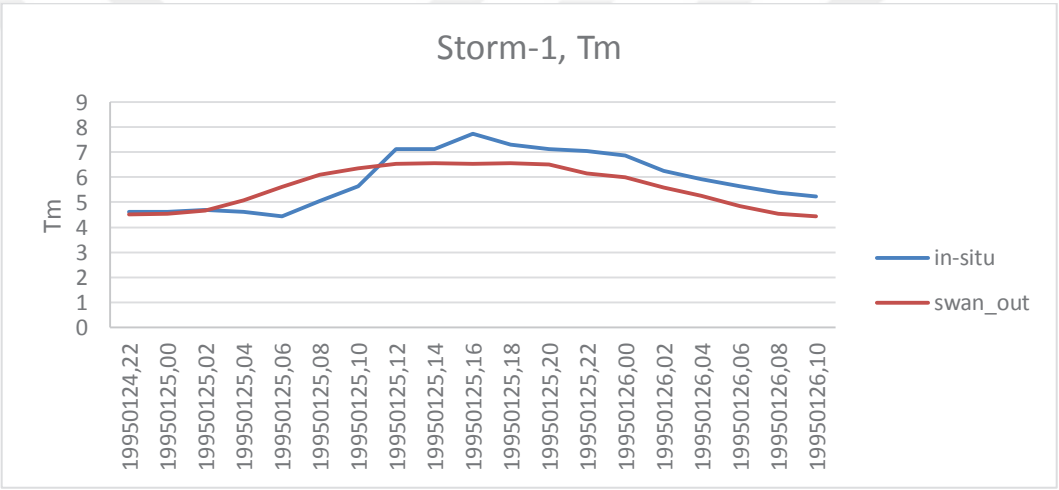

Figure 58.Time-series comparison for Tm of in-situ measurement and SWAN-out for the storm-1,

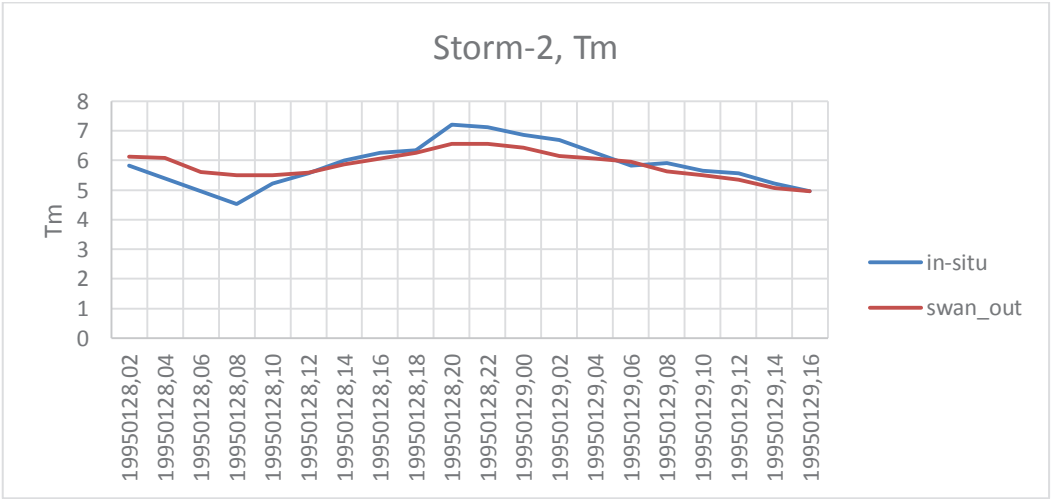

Figure 59. Time-series comparison for Tm of in-situ measurement and SWAN-out for the storm-2,

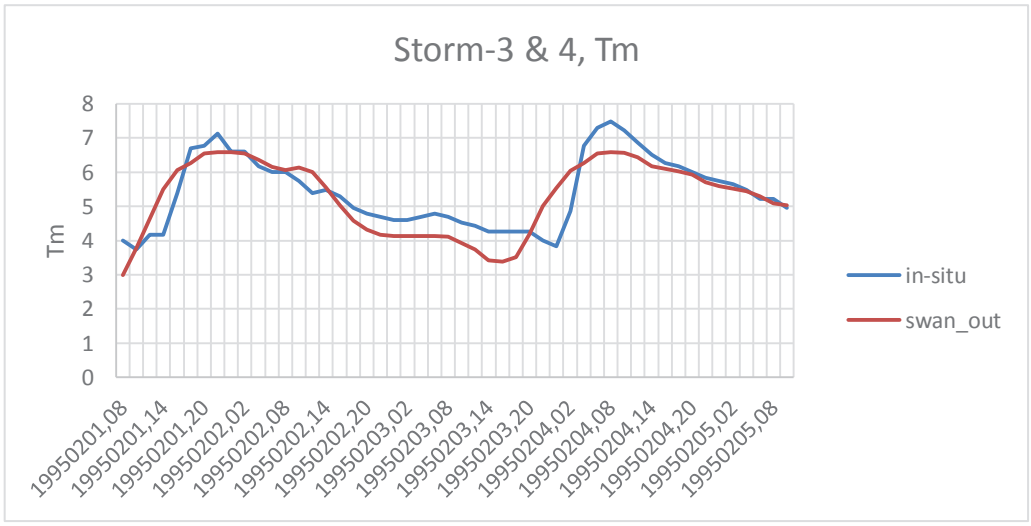

Figure 60. Time-series comparison for Tm of in-situ measurement and SWAN-out for the storm-3-4,

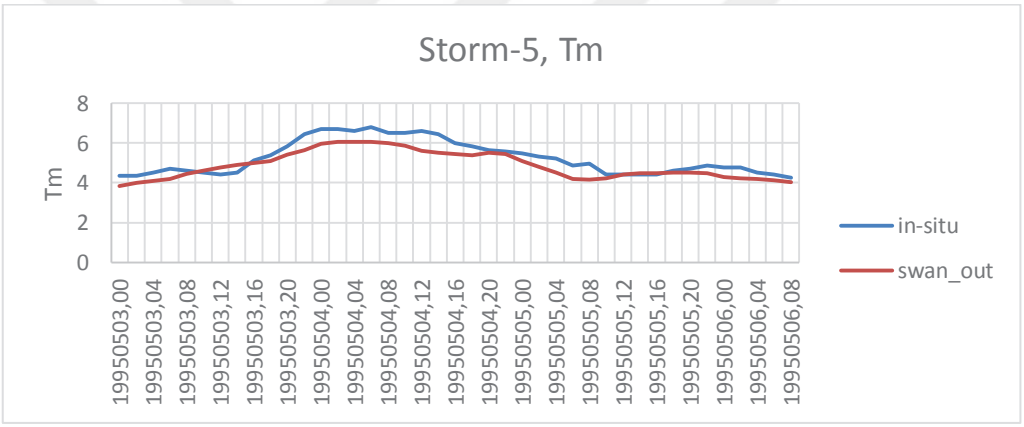

Figure 61.Time-series comparison for Tm of in-situ measurement and SWAN-out for the storm-5,

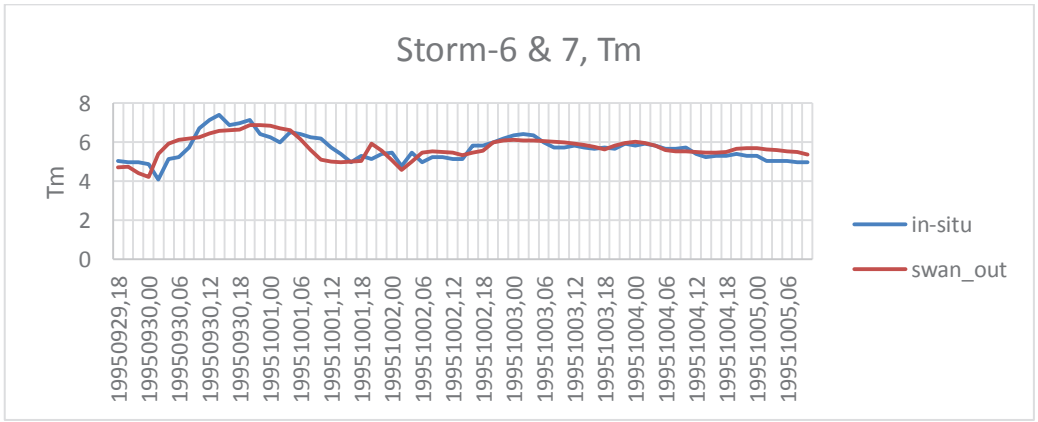

Figure 62.Time-series comparison for Tm of in-situ measurement and SWAN-out for the storm-6-7,

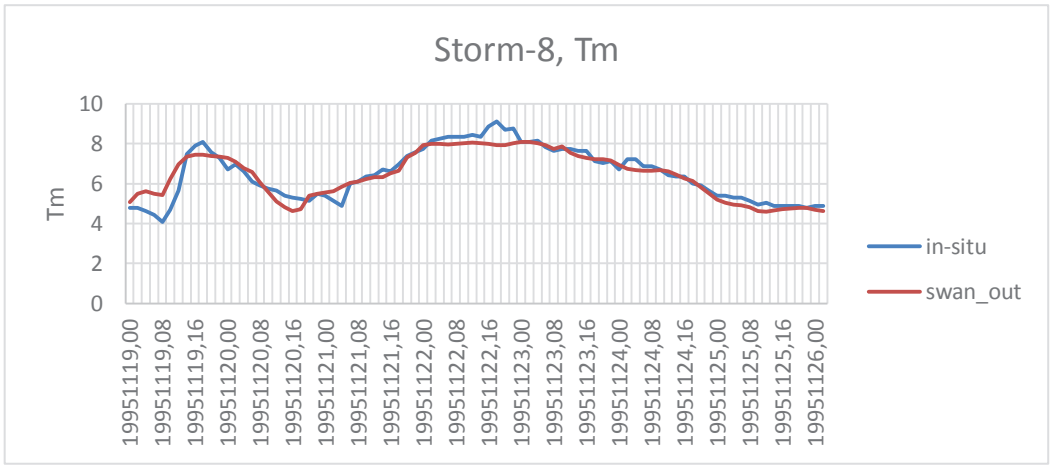

Figure 63.Time-series comparison for Tm of in-situ measurement and SWAN-out for the storm-8,

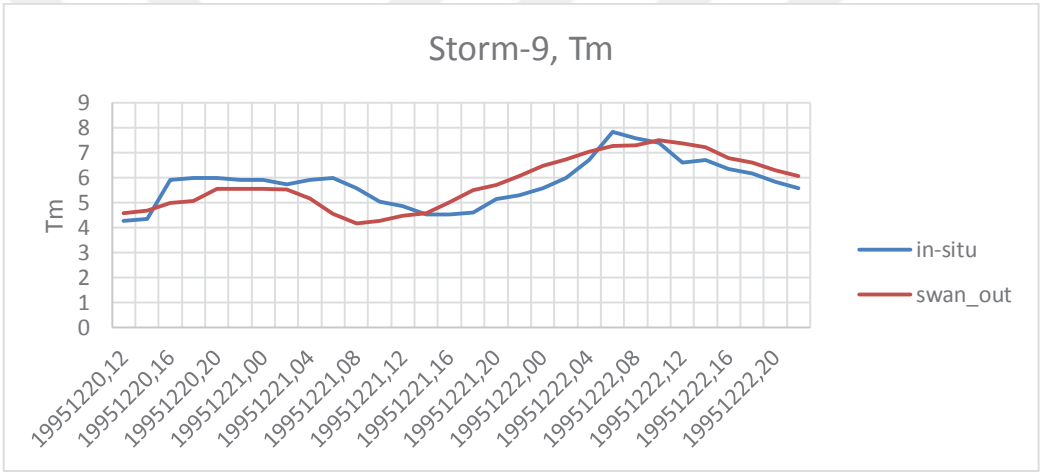

Figure 64.Time-series comparison for Tm of in-situ measurement and SWAN-out for the storm-9,

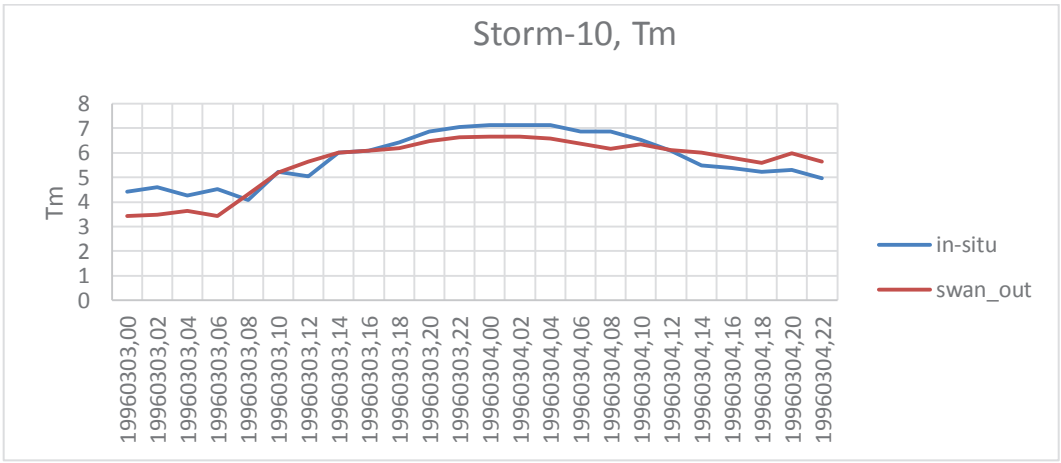

Figure 65.Time-series comparison for Tm of in-situ measurement and SWAN-out for the storm-10,

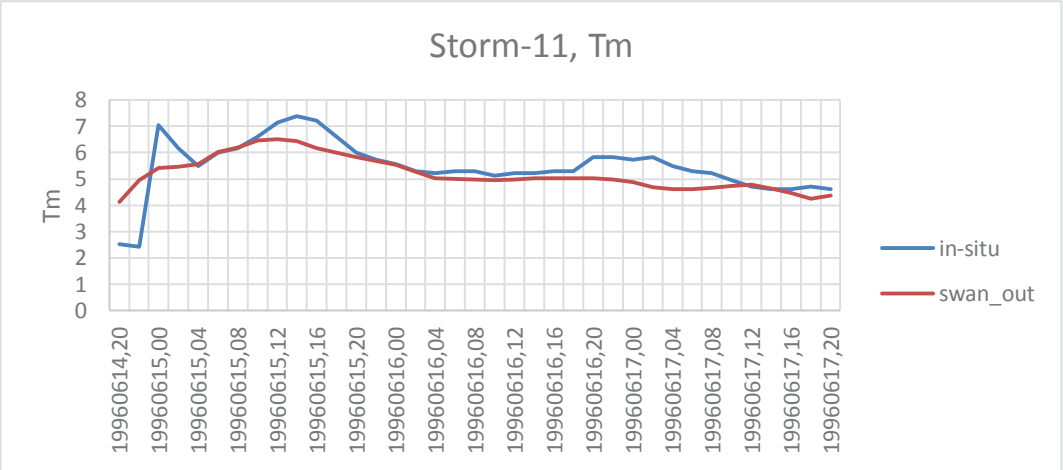

Figure 66.Time-series comparison for Tm of in-situ measurement and SWAN-out for the storm-11,

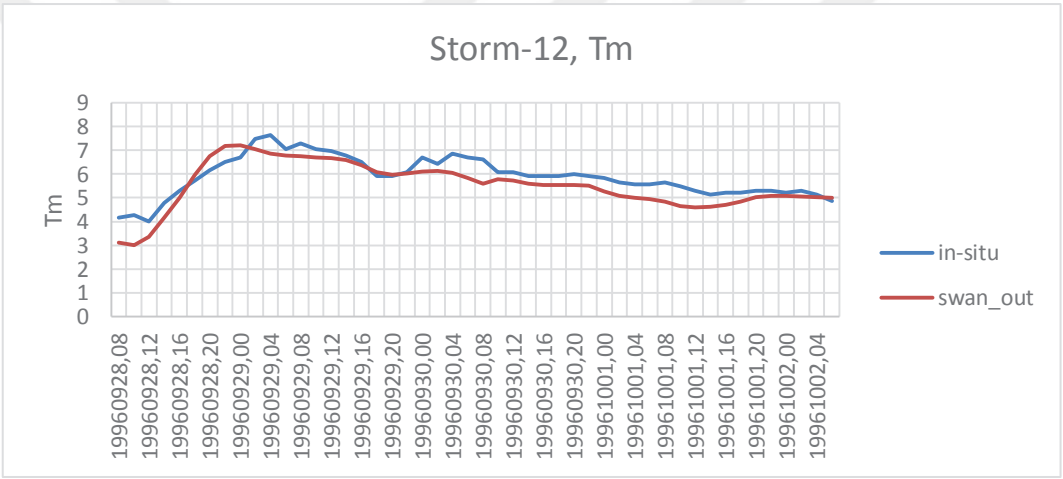

Figure 67.Time-series comparison for Tm of in-situ measurement and SWAN-out for the storm-12,

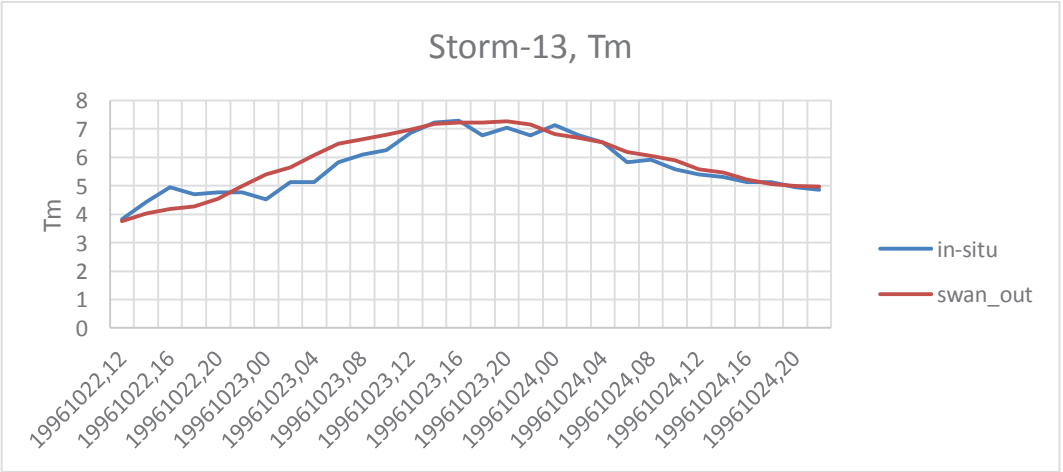

Figure 68.Time-series comparison for Tm of in-situ measurement and SWAN-out for the storm-13,

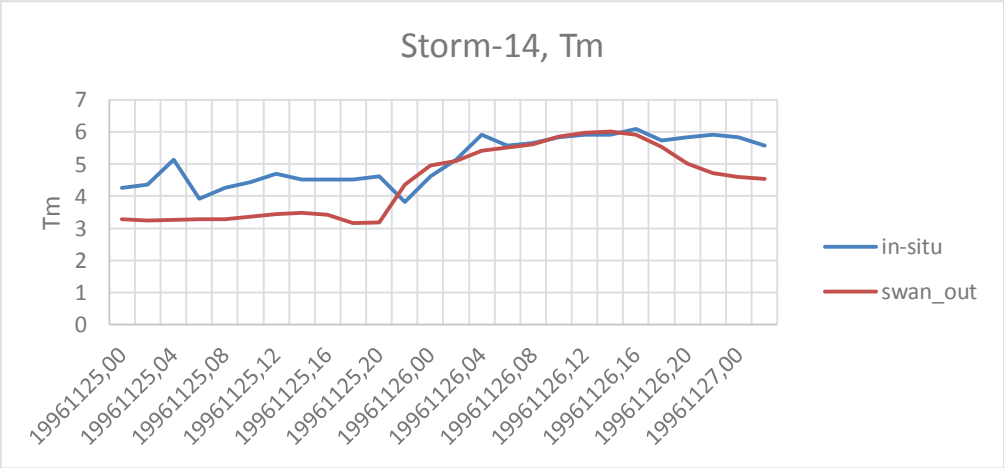

Figure 69.Time-series comparison for Tm of in-situ measurement and SWAN-out for the storm-14,

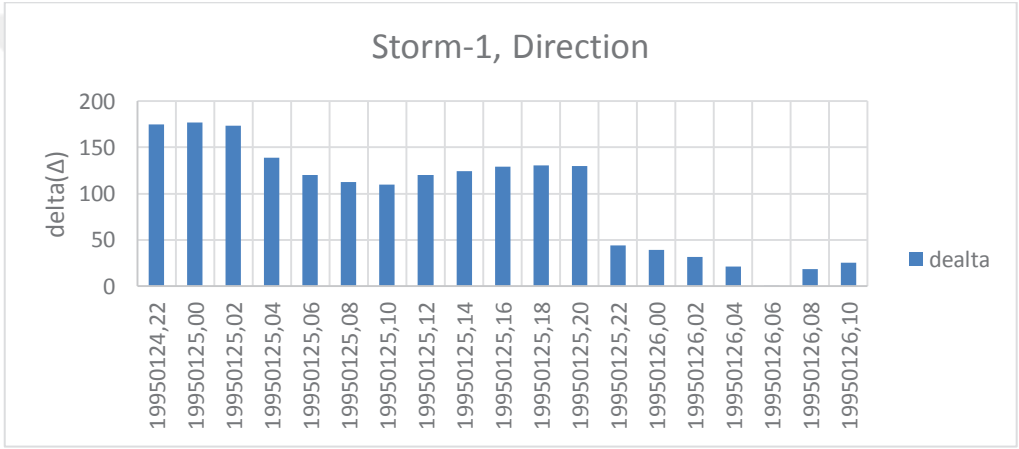

Figure 70.Time-series comparison for the direction of in-situ measurement and SWAN-out for the storm-1,

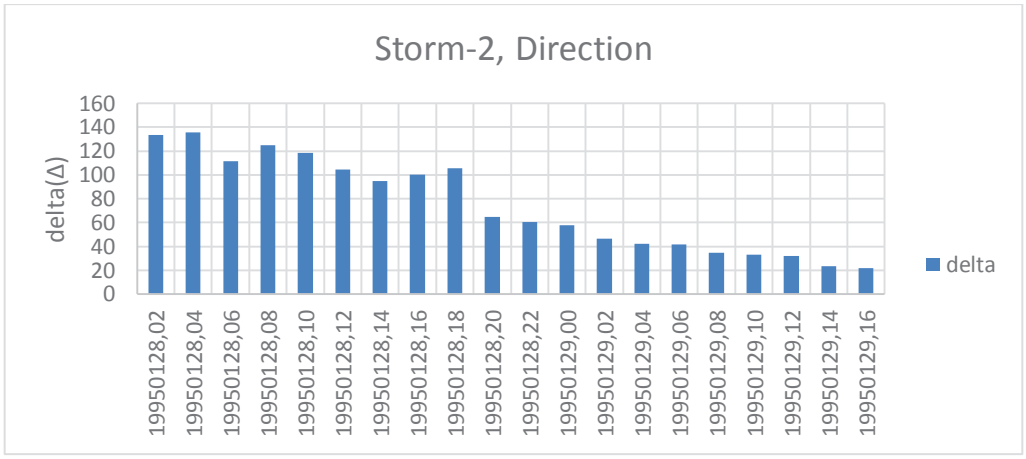

Figure 71.Time-series comparison for the direction of in-situ measurement and SWAN-out for the storm-2,

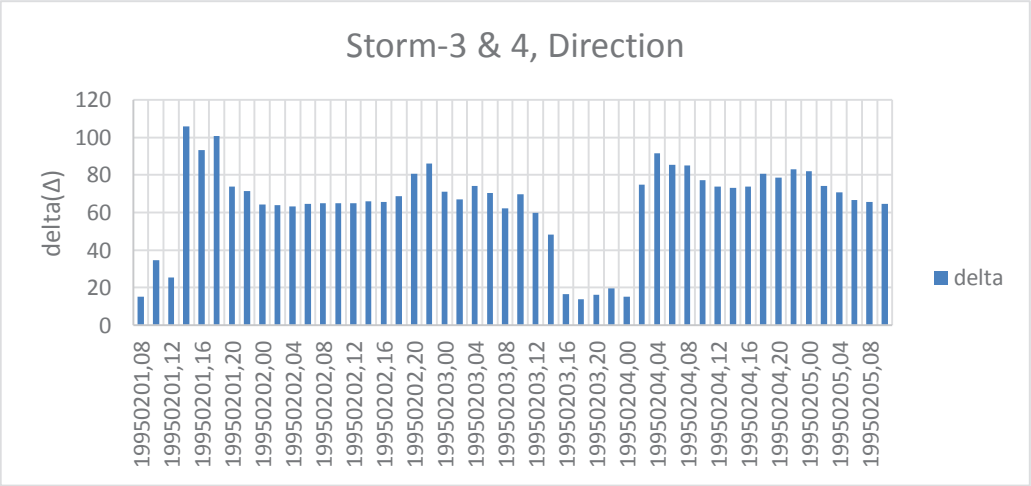

Figure 72.Time-series comparison for the direction of in-situ measurement and SWAN-out for the storm-3-4,

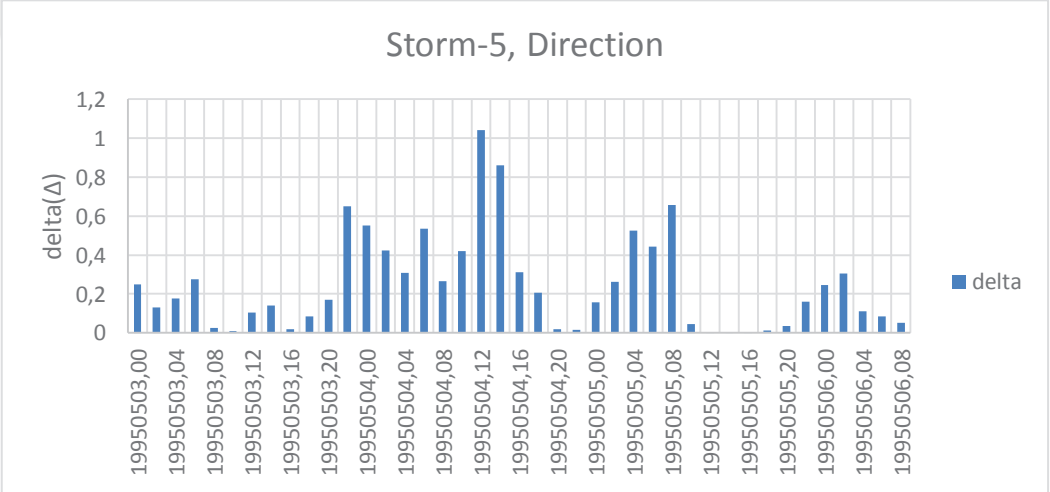

Figure 73.Time-series comparison for the direction of in-situ measurement and SWAN-out for the storm-5,

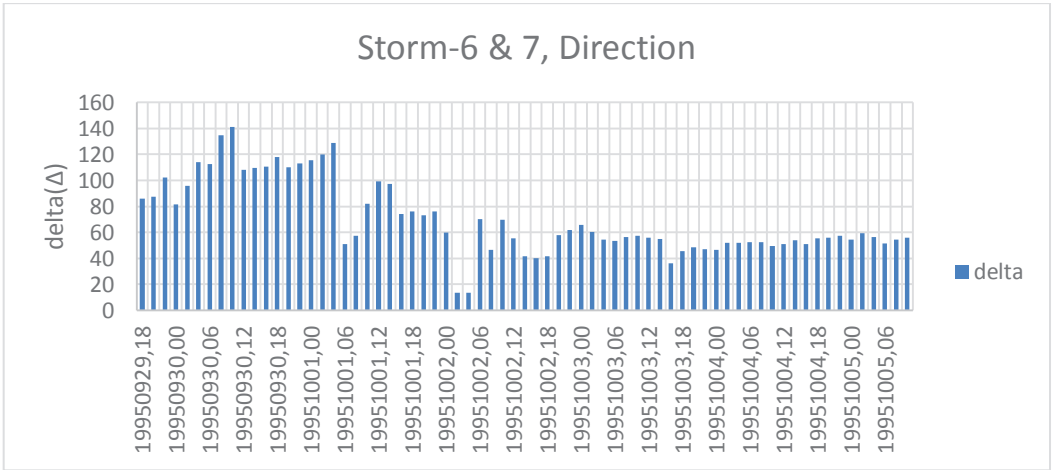

Figure 74.Time-series comparison for the direction of in-situ measurement and SWAN-out for the storm-6-7,

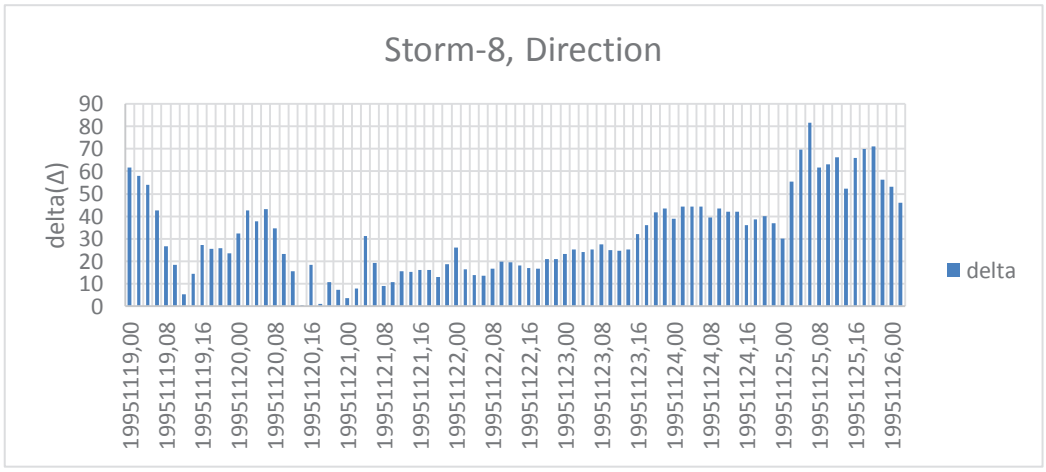

Figure 75.Time-series comparison for the direction of in-situ measurement and SWAN-out for the storm-8,

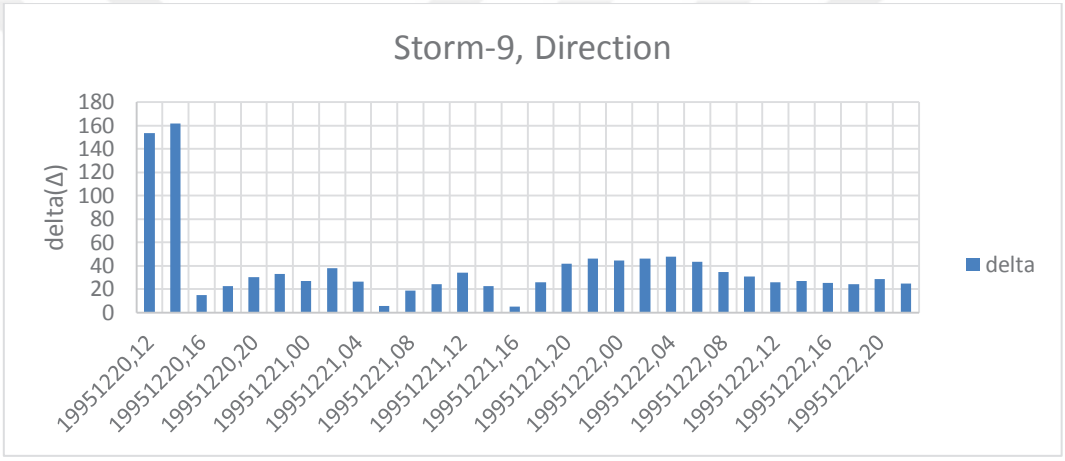

Figure 76.Time-series comparison for the direction of in-situ measurement and SWAN-out for the storm-9,

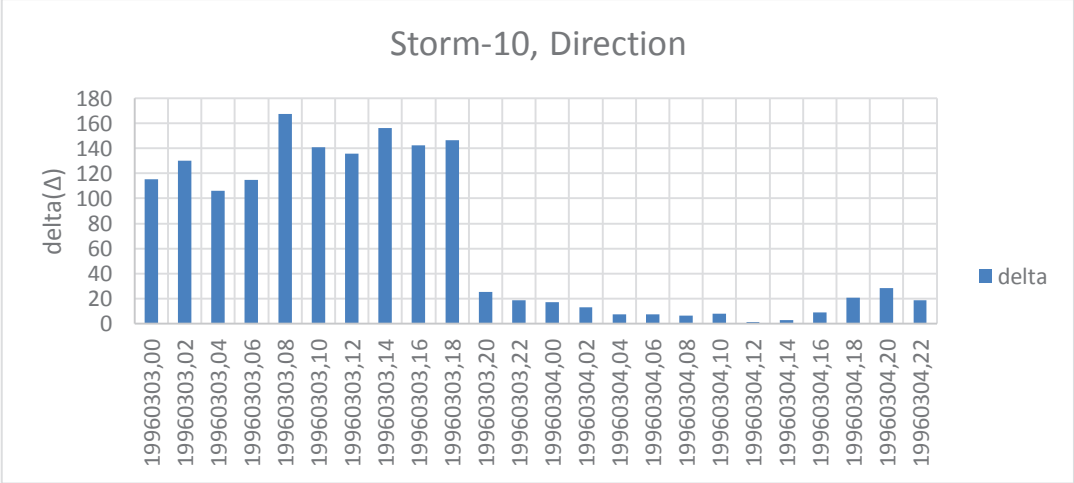

Figure 77. Time-series comparison for the direction of in-situ measurement and SWAN-out for the storm-10,

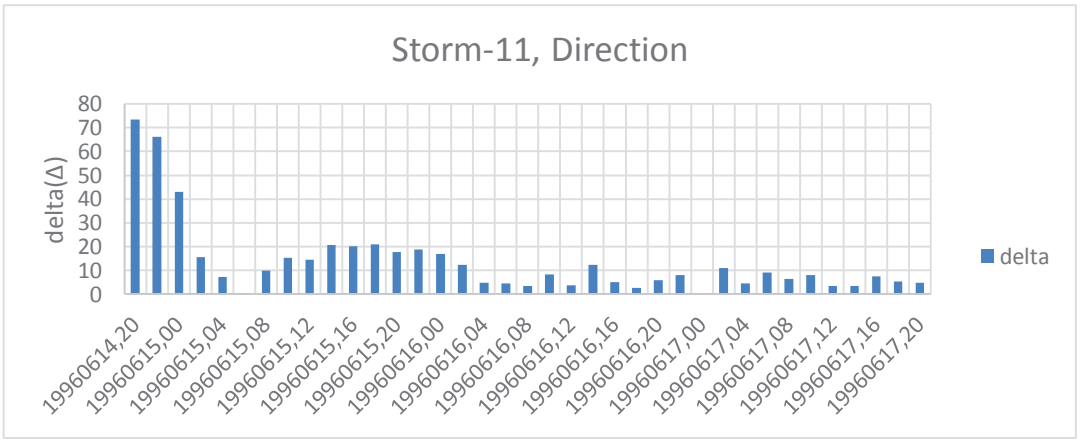

Figure 78.Time-series comparison for the direction of in-situ measurement and SWAN-out for the storm-11,

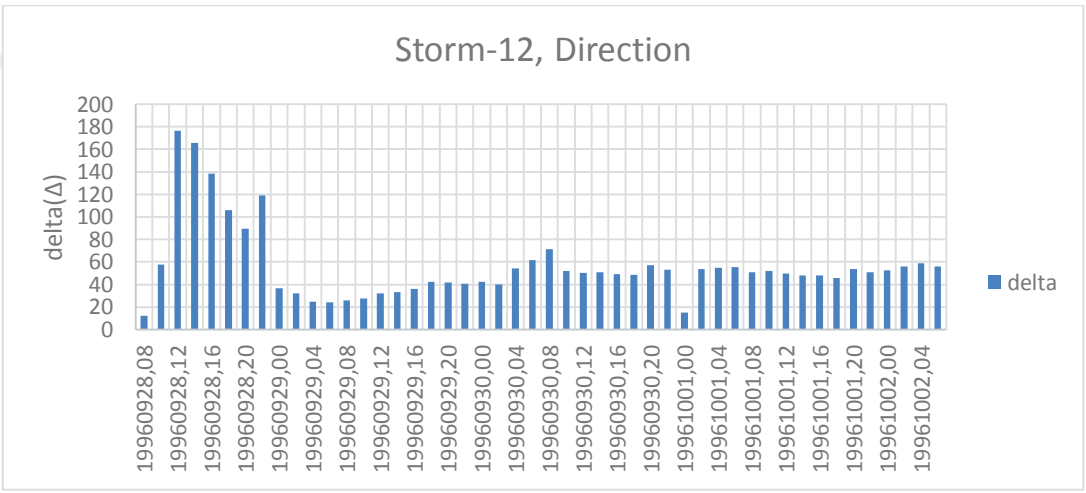

Figure 79.Time-series comparison for the direction of in-situ measurement and SWAN-out for the storm-12,

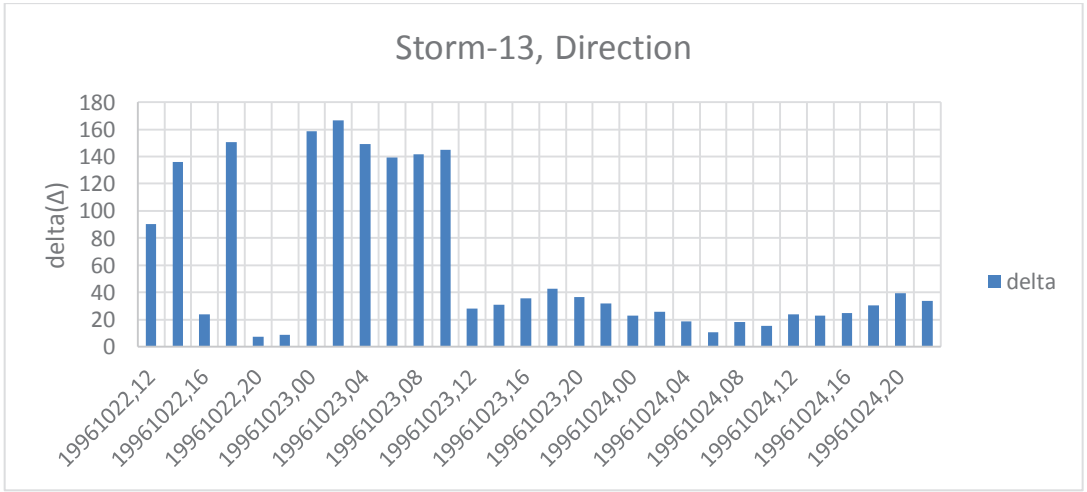

Figure 80.Time-series comparison for the direction of in-situ measurement and SWAN-out for the storm-13,

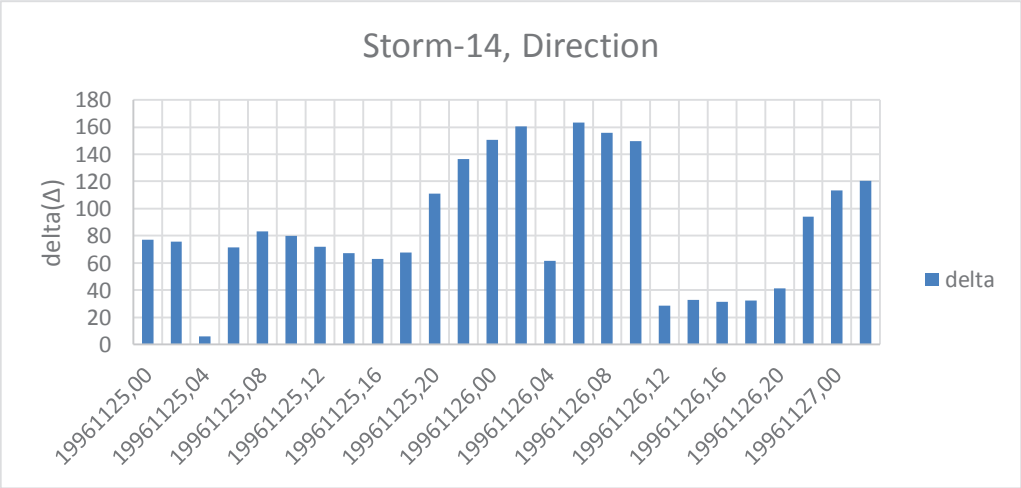

Figure 81.Time-series comparison for the direction of in-situ measurement and SWAN-out for the storm-14,